MEASUREMENTS AND ANALYSIS OF OZONE PRODUCTION IN HOUSTON AND LOS ANGELES

A Dissertation

Presented to

the Faculty of the Department of Earth and Atmospheric Sciences

University of Houston

In Partial Fulfillment

of the Requirements for the Degree

Doctor of Philosophy

By

James Howard Flynn III

May 2013

MEASUREMENTS AND ANALYSIS OF OZONE PRODUCTION IN HOUSTON AND LOS ANGELES

_____

James Howard Flynn III

APPROVED:

_____

Dr. Barry Lefer, Chairman

_____

Dr. Robert Talbot

_____

Dr. Xun Jiang

_____

Dr. Winston Luke, NOAA Air Resources Laboratory

_____

Dean, College of Natural Sciences and Mathematics

ACKNOWLEDGEMENTS

My special thanks go to Dr. Barry Lefer for providing me the opportunity to work with him since arriving at the University of Houston and for his invaluable support and instruction over the years. I would also like to thank Dr. Robert Talbot, Dr. Xun Jiang, and Dr. Winston Luke for agreeing to be on my committee and for providing input into this work. I am also grateful for the many students in the Atmospheric Science group who assisted me in collecting these measurements and who helped maintain the lab while allowing me time to complete this work. Finally, I would like to extend my deepest gratitude to my very understanding and tolerant wife and all of my family who assisted me in too many ways to count while I completed this degree.

MEASUREMENTS AND ANALYSIS OF OZONE PRODUCTION IN HOUSTON AND LOS ANGELES

An Abstract of a Dissertation
Presented to
the Faculty of the Department of Earth and Atmospheric Sciences
University of Houston

In Partial Fulfillment
of the Requirements for the Degree
Doctor of Philosophy

By
James Howard Flynn III

May 2013

ABSTRACT

Ozone is a respiratory irritant that affects all groups of people, but can be of significant concern to young children, those with respiratory illnesses such as asthma, and the elderly. Repeated exposure can cause permanent lung damage. An estimated 123 million people in the Unites States live in regions designated as non-attainment for the 2008 8-hour ozone standard of 75 ppbv. Nearly 5.9 million people live in the Houston-Galveston-Brazoria non-attainment area, and over 15.7 million live in the Los Angeles-South Coast Air Basin non-attainment area.

The work presents the results and analysis of measurements collected during several field campaigns in Houston, TX between 2006 and 2012, as well as in Pasadena, CA (CalNex) in the summer of 2010. Part one focuses on the comparison of O_3, CO, NO, and NO_2 measured continuously at two heights on the UH main campus in the fall of 2011 and 2012 and finds that the titration of O_3 to NO_2 accounts for ~50% of the observed nighttime differences on average, while it accounts for nearly 100% of the differences during some mornings. The second part presents the results of photochemical box modeling of O_3 production rates during three campaigns in Houston and during CalNex, which shows the effects of VOC reductions on O_3 production and the differences between the spring and fall O_3 seasons in Houston. Finally, an examination of the NOy budget during CalNex and the impacts that the choice of classification of days has on the analysis will be discussed reports that the overall agreement between measured NOy and the sum of individual NOy species is good, and that distinctly different results for calculated O_3 production efficiencies are found depending on which classification method is applied to the measurements.

Table of Contents

1. INTRODUCTION

Ozone is a respiratory irritant that affects all groups of people, but can be of significant concern to young children, those with respiratory illnesses such as asthma, and the elderly. Repeated exposure can cause permanent lung damage. An estimated 123 million people in the Unites States live in regions designated as non-attainment for the 2008 8-hour ozone standard of 75 ppbv. The Houston-Galveston-Brazoria (HGB) region of southeast Texas has been designated as a marginal non-attainment area for ozone with a design value of 84 ppbv. Design values for O_3 are calculated by averaging the 4th highest 8-hour O_3 value for the most recent three years and are used to determine whether an area is in attainment with the NAAQS. Nearly 5.9 million people reside in the eight counties included in the HGB non-attainment area. Additionally the Los Angeles-South Coast Air Basin in California is designated as being in extreme non-attainment with a design value of 112 ppbv, the highest in the nation, affecting over 15.7 million people in the affected 4 county area (http://www.epa.gov/oaqps001/greenbk/hntc.html).

Tropospheric ozone forms by reactions of oxides of nitrogen (NO_x), volatile organic carbon (VOC), and oxygen in the presence of solar radiation. Ozone photochemistry occurs when NO_2 is photolyzed in sunlight. Ozone formation is the result of the following reactions:

$$NO_2 + h\nu \rightarrow NO + O(^3P) \qquad \text{(where } h\nu < 420 \text{ nm)} \qquad (1.1)$$

$$O(^3P) + O_2 + M \rightarrow O_3 + M \qquad (1.2)$$

Once formed, ozone reacts with NO to regenerate NO_2.

$$O_3 + NO \rightarrow NO_2 + O_2 \quad (1.3)$$

Net ozone production is not possible unless a peroxy radical is present to react with NO to regenerate the NO_2 without destroying an ozone molecule as in reaction 3.

$$RO_2 + NO \rightarrow NO_2 + RO \text{ (where R can be: H, } CH_3, C_2H_5, \text{ etc.)} \quad (1.4)$$

Measurements of O_3 can be affected by the proximity of the site to emission sources such as power plants or roadways. In these locations emissions of NO can react with O_3 by equation (3) above to form NO_2. In order to account for these reactions O_x (O_3+NO_2) can be used. In areas with strong emissions NO_2 can comprise a significant portion of Ox while measurements in other areas tend to be comprised primarily of O_3 (Murphy et al., 2007). The same variability in O_3 in the horizontal also occurs in the vertical where measurements from ozonesondes routinely show gradients near the surface with higher O_3 aloft in the lowest few hundred meters (Tang et al., 2011). Ground level emissions of NO react with O_3 to form NO_2 near the surface which changes the O_x partitioning in the vertical and are responsible in part for the gradient in O_3 seen in the ozonesonde data. Differences are regularly seen in O_3 and NO_2 measurements from the Launch Trailer at the surface and Moody Tower at 70 m on the UH campus when vertical mixing is weak, such as nighttime and early morning. Stutz et al. (2004) showed that there is a strong altitude dependence on observed mixing ratios in the lowest part of the nocturnal atmosphere. The long term measurements at the Launch Trailer and Moody Tower, along with continuous measurements of boundary layer heights, provide a unique opportunity to examine the relationship between O_3 and NO_2 at two heights.

Under the Clean Air Act states with areas designated as non-attainment are required to develop control strategies to reduce pollution and attain (and maintain) compliance with the National Ambient Air Quality Standards. For O_3, these control strategies typically focus on reductions of NO_x and/or VOCs. In Houston for instance, the finding that highly reactive VOCs may be responsible for large fraction of instantaneous O_3 production rates (Ryerson et al., 2003) which lead to the implementation of additional restrictions on flares and cooling towers for ethylene, propylene, 1,3-butadiene, and isomers of butane. Since 2000, ambient NO_x in Houston has decreased by ~40%, and ethylene has decreased by nearly 75% since 1998 (Figure 1-1). Warneke et al., (2012) showed that over the last 50 years, tighter emission controls have reduced VOC emissions in the LA basin by nearly two orders of magnitude.

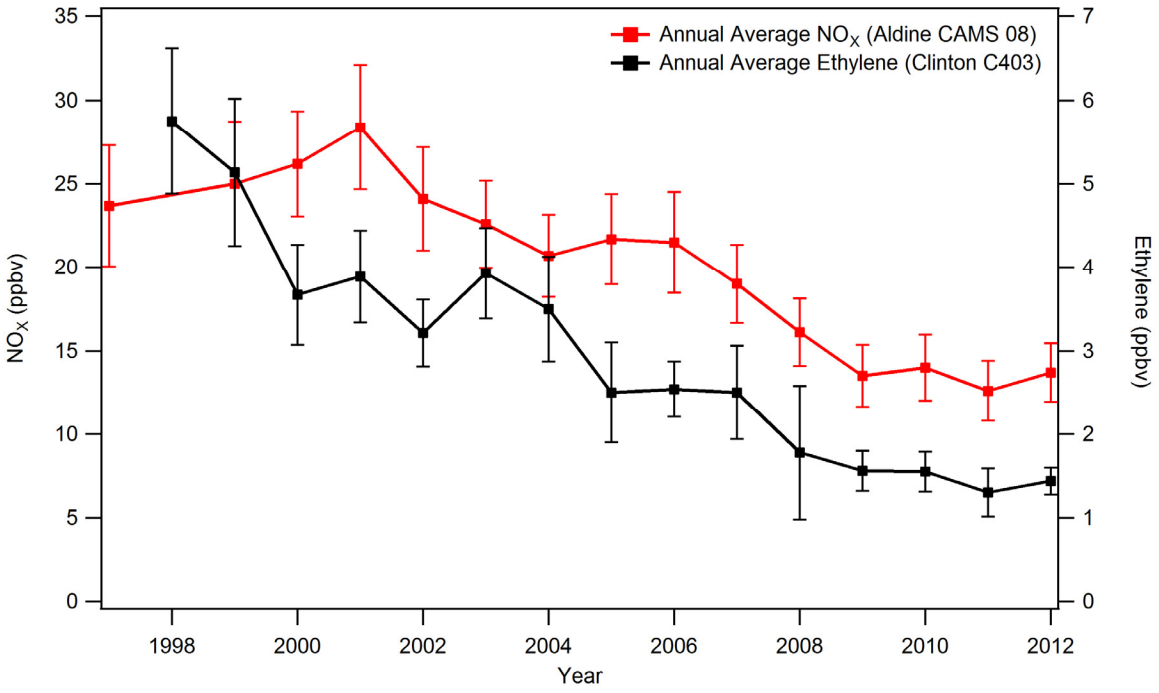

Figure 1-1. Time series of NOx and ethylene reflect reductions in NOx and VOC emissions in Houston. NO_x error bars represent one standard deviation divided by 50. Error bars for ethylene are one standard deviation divided by 10.

As a result of these controls ozone levels in both Houston and Los Angeles have decreased over the last two decades. Figure 1-2 shows the number of exceedances of the 125 ppbv 1-hour O_3 standard from the late 1980's to 2006 for Houston and Los Angeles. Where Los Angeles once had nearly half of the days each year above the standard, now less than 40 days per year exceed this standard. In Houston during the 1980's there were fewer exceedances than Los Angeles, but still occurred on at least 60 days per year. By 2006 exceedances in Los Angeles had dropped to ~30-40 days per year while Houston had slightly less. The most rapid improvement in the number of 1-hour exceedances in Houston took place between 2005 and 2008 which coincides with the full implementation of the NO_x and HRVOC rules in the HGB area. During this time exceedances of the 1-hour standard dropped from ~20 per year to only a few. While the 125 ppbv 1-hour

standard is still in effect as an anti-backsliding measure to ensure that pervious standards are still met, the current NAAQS for O_3 is 75 ppbv for an eight-hour average. Although significant improvement in reducing the number of 1-hour exceedances was achieved in Houston, the current standard is still exceeded 35 times a year. Los Angeles violated the 8-hour 75 ppbv standard 115 times in 2012.

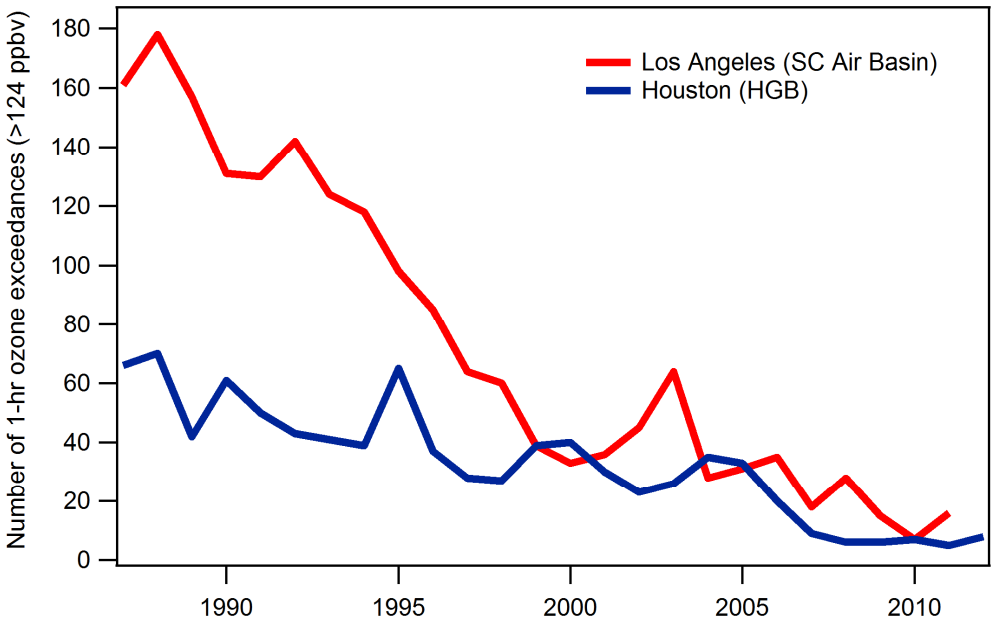

Figure 1-2. Number of days each year with peak 1-hour O_3 values above 125 ppbv for Houston and Los Angeles. Figure courtesy B. Lefer. Data courtesy TCEQ and CARB.

As mentioned previously, O_3 production is dependent on several variables, such as NO_x, VOCs, and sunlight. Lefer et al. (2003) showed that reductions in the jNO_2 photolysis rate always resulted in a reduction in O_3 production, and therefore O_3 production was always limited. Clouds and aerosols can reduce the number of photons that reach the lowest part of the atmosphere compared to cloud and aerosol free conditions, resulting in ~3% lower net O_3 production by aerosols alone, and a 17%

reduction due to the combined effects of clouds and aerosols (Flynn et al., 2010). The use of a photochemical box model can be used to calculate the instantaneous rates of O_3 formation, destruction, and net production, as well as calculate the individual contributions of reactions to the formation and destruction terms. These terms can be used as an indicator of the photochemical regime in which they took place, such as being NO_x-saturated or NO_x-sensitive.

In a NO_x-saturated condition, increases in NO_x tend to reduce O_3 production rates, whereas in a NO_x-sensitive condition O_3 production rates increase with greater NO_x. This can lead to a situation where reductions in NO_x can actually increase ambient O_3. In some cases, such as urban environments, the conditions can change from a NO_x-saturated situation in the morning to NO_x-sensitive in the afternoons. The combination of emissions from the morning rush hour and a low boundary layer can lead to high mixing ratios of NO_x. As the boundary layer deepens though the day, these and additional emissions are diluted into a larger volume resulting in lower mixing ratios. The point at which the transition from NOx-saturated to NO_x-sensitive depends on the reactivity of the VOCs present as the VOCs and NO_x compete for OH radicals. In the case of NO_x-saturation, OH reacts with NO_2 to form HNO_3, a terminal species in the troposphere for both OH and NO_2. As VOC reactivity increases, the point at which the NO_x-saturated/NO_x-sensitive transition occurs moves towards higher levels of NO_x. Consequently, reductions in VOC reactivity can drive conditions to a more NO_x-saturated situation, reducing the net instantaneous O_3 production rates.

As NO_x is consumed in the photochemical process, such as in the formation of HNO_3 described above, the overall composition of NO_y changes. NO_y is defined as the sum of NO, NO_2, HNO_3, PAN, HONO, PPN, N_2O_5, NO_3, $ClNO_2$, etc. Measurements of NO_y are typically made with either gold tubes or molybdenum mesh cartridges heated to 300ºC or above and catalytically reduce the NO_y species to NO, which is easily measured with a chemiluminescence detector. Some work has found that additional non-NO_y species such as NH_3 may also be converted to NO in these converters (Sather et al., 2006, Fitz et al., 2003, Geddes, 2013, Dunlea, et al., 2007,Williams et al., 1997, Xue et al., 2011). In many cases commercial instrumentation relies on the use of the same catalytic converters to measure NO_x. Because these converters also convert other NO_y components, the resulting NO_x is often an over estimation. This is particularly true during periods of strong O_3 photochemistry (Sather et al., 2006, Dunlea, et al., 2007). Photolytic NO_2 converters were developed as an alternative to the catalytic converter in an attempt to reduce interferences, however some species (i.e. HONO) can be partially photolyzed to form NO, resulting in small but measurable interferences (Pollack et al., 2010).

As described previously, when an area is NO_x-saturated reductions in NO_x levels can lead to an increase in the instantaneous O_3 production rates. Reductions in NO_x emissions can be brought about by regulation or by variable emissions. One change in emissions that occurs on a regular basis is what has become to be known as the "weekend effect", where levels of NO_x on the weekends are lower than during weekdays because there is less vehicle traffic, and therefore emissions, on weekends in most locations. In a NO_x-saturated environment where the dominant source is from vehicles, this weekend effect can lead to increases in O_3 on weekends (Pollack et al., 2012, Murphy et al., 2007).

Because of these differences many studies have focused on the differences between weekdays and weekends. Although this approach yields valuable information, particularly in regards to the effects of emissions on O_3, it neglects other important factors which impact O_3 levels. While emissions may be more conducive to greater O_3 production rates on weekends, the meteorological conditions may not be. Factors such as temperature, wind speed, and cloud-cover also have significant impacts on O_3. Classifying days by meteorological conditions is also problematic because variations in emissions are ignored. However, if analyses are performed by separation of days based on actual O_3 levels, both emissions and meteorology are incorporated into the analysis by default.

The following chapters will present the results and analysis of measurements collected during several field campaigns in Houston, TX between 2006 and 2012, as well as in Pasadena, CA (CalNex) in the summer of 2010. Chapter 2 focuses on the comparison of O_3, CO, NO, and NO_2 measured continuously at two heights on the UH main campus in the fall of 2011 and 2012. Chapter 3 presents the results of photochemical box modeling and O_3 production rates during three campaigns in Houston and during CalNex. The fourth chapter examines the NO_y budget during CalNex and the impacts that the choice of classification of days has on the analysis.

2. CONTINUOUS MEASUREMENTS OF O_3 AND NO_2 AT TWO HEIGHTS ON THE UNIVERSITY OF HOUSTON-MAIN CAMPUS

2.1 INTRODUCTION

Ozone is a respiratory irritant that affects all groups of people, but can be of significant concern to young children, those with respiratory illnesses such as asthma, and the elderly. Repeated exposure can cause permanent lung damage. An estimated 123 million people in the Unites States live in regions designated as non-attainment for the 2008 8-hour ozone standard of 75 ppbv (http://www.epa.gov/oaqps001/greenbk/hntc.html).

Tropospheric ozone is formed by the reactions of VOCs and NO_x in the presence of sunlight, where:

$$RO_2 + NO \rightarrow NO_2 + RO \qquad \text{(where R can be: H, } CH_3\text{, } C_2H_5\text{, etc.)} \qquad (2.1)$$

$$NO_2 + h\nu \rightarrow NO + O(^3P) \qquad (\text{where } h\nu < 420 \text{ nm}) \qquad (2.2)$$

$$O(^3P) + O_2 + M \rightarrow O_3 + M \qquad (2.3)$$

Once formed, ozone can then react with NO to regenerate NO_2.

$$O_3 + NO \rightarrow NO_2 + O_2 \qquad (2.4)$$

By taking O_x as the sum of $NO_2 + O_3$, O_x is conserved in reactions 2-4, although the partitioning of O_x can be controlled by emissions of NO and intensity of sunlight. Site-to-site comparisons of O_3 can be affected by proximity of the sites to sources of

NO_x, such as roadways, parking lots, or industrial sources, by reaction 3 above. This can be especially true when nearby sites are separated by significant vertical differences. To better quantify the total oxidant level at a given site, O_x should be considered in addition to O_3.

In 2009 the Texas Commission on Environmental Quality (TCEQ) began funding the University of Houston (UH) to collect measurements of O_3 and meteorology from the UH-Sugar Land campus and submit the data into the TCEQ LEADS system as CAMS 696. The following year the scope of the TCEQ funding was expanded to include measurements of O_3 and meteorology from four additional UH measurement sites on the UH main campus (C695), UH Coastal Center (C697), West Liberty airport (C699), and WG Jones State Forest (C698) (www.hnet.uh.edu). Measurements of CO at the Moody Tower were also included in the expanded funding. In 2011 the program was further expanded to include CO from all five sites. Although none of the trace gas data from the five UH operated sites meet the EPA quality assurance criteria for regulatory use, the data can be used for informational purposes and to assist in modeling efforts. Two of these sites, UH-Sugar Land and West Liberty airport, are the only monitors in Ft. Bend and Liberty counties, respectively and serve to fill gaps in the existing O_3 monitoring network.

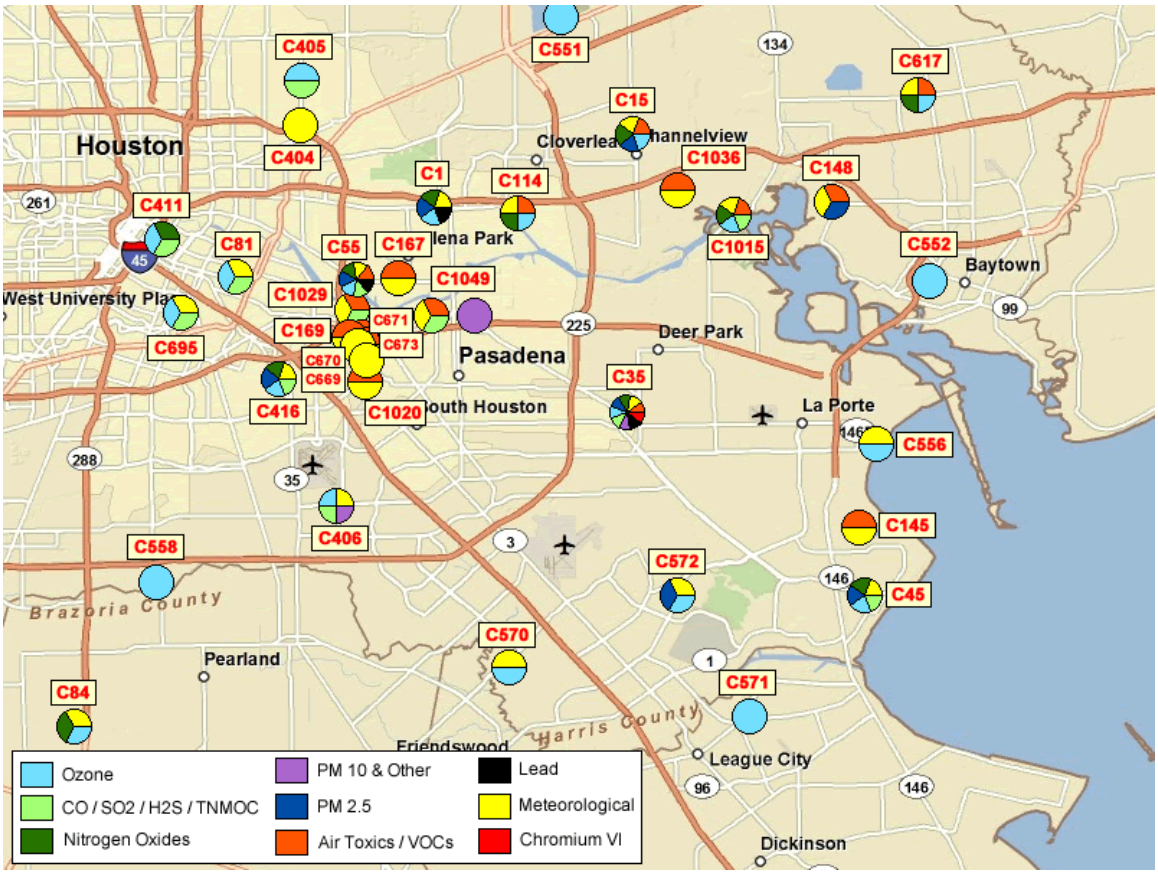

Figure 2-1. CAMS locations in southeast Houston. Moody Tower (C695) is located ~4 km south of downtown. The four additional UH monitoring sites are outside this map domain. Map courtesy TCEQ.

As part of the measurement program UH submits monthly comparisons of 13:00 CST hourly O_3 data from each of the five sites to three nearby O_3 monitors (Figure 2-1). Early afternoon was chosen as the comparison time with the assumption that photochemical O_3 production would be nearing its peak and the ambient values would be more uniform in the local area. Comparisons of the Moody Tower data often showed a good correlation with the nearby CAMS sites however the slope was up to 10-15% different (higher or lower) and with a 5-10 ppbv offset, with the Moody Tower measuring consistently higher (Figure 2-2). This phenomenon was also seen to a lesser extent in the data from the Jones Forest site. Both of these sites sample from elevated heights, the

Moody Tower at 70 m and Jones Forest at 41 m, and are compared to monitoring sites with typical EPA sample heights of 4-5 m.

Initially theories included differences in calibration, O_3 titration near the surface by vehicle exhaust, dry deposition of O_3 to surfaces, and differences in O_3 production rates. In order to begin addressing some of these theories the TCEQ again expanded the scope of the monitoring project in the fall of 2011 and 2012 to include measurements of NO and NO_2 at the Moody Tower and to measure O_3, CO, NO, NO_2, and meteorology at the Launch Trailer, a nearby surface site on the UH campus typically used for ozonesonde and radiosonde launches, with an inlet height of approximately 5m. The data presented here will examine the observed differences in the continuous measurements collected at the two sites on the UH campus during the fall of 2011 and 2012.

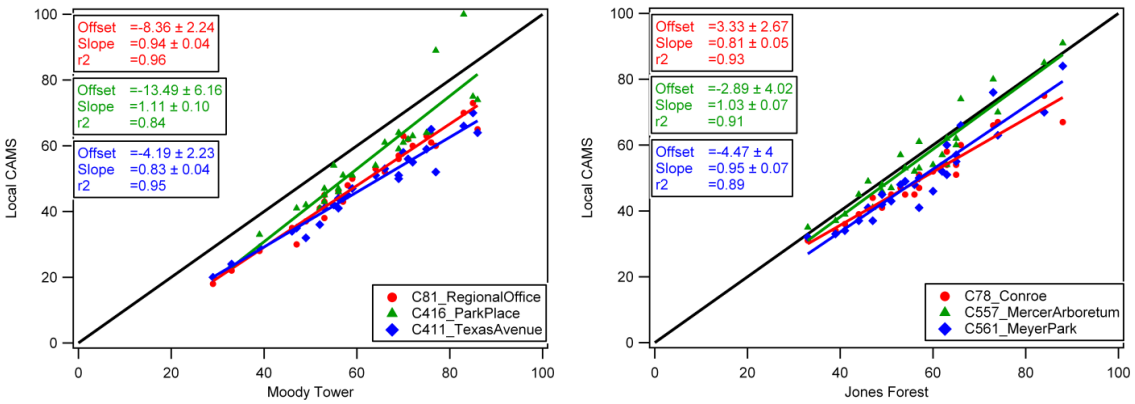

Figure 2-2. Scatter plot of 13:00 CST Moody Tower and Jones Forest O_3 values vs. the three nearest CAMS data for October 2010.

2.2 METHODS

2.2.1 Measurement sites

Both measurement sites are on the University of Houston main campus, located approximately 4 km south of downtown Houston. Measurements were collected from two heights, the roof of a high-rise dormitory and a converted truck trailer approximately ½ mile north of the dormitory.

North Moody Tower (29°43'3.04"N, 95°20'28.32"W)

The North Moody Tower is an 18-story dormitory on the southern side of the UH campus (Figure 2-3). An atmospheric chemistry laboratory is located on the 18th floor along with a 10 m sampling tower on the balcony. Trace gas and meteorological measurements are collected from the top of the sampling tower, approximately 70 m above the ground. An aluminum wrapped ½" PFA tube was used as the sample inlet for the sample manifold with a vacuum pump providing a residence time of ~1 second from the tip of the inlet to the manifold. Three-way Teflon solenoid valves were used to automatically switch between sample and calibration modes for the trace gasses.

Figure 2-3. Photo of North Moody Tower, left, and sample inlet mast with downtown Houston in the background, right.

Launch Trailer (29°43'26.11"N, 95°20'20.96"W)

Surface level (5 m) measurements were collected from a commercial truck trailer that was converted into an atmospheric chemistry laboratory with central air conditioning, instrument racks, electrical power, and high-speed internet connection (Figure 2-4). An aluminum sampling tower is bolted to the outside of the trailer providing the mast for the meteorological sensors and sample inlet. Like the Moody Tower, the sampling inlet was composed of aluminum wrapped PFA tubing, three-way Teflon solenoid valves, and a vacuum pump to maintain a residence time under 1s.

In 2011 the Launch Trailer was located in a grassy area approximately 20' off of an internal campus road with light traffic, however during the summer of 2012 the trailer

was moved approximately 120' east and a gravel parking lot was built immediately adjacent to the trailer. Due to the close proximity of the parking lot vehicle emissions are often sampled, but the narrow plumes quickly dissipate and do not appear to have any significant impact on the measurements.

Figure 2-4. UH Launch trailer in its' current location. Sample inlets are mounted to tower on left, ~1.5m above roof of the trailer.

2.2.2 Instrumentation

Trace gasses

Trace gas measurements at the Moody Tower and Launch Trailer were collected using a PC based data acquisition system running DAQFactory (www.Azeotech.com) software and LabJack USB hardware. The computer times were synchronized with one of the clocks at the US Naval Observatory every 15 minutes, thus keeping both data PC's on the same time base. Each of the trace gas instruments were set to a 10s averaging time

and were queried serially and logged by DAQFactory to a delimited text file once every 10s, ensuring that each value was recorded. LabJack hardware was used to control various components of the sampling and calibration system, including solenoid valves used to selectively switch each instrument between sample and measurement modes. The 10s data was subsequently averaged to 5-minute values after applying slope, offset, and conversion efficiency corrections to the data as needed.

Calibrations of the trace gas instruments were performed by feeding test atmospheres to the sample inlets of the instruments via three-way Teflon solenoid valves. The ozone test atmospheres were generated by a Thermo 49c Primary Standard ultraviolet photometric calibrator. Multipoint calibrations typically consisted of 4-5 upscale points between 25 and 200 ppbv plus a zero. Spans at the Launch Trailer were typically 50 ppbv and a zero while the Moody Tower was 160 ppbv and a zero. The Moody Tower span values were set by the agreement with the TCEQ; however Launch Trailer span values were selected to more closely represent typical ambient values.

Thermo 146c & -i series calibrators were used to generate the test atmospheres for the CO, NO, and NOx instruments. An AADCO 737 pure air generator was used to provide a continuous source of dilution air while compressed gas cylinders of nominally 25 ppmv CO in N_2, 5 ppmv NO in N_2, and 5 ppmv NO_2 in N_2 from Scott-Marrin Inc. (Riverside, CA) were used as the blend gases. The gases from Scott-Marrin were ±2% NIST traceable calibration standards. Multipoint calibrations of CO typically consisted of 4-5 upscale points from 800-1000 ppbv through 100 ppbv plus a zero. Single point span levels were typically 200-250 ppbv plus a zero. NO and NO_2 multipoint calibration

levels corresponded to five upscale points between 100 and 5 ppbv and a zero. Cross calibrations between the Moody Tower and the Launch Trailer were accomplished by exchanging gas and O_3 standards to ensure that the measurements at each site were comparable. Additionally, the O_3 calibration standards were checked against the EPA Region 6 standard reference photometer annually. The 5-minute average detection limits defined as three times the standard deviation of zero and the detailed uncertainties for the trace gas measurements at both sites are shown in Table 2-1.

	Detection Limit (ppbv)	Calibration Standard	100 sccm MFC	10 slm MFC	Repeatability	Conversion Efficiency	Combined Uncertainty
Moody Tower							
Ozone	1.5	2%	-	-	2.2%	-	3.0%
CO	40	2%	2%	2%	3.5%	-	4.9%
NO	0.03	2%	2%	2%	1.9%	-	4.0%
NO_2	0.11	2%	2%	2%	1.8%	0.30	3.9%
Launch Trailer							
Ozone	1.5	2%	-	-	1.2%	-	2.3%
CO	40	2%	2%	2%	3.3%	-	4.8%
NO	0.04	2%	2%	2%	4.1%	-	5.4%
NO_2	0.19	2%	2%	2%	6.8%	0.21	7.6%

Table 2-1. Detection limits and uncertainties for Moody Tower and Launch Trailer in situ trace gas measurements.

In situ measurements

Ozone

A Thermo Environmental 49c UV-photometer was used at both the Moody Tower and Launch Trailer to collect measurements of ozone (Williams et al., 2006). Daily zero/span checks were performed on each instrument to track stability. Bi-weekly multipoint calibrations were used to establish the response of the instrument at the Moody Tower, while the Launch Trailer instrument received multipoint calibrations nominally twice weekly. Calibration approaches were dictated by the requirements of the H-NET

monitoring project for TCEQ. The ozone calibrators used were evaluated by the EPA Region 6 calibration laboratory and are traceable back to SRP #5. The ozone calibrators were controlled via commands from DAQFactory which also controlled the Teflon solenoid valves used to switch the ozone instrument from sample to calibration mode. Both valve position and sample state flags were recorded in the data file to facilitate data processing.

CO

CO measurements at the Moody Tower were collected with a Thermo Environmental 48c-TLE while a 48i-TLE was used at the Launch Trailer. Both instruments use an infrared detector with gas filter correlation wheel and feature an internal catalytic scrubber used to periodically determine the baseline of the instrument. Every hour the instruments were placed into zero mode and the averaging was changed from 10s to 180s. After eight minutes the baseline was automatically reset to the current value and placed back into measurement mode with a 10s averaging time. The status flag was held in the zero state for an additional 120s after the instrument returned to sample mode to allow the instrument to recover from the zero and provide a clean status wave for removing non-measurement data during processing. As with the ozone measurements, zero/span checks were automatically performed each day at both the Moody Tower and Launch Trailer to track stability while bi-weekly multipoint CO calibrations at the Moody Tower were used to determine instrument sensitivity. Multipoint calibrations at the Launch Trailer were conducted approximately twice per week to determine the sensitivity of the CO instrument at the surface site.

NO and NO_2

Measurements of NO and NO_2 at the Moody Tower were collected using a Thermo Environmental 42i-TL chemiluminescence instrument operated in NO_x mode and reported both NO and NO_x measurements every 10s. An LED-based photolytic converter from Air Quality Design was used in place of the standard molybdenum converter. This LED photolytic converter is more selective in converting NO_2 to NO and does not exhibit the interferences that are possible when using molybdenum or other high power UV LED converters (Sather et al., 2006; Pollack, Lerner, & Ryerson, 2010). As part of the 10s measurement sequence, the 42i-TL instrument performs a pre-reactor zero which is used in the calculation of each 10s value produced by the instrument, therefore additional pre-reactor zeros or baseline corrections are not necessary. One drawback to using one instrument to measure NO and NOx sequentially is that when ambient concentrations are highly dynamic it is possible for the instrument to report NO greater than NO_x. This effect is more pronounced when plumes are narrow and have sharper edges. The Launch Trailer measurements, which were more likely to see narrow strong plumes from individual vehicles, were made using separate instruments for NO (42c) and NO_x (42c-TL with AQD photolytic converter). These instruments were configured for continuous operation without switching modes. Pre-reactor baseline determinations were conducted hourly on both the NO and NOx instruments. The average of each pre-reactor baseline check was interpolated during processing and then subtracted from the measurement data resulting in continuously variable baseline-corrected data.

Calibrations of the NO_x instruments were performed automatically with the dilution and valve system described above. Test atmospheres of NO were used to evaluate the sensitivity of the detector while NO_2 dilutions were used to assess the conversion efficiency of the photolytic converter. Although one instrument was used to measure NO and NO_x at the Moody Tower, the minor differences in the sample flow path and operating pressures resulted in slightly different sensitivities to NO calibrations, therefore during data processing the NO and NO_x data were treated as if they were from separate instruments. NO_2 data was calculated by first correcting the NO and NO_x data for baseline and sensitivity calibrations and then subtracting NO from the NO_x values. The resulting difference was then divided by the conversion efficiency determined by the NO_2 calibrations, producing corrected NO_2 values.

Long-path Differential Optical Absorption Spectrometer (DOAS)

As described in Williams et al. (2006) and Wong et al. (2011), the long-path DOAS instrument deployed at the Moody Tower site during the 2009 Study of Houston Aerosol and Radical Precursor (SHARP) project was used to measure path averaged mixing ratios of O_3 and NO_2. The DOAS system used a double Newtonian telescope to send and receive a white beam of light from a Xe-arc lamp. Retroreflectors on the roofs of three buildings in downtown Houston (George R. Brown Convention Center, 30 m; Five Houston Center, 130 m; JPMorgan Chase Tower, 300 m) reflected the light back to the detector, giving a total path length of 8-10 km. The received light is passed to a Czerny-Turner spectrograph and photodiode array, yielding a spectral resolution of 0.55 nm. The DOAS technique does not require calibration and has a variable sample time depending

on atmospheric conditions. Detection limits vary with path length and atmospheric conditions while the overall uncertainty is approximately 3% for O_3 and 8% for NO_2 (Stutz et al., 2004).

Meteorology

Both measurement sites recorded basic meteorological parameters of wind speed and direction (RM Young 05103), temperature and relative humidity (Vaisala HMP-45C), station pressure (Setra 278), and rainfall (Texas Electronics TE525). These measurements were recorded once every 10 seconds by a Campbell Scientific CR1000 datalogger. Data were downloaded to the same PC as the trace gas data. The datalogger's clock was set so that the clock would be reset if the difference between the datalogger was greater than 1 second. By coordinating the various clocks in this way it was possible to maintain the synchronization of all of the measurements at both sites. Because of the local interferences by buildings and trees of the winds measured at the Launch Trailer, the results and analysis presented will focus on meteorological data from the Moody Tower since the wind fields are more likely to be representative of the overall wind field.

Additional measurements of NO_2 photolysis rates (jNO_2) and boundary layer (BL) heights were also collected at the Launch Trailer. Measurements of jNO2 were made using a MetCon filter radiometer (Shetter et al., 2003). Boundary layer heights were measured with a Vaisala CL-31 ceilometer with modified firmware and processed with Vaisala's BL-View software in real time. Additional details regarding the operation and characteristics of the CL-31 can be found in Haman et al. (2012).

2.3 RESULTS

2.3.1 Ozone at Moody Tower and Launch Trailer

The data examined here for each site were collected between 10/7-12/12/2011 (66 days) and 9/17-11/13/2012 (57 days). These periods were selected for maximum overlap when all of the instruments were operating well and for comparable periods during both years. Figure 2-5 and Figure 2-6 show the time series of O_3 data collected in the fall of 2011 and 2012, respectively. In general the Moody Tower O_3 measurements were slightly higher during the daytime and significantly higher overnight compared to the Launch Trailer. Meteorological conditions were similar for both periods and were dominated by winds from the south-southeast. Polar plots of wind direction histograms for each measurement period (Figure 2-7 and Figure 2-8) show that there was a more significant northeasterly component in 2012.

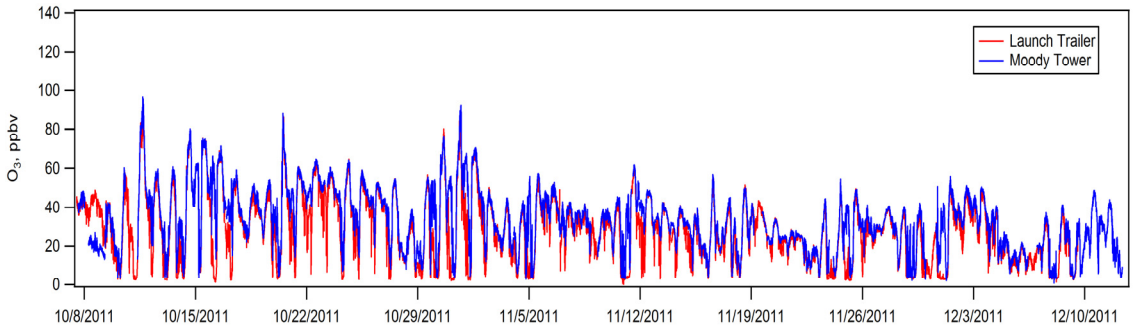

Figure 2-5. Time series of O_3 data coverage at the Moody Tower and Launch Trailer during fall 2011.

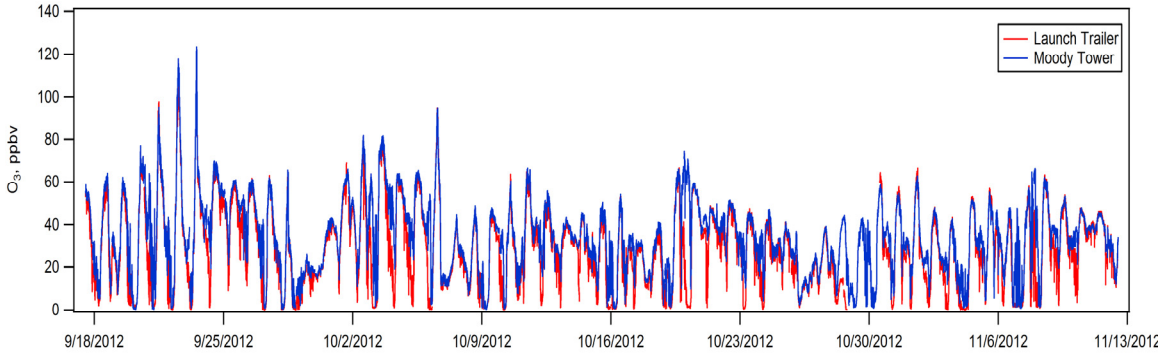

Figure 2-6. Time series of O_3 data coverage at the Moody Tower and Launch Trailer during fall 2012.

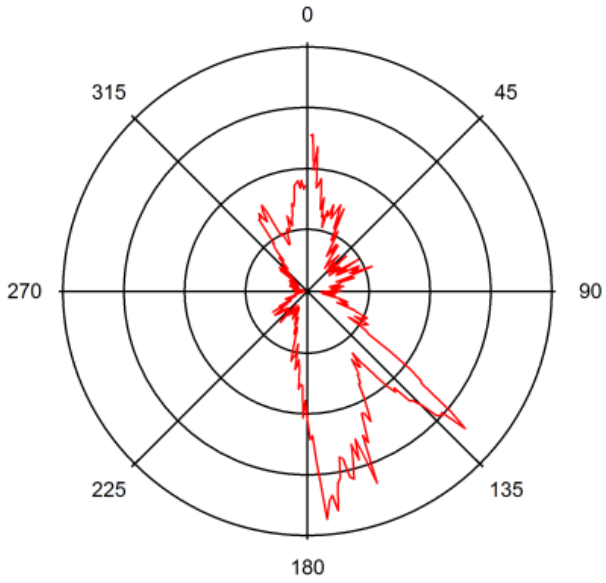

Figure 2-7. Polar plot of wind direction histogram during the fall 2011 measurement period for the Moody Tower.

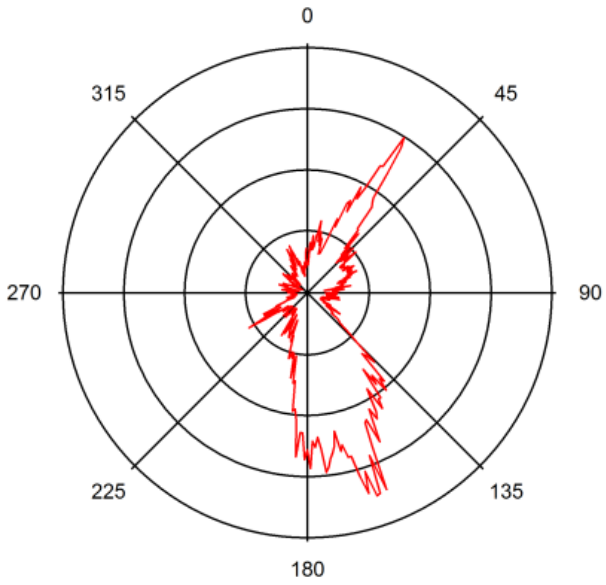

Figure 2-8. Polar plot of wind direction histogram during the fall 2012 measurement period for the Moody Tower.

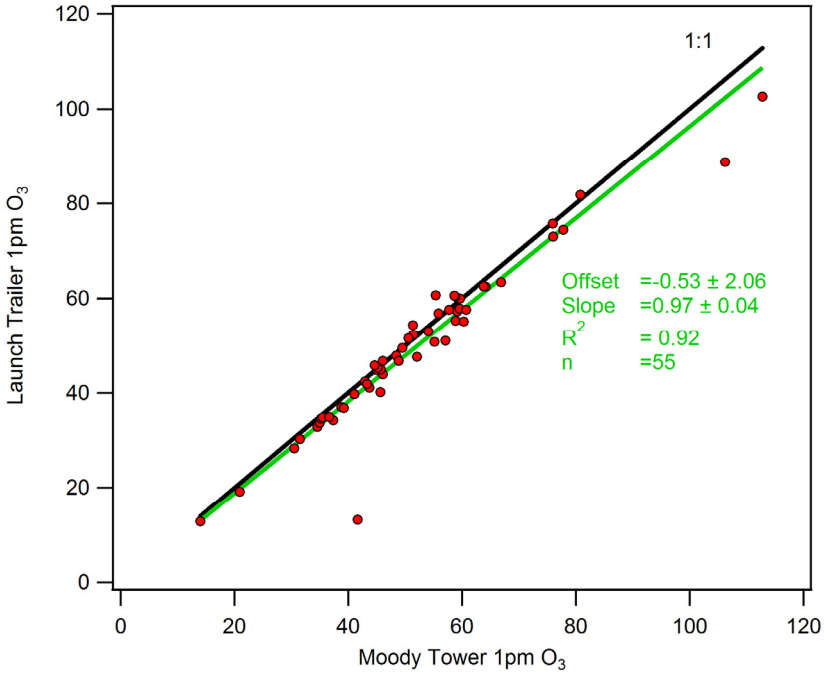

Figure 2-9. Comparison of Launch Trailer vs. Moody Tower 13:00 CST hourly O_3 for Fall 2012.

A scatter plot of the 13:00 CST hourly O_3 averages from the fall 2012 period (Figure 2-9) indicates that the afternoon ozone measurements agree well between the two sites. This is in contrast with the previous comparisons of the Moody Tower to nearby CAMS stations (Figure 2-2) and may be due in part to the close proximity of the two sites. In addition to the reasons for selecting 13:00 CST for the comparisons mentioned previously, it should be noted that convective mixing at this time of day tends to reduce the vertical gradient in O_3.

2.3.2 O_3 vs. O_x

While the afternoon O_3 observations show good agreement between the two sites, there are more significant differences between the sites during other times of day. Differences in O_3 during the overnight and early morning hours can be quite significant, up to 40 ppbv at times (Figure 2-10, upper panel) with the Moody Tower values higher than the Launch Trailer. An examination of the NO_2 data, Figure 2-10 middle panel, shows that there are also significant differences between the two sites, however in this case the Launch Trailer values are greater than the Moody Tower. Because NO_2 is easily photolyzed to create O_3, it has been suggested that O_x (the sum of O_3 + NO_2) be considered instead of O_3 (Murphy et al. 2007). O_x can be especially important when comparing urban or polluted sites where traffic emissions are significant. O_x for the Moody Tower and Launch Trailer, shown in the lower panel of Figure 2-10, shows quite clearly that most of the differences that were seen in O_3 and NO_2 are not present when considering O_x, indicating that much of the overnight and early morning differences seen in O_3 are due to titration with NO emitted near the surface. Additionally, the diurnal

profile of O_x is much flatter than O_3, and the rate of increase in O_x in the morning is less than the rate for O_3.

Figure 2-10 also shows that the rate of O_3 increase seen on the mornings of October 11 and 12, ~15 ppbv/hr and ~40 ppbv/hr at the Launch Trailer, respectively, are significantly reduced when considering O_x. On October 11, the increase in O_x is delayed almost 90 minutes from the beginning of the increase in O_3, and once O_x begins to increase around 8:00 CST the rate is ~5 ppbv/hr lower than the rate for O_3. In the case of October 12, O_3 at the Launch Trailer increases approximately 20 ppbv in just 30 minutes; however the O_x levels remain constant. While these observed increases in morning O_3 do show significant O_3 production rates, a portion of the rates are due to the reconversion of NO_2 back to O_3 after it was initially titrated by morning rush hour emissions (Murphy et al., 2007). In the case of October 12th, all of the morning increase in O_3 can be attributed to this reconversion of NO_2 rather than "new" O_3 production, as evidenced by the lack of change in O_x during this period.

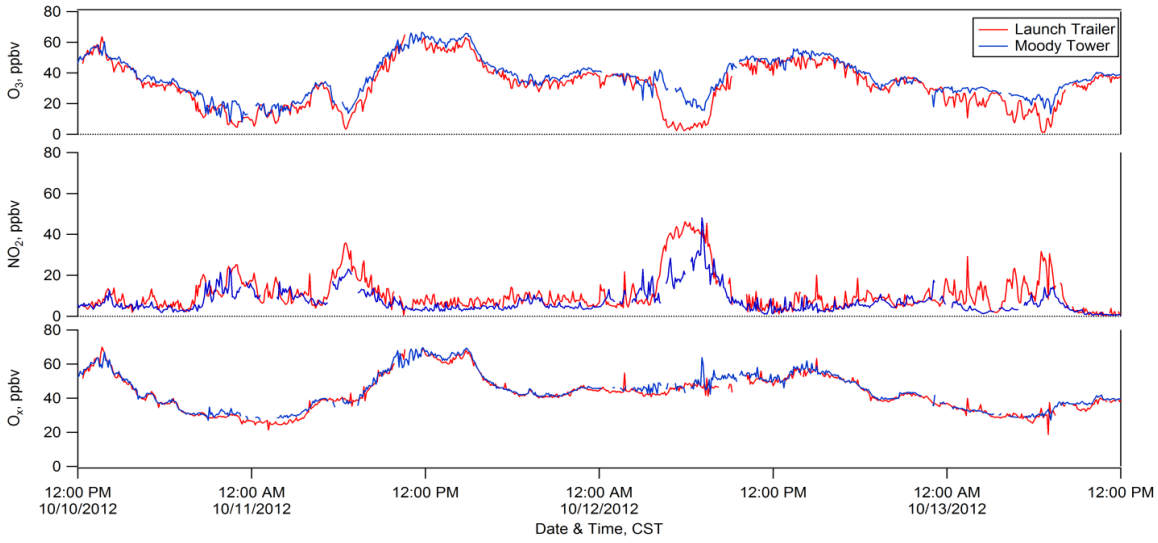

Figure 2-10. Seventy-two hour time series of O_3, NO_2, and O_x during the fall 2012 measurement period.

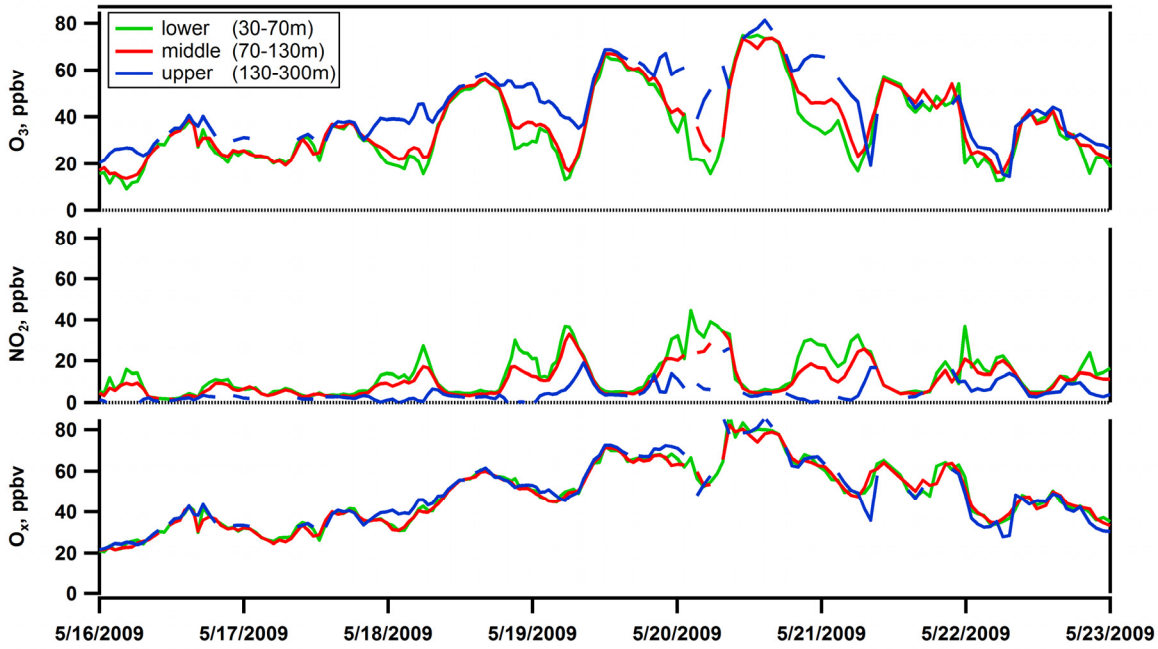

Figure 2-11. One-week time series of O_3, NO_2, and O_x from the UCLA LP-DOAS at the Moody Tower during spring 2009.

Measurements of O_3 and NO_2 from the LP-DOAS from UCLA during the SHARP campaign during the spring of 2009 (Figure 2-11) show similar results to the in situ measurements made in 2011 and 2012, however the altitudes (30-300 m) and area (4-5 km between DOAS and retroreflectors) covered by the DOAS are much greater. As with the in situ measurements, this would tend to indicate that O_x is largely conserved over a range of altitudes and that the in situ measurements are representative of a larger area. In addition, the increase in O_x over the course of the first 5 days during this period is more evident than what can readily be seen in the O_3 data.

2.4 DISCUSSION

2.4.1 High and low O_3 days

The data were separated into high and low O_3 days. For the purposes of this study high O_3 days were defined as days with peak 1h $[O_3] > 70$ ppbv and low O_3 days had peak 1h $[O_3] < 40$ ppbv. In the fall 2012 period, there were eight high O_3 days and seven low O_3 days. Average diurnal profiles of O_3, NO_2, and O_x were calculated for both sites. Figure 2-12 shows the diurnal profiles for fall 2012, with the high O_3 days in the left column and low O_3 days in the right column. In general, under all conditions for all measurements the two sites agree during the day time, however large differences can exist during periods with weak vertical mixing. During the late night and early morning, differences in the diurnal profiles of O_3 on high O_3 days can approach 20 ppbv. Both locations show a minimum in O_3 that coincides with the local morning rush hour. The NO_2 profiles for both locations show that the daily maximum also occurs during morning

rush hour, primarily due to titration of O_3 with NO from vehicle emissions. The CO/NO_x ratio for days with high O_3 in Figure 2-13 and Figure 2-14 (LT: CO/NO_x 5.33 ± 0.05; MT: 5.25 ± 0.07) is consistent with vehicle emissions (Parrish, 2006; Luke et al., 2010), and the timing of the emissions would indicate that the highest levels were seen during the morning rush hour. Because the surface emissions of NO from the morning rush hour occur at a time when vertical mixing is reduced, more O_3 is titrated to NO_2 at the height of the Launch Trailer than the Moody Tower. Not shown, there is also approximately an hour delay in the morning rush hour peak of NO and CO in the diurnal profile at the Moody Tower compared to the Launch Trailer, with the Launch Trailer measuring higher values for both NO and CO. These differences can give an indication of the dilution and mixing time it takes for surface emissions to reach the sample height of the Moody Tower. The nighttime and early morning differences seen in the O_x diurnal profiles at both sites are roughly 50% less than the differences seen in the O_3 diurnal profile, therefore O_3 titration accounts for ~50% of the differences in nighttime [O_3]. Since these differences occur before sunrise when O_3 production is not taking place, the remainder of the nighttime differences is likely due to dry deposition to surfaces and other O_3 reactions, such as O_3 + Alkenes. Not only are the differences in O_x on low O_3 days insignificant at all times of day, the diurnal profile is nearly flat, indicating that very little new O_3 was produced on these days. Data from fall 2011 also show similar results.

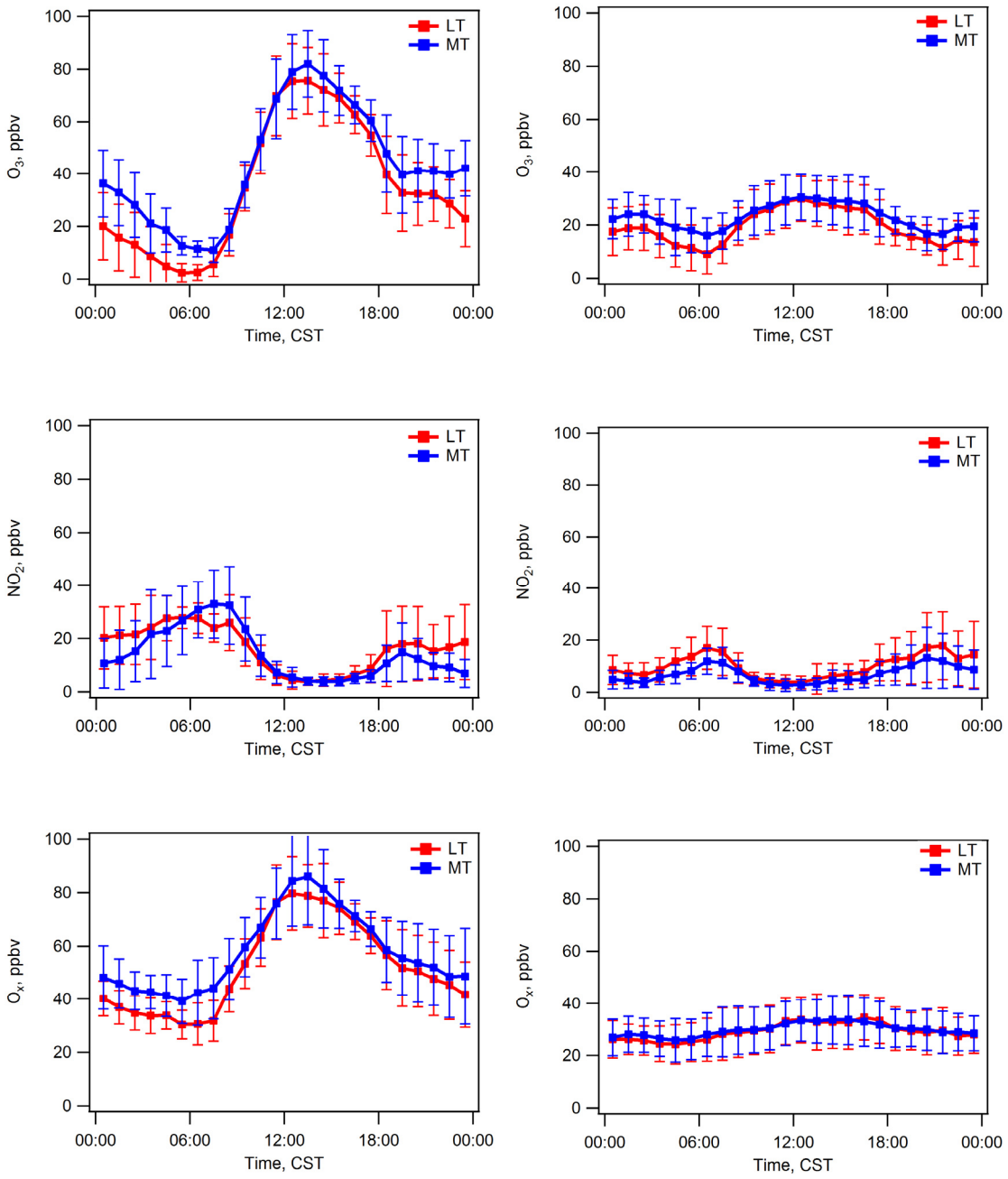

Figure 2-12. Diurnal profile of fall 2012 measurements for O_3, NO_2, and O_x for days with high O_3 days (peak 1h [O_3] > 70 ppbv), left column, and low O_3 days (peak 1h [O_3] < 40 ppbv), right column.

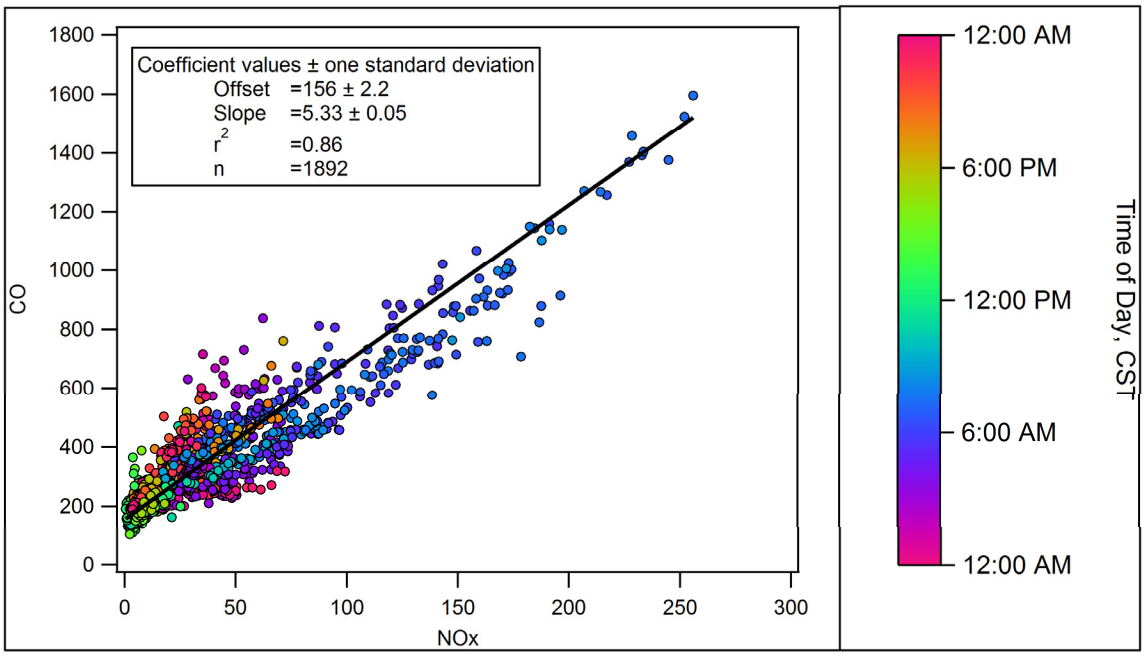

Figure 2-13. CO vs. NO_x at the Launch Trailer for high O_3 days during fall 2012.

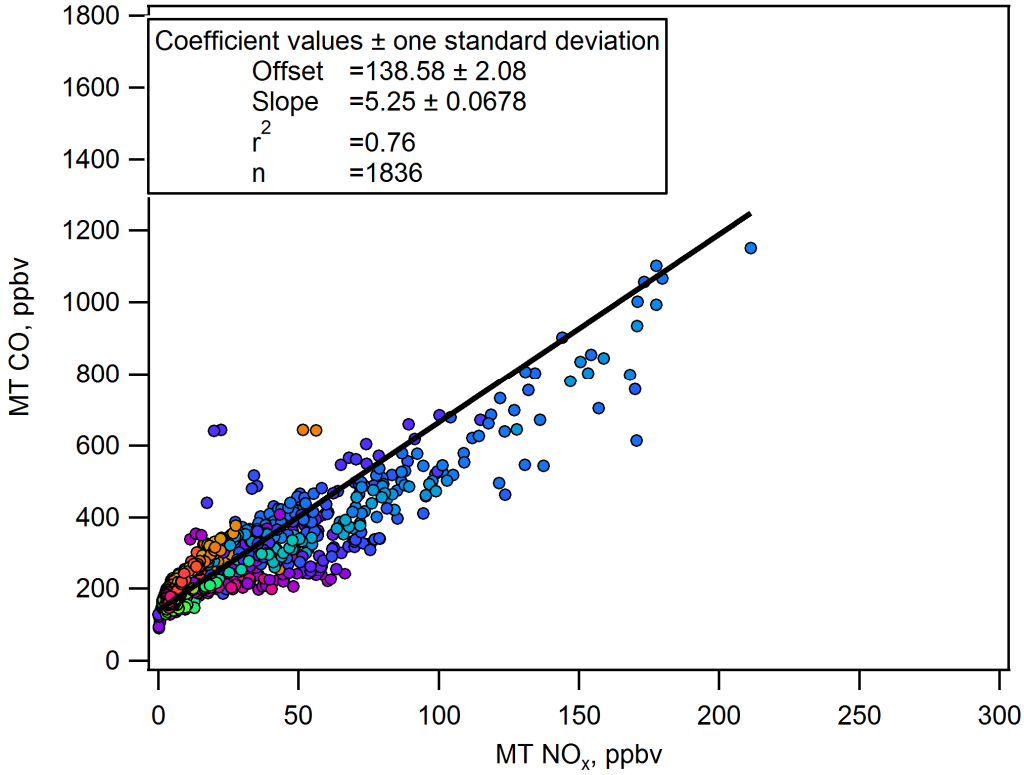

Figure 2-14. CO vs. NO_x at the Moody Tower for high O_3 days during fall 2012. The color scale is the same as for Figure 2-13.

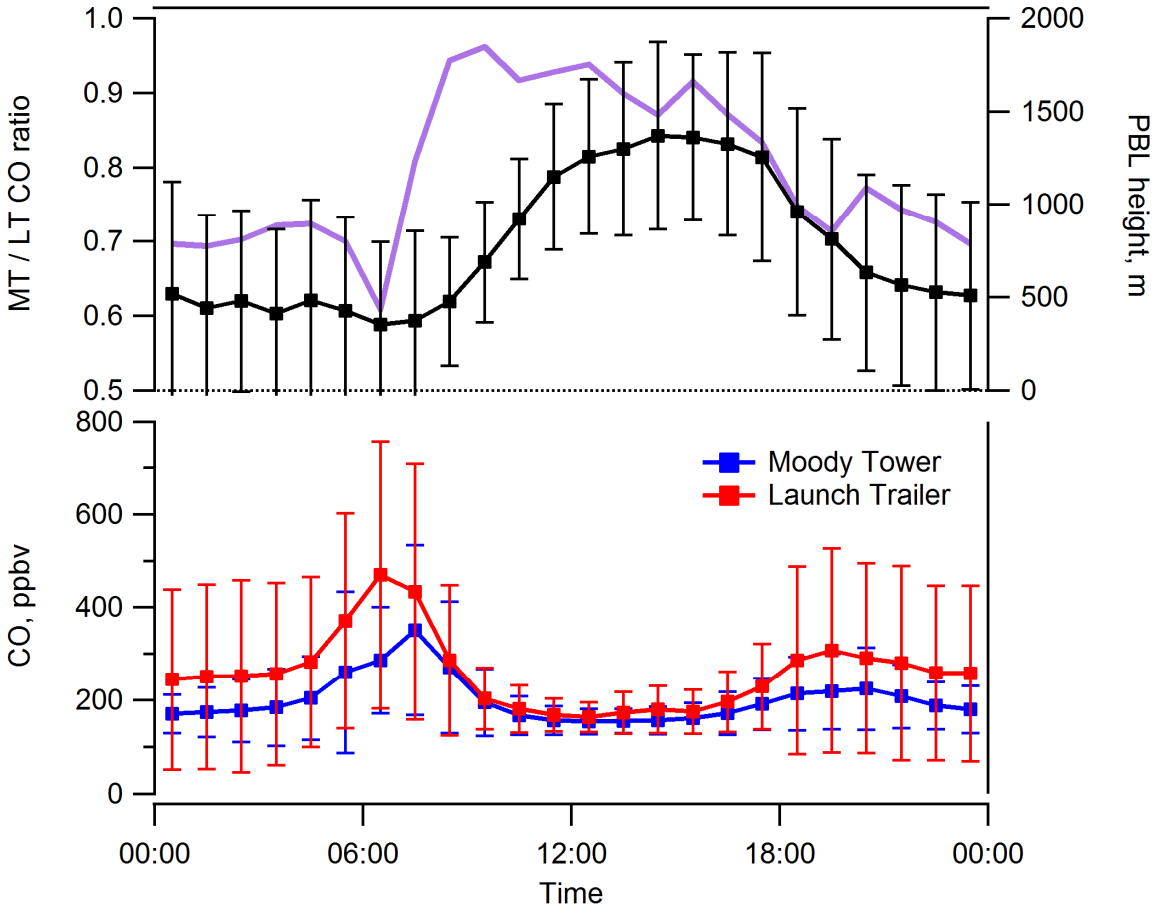

Figure 2-15. Diurnal profiles of CO for Moody Tower and Launch Trailer (lower panel). Upper panel shows the ratio of the MT/LT CO diurnal profile and PBL height.

Diurnal profiles show the Moody Tower CO is lower than at the Launch Trailer all day, but the greatest differences are evening through mid-morning when vertical mixing is weakest. Examination of the Moody Tower/Launch Trailer CO ratio shows that after the boundary layer has deepened, CO at the Moody Tower was about 10% lower than at the Launch Trailer because of the dilution that occurs while mixing the surface emissions up to the 70 m sample height of the Moody Tower. Overnight, when vertical mixing is weakest, CO at the Moody Tower is about 30% less than at the Launch Trailer.

However, the largest difference between the two heights coincides with the morning rush hour, when the Moody Tower measurements show that the surface emissions are diluted by nearly 40% by the time they reach the Moody Tower. The ratio of the Moody Tower and Launch Trailer NO_x diurnal profiles (not shown) also show a similar dilution during the morning rush hour. Because both CO and NO_x are diluted a similar amount, the CO/NO_x ratio is maintained between the two measurement heights (Figure 2-13 andFigure 2-14).

2.4.2 Differences in O_x

While much of the observed differences can be attributed to O_3 titration, there are several periods in which there are significant differences in O_x between the two heights. Figure 2-16 shows an example of a time series of O_3, CO, NO, NO_2, O_x, and jNO_2 for a four day period in September 2012. The differences in O_x appear to have two general causes. First, during the overnight periods of September 21, 22, and 23 the difference in O_x is slightly greater than during most other times. Upon closer examination O_3 was found to have increased at the Moody Tower but not at the Launch Trailer. At the same time, CO levels at the Moody Tower either decreased or stayed constant while CO at the Launch Trailer generally increased. Boundary layer height data from the CL-31 at the Launch Trailer showed that on these nights the height of the nocturnal inversion was within a few tens of meters above or below the 70 m sample height of the Moody Tower. Based on these observations, it is likely that on these occasions the Moody Tower was sampling from the residual layer or a mixture of the residual layer and surface layer rather than entirely from the surface layer like the Launch Trailer. Errors in nocturnal

inversion height measurements and/or mechanical turbulence may account for sampling the residual layer when inversion heights were slightly above the Moody Tower sample height.

Differences in O_x also may be driven by a loss of O_x at one of the locations, as seen in Figure 2-16 on the morning of September 20 and 21. On these and several other occasions pre-dawn O_x at the Launch Trailer was reduced while the Moody Tower remained relatively constant. Examination of O_3 and NO_2 at the Launch Trailer show that in both cases O_x was almost entirely composed of NO_2 as O_3 had been near zero for several hours prior to the reduction in O_x; therefore, a loss of NO_2 is responsible for the reduction in O_x during these periods. Measurements of CO and NO during these periods are particularly high, with [NO] $\geq$ 150 ppbv. A scatter plot of the difference between O_x at the Moody Tower and Launch Trailer versus NO measured at the Launch Trailer (Figure 2-17) shows that differences between the two locations can occur with any wind direction at low [NO], with the Moody Tower most often higher than the Launch Trailer. Higher levels of NO are correlated with wind directions from the NNE-ENE and show somewhat smaller differences in [O_x] up to ~50-75 ppbv of NO. At NO levels greater than 75 ppbv, the differences in O_x begin to increase, with Moody Tower O_x greater than the Launch Trailer by as much as 60 ppbv or more. Other species that are co-emitted with NO and CO are likely responsible for the loss of NO_2 during these extreme events. Although the conversion of NO_2 to HONO by heterogeneous reaction on the surface of aerosols, including soot, the formation of $ClNO_2$, and reactions on PAH coated particles have been well documented (Ziemba, et al., 2010, Sarwar et al., 2012, Esteve, et al., 2006), these reactions are not likely to explain the loss of up to 30 ppbv of NO_2 during

these events. Unfortunately measurements of NO_y, aerosols, and VOCs were not collected during either 2011 or 2012 which would likely be useful in better determining the NO_2 loss mechanism.

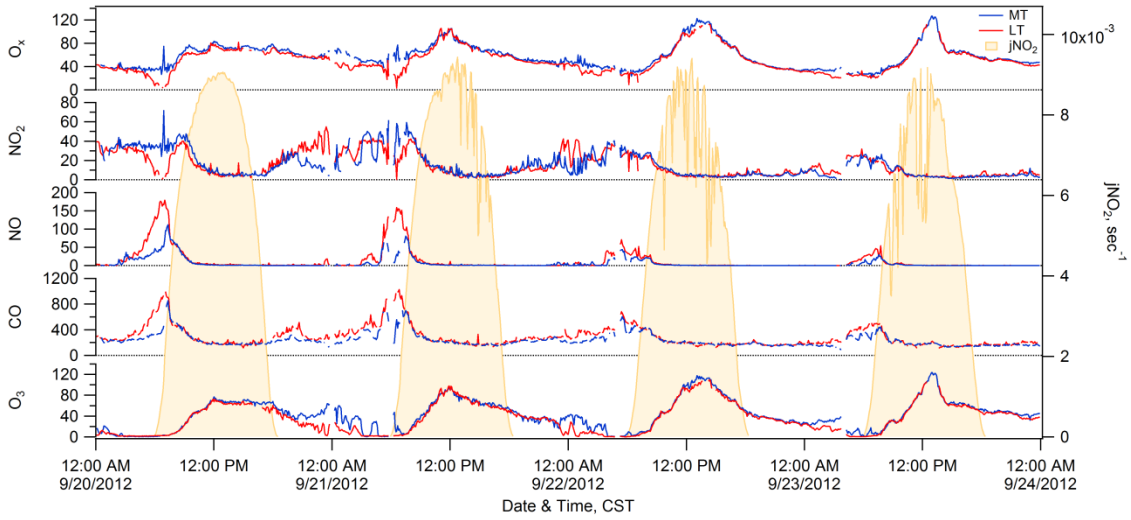

Figure 2-16. Four day time series of O_3, CO, NO, NO_2, O_x, and jNO_2 during fall 2012.

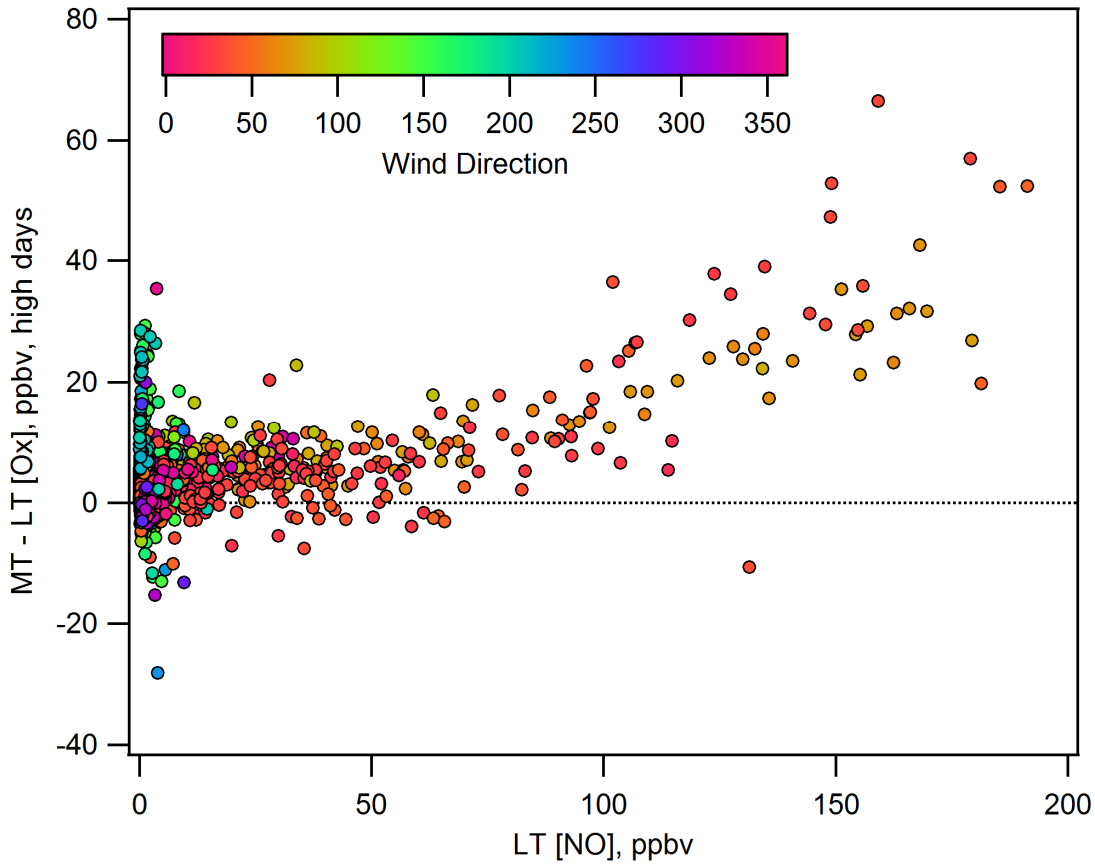

Figure 2-17. Scatter plot of the difference between O_x at the Moody Tower and Launch Trailer on days with high O_3 versus NO measured at the Launch Trailer with marker color showing wind direction.

2.4.3 Comparisons of Moody Tower to CAMS sites

Comparisons for the monthly reports were performed using the 13:00 CST hourly O_3 averages from the Moody Tower. Other near-by monitoring sites that initially highlighted the differences in O_3 measurements were also examined for the 2011 and 2012 measurements presented here.

Fall 2011 Moody Tower measurements were compared to two nearby sites and two distant sites (Figure 2-18). Figure 2-19 shows the 13:00 CST hourly averaged O_3

measured at two nearby sites, C411 (Houston Texas Avenue, 3.5 km north) and C416 (Park Place, 6 km southeast), plotted against Moody Tower data. Reduced major axis regressions were calculated and found slopes of 0.83±0.04 and 0.87±0.05 for C411 and C416 respectively. R-squared values were 0.81 for C411 and 0.87 for C416. These results are consistent with the differences that were previously found in the monthly reports to the TCEQ. Additionally, the majority of the 400-series monitoring sites show a similar grouping with slopes nominally in the 0.8-0.9 range. These sites are located throughout the Houston area, as much as 30 km from the Moody Tower. It should be noted that all of the 400-series monitoring sites in the Houston area are maintained by the City of Houston rather than the TCEQ and the ozone data from these sites meet the requirements to be used for regulatory purposes.

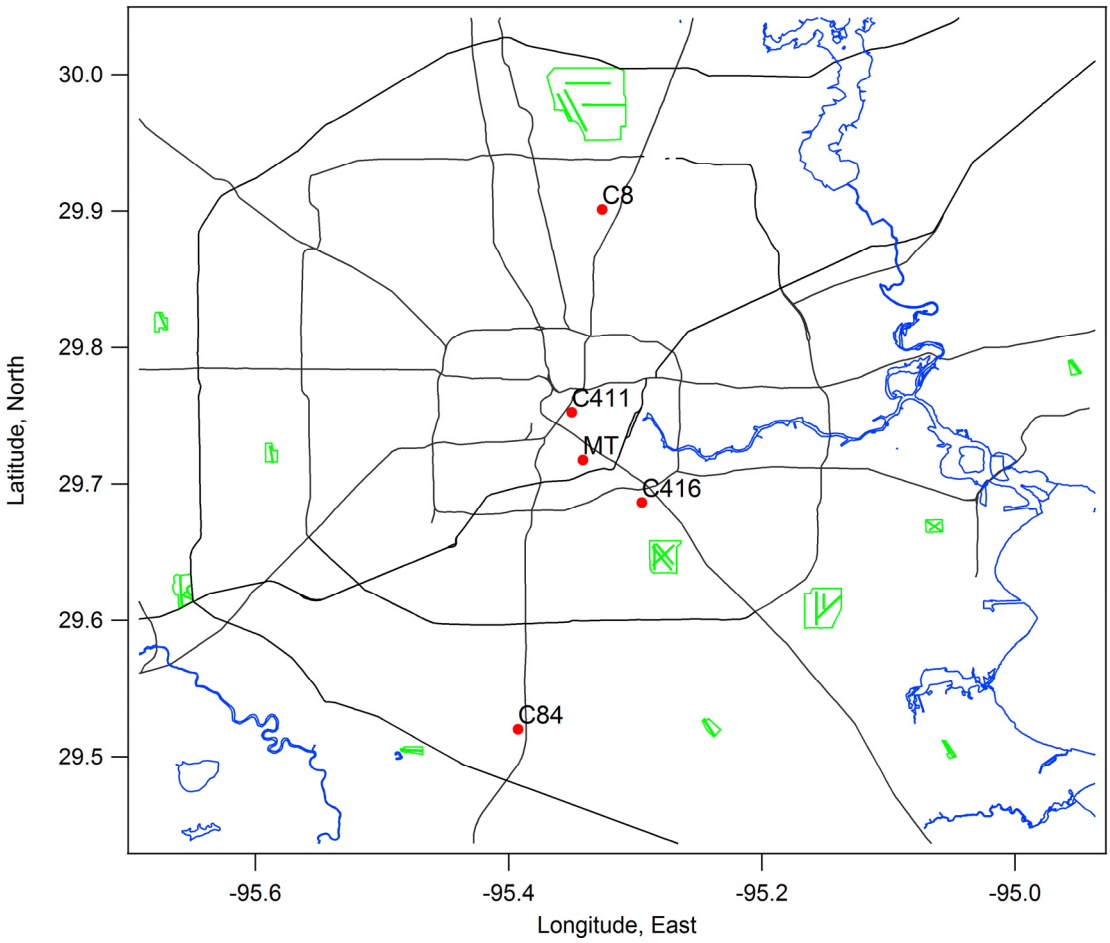

Figure 2-18. Houston area map showing the Moody Tower and CAMS sites used in comparisons.

A comparison to other monitors in the Houston area, however, yields different results with much better agreement. Comparisons to CAMS sites with one- and two-digit identification numbers in the Houston area show slopes much closer to 1. These sites are operated by the TCEQ Houston Regional Office with the exception of C35, Houston Deer Park, which is operated by a contractor for the TCEQ. Figure 2-20 shows the comparison of C8 (Houston Aldine, 20 km north) and C84 (Manvel Croix Park, 23 km south) to the Moody Tower for the same period. Linear fits of the data give slopes of 1.01±0.05 for C8 and 1.03±0.06 for C84.

Both the TCEQ and City of Houston sites are distributed through the Houston area with good coverage. The agreement with the TCEQ monitoring sites and disagreement with the City of Houston sites may be an indication of a systematic difference between TCEQ and COH sampling protocols. Perhaps it is something as simple as a poor ozone calibration standard, or something related to the COH sampling approach. In September of 2012 it was found that the Teflon inlet to the UH Launch Trailer (installed new in August 2011) appeared to be "dirty" or coated with particles. Tests were performed where a second inlet from a brand new piece of Teflon tubing was installed in parallel with the "dirty" launch trailer inlet. Switching between the old and new inlets several times found that the new particle free inlet may be 2 ppbv (~6-7%) higher than the old inlet, but the tests were done under variable conditions so the old inlet was place in storage and additional lab testing may be conducted. Comparisons between the Launch Trailer and Moody Tower in May 2012 showed that the Launch Trailer may have been as much as 6 ppbv (~11.5%) lower than the Moody Tower during the afternoons when vertical mixing should minimize the differences between the two heights. Because it was uncertain when the inlet may have begun affecting the 2012 measurements five months (April 11 – September 12) were invalidated.

The effects of the "dirty" inlet were not evident in the calibrations because calibrations through the inlet were not feasible with the equipment used. Attempts to calibrate through the length of the inlet caused excess back pressure in the O_3 calibrator resulting in noisy calibrations. As a result, calibration gas was added through a Teflon solenoid inside the launch trailer. This approach resulted in stable calibrations of the O_3 instrument but did not account for losses that may have been happening in the inlet.

Discussions with the site operators for the City of Houston sites confirmed that they do not calibrate their O_3 instruments through the inlet; however, the TCEQ does conduct an annual technical audit where the instruments are challenged through the full length of the sample line. The City of Houston follows the guidance of the TCEQ and changed their sample inlets every six months until April 2012, when the TCEQ guidance changed to an annual replacement schedule. Filters are not used on the inlet of the sample lines. The Moody Tower monthly reports do not appear to show significant differences in the comparison to surrounding sites until August 2012 (offsets 1.4-3.4 ppbv, slopes 0.98-1.06). While these findings may affect the comparisons between the Moody Tower and surrounding CAMS sites, they do not affect the comparisons of O_3 and O_x on the UH campus.

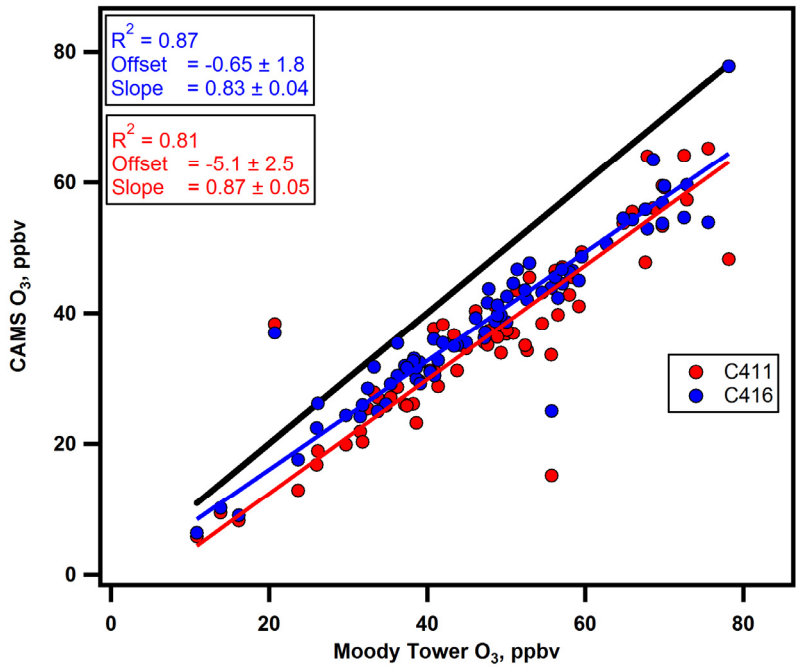

Figure 2-19. Scatter plot of O_3 from two nearby monitoring sites and the Moody Tower. Comparisons of other 400-series monitoring sites show similar results.

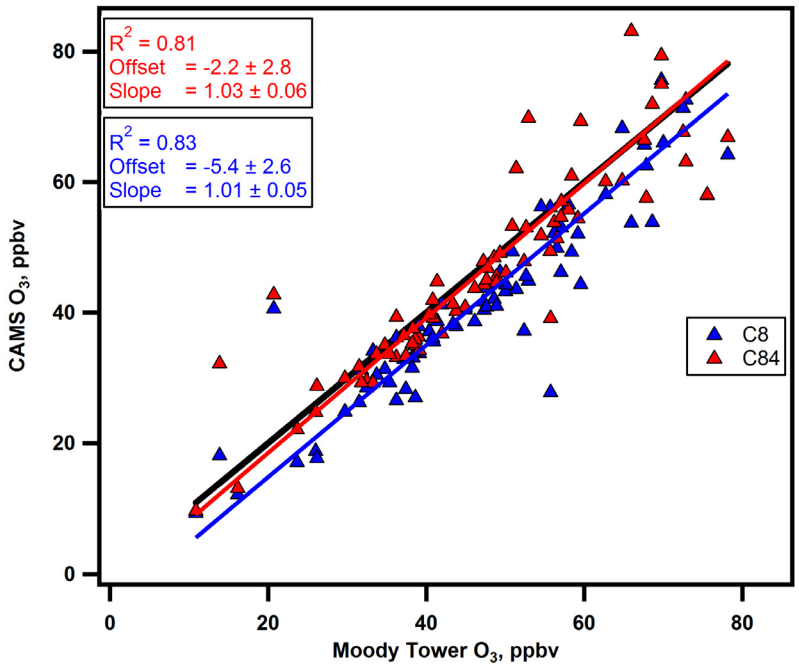

Figure 2-20. Scatter plot of O_3 from two distant monitoring sites and the Moody Tower. Comparisons of Houston area one- and two-digit sites show similar results.

In contrast to the fall 2011 comparisons, data from fall 2012 show much better agreement between the Moody Tower and the 400-series CAMS sites. Figure 2-21 through Figure 2-23 show the 13:00 CST hourly average O_3 comparisons between Moody Tower and C416 for September, October, and November. Hourly averages for the entire month are shown as grey points while the 13:00 CST data are shown as red points, with the 1:1 line in black. The agreement for all three of these months shows a significant improvement over previous years with slopes between 0.93 and 1.05. This may indicate that an adjustment was made to the calibrations of the 400-series measurements since sample inlets were changed on a regular basis.

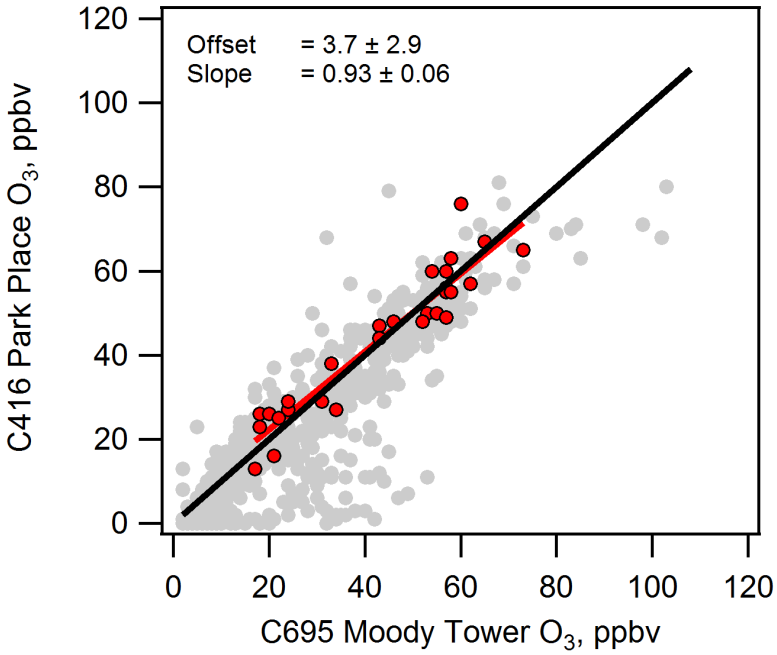

Figure 2-21. Scatter plot of hourly averaged O_3 for C416 and Moody Tower for September 2012. Points for all hours are shown in grey; red points indicate 13:00 CST values.

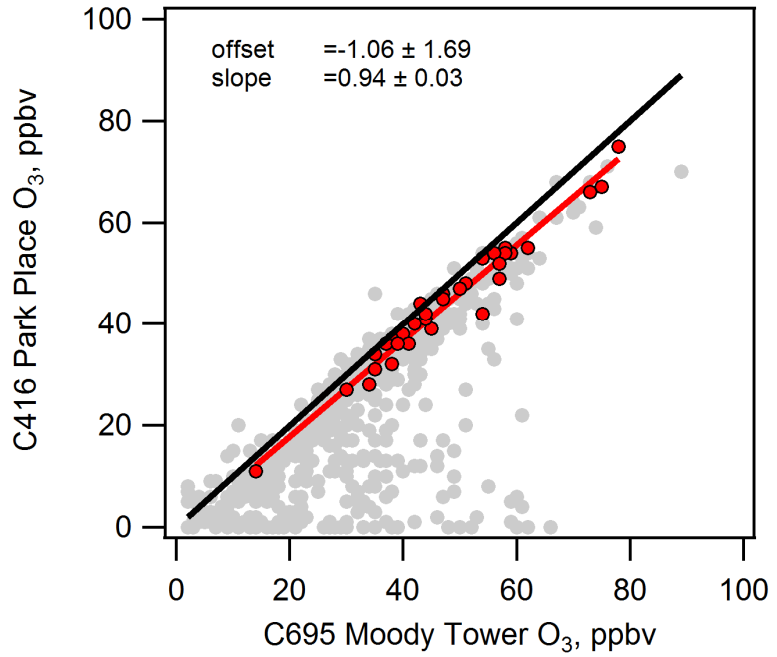

Figure 2-22. Scatter plot of hourly averaged O_3 for C416 and Moody Tower for October 2012. Points for all hours are shown in grey; red points indicate 13:00 CST values.

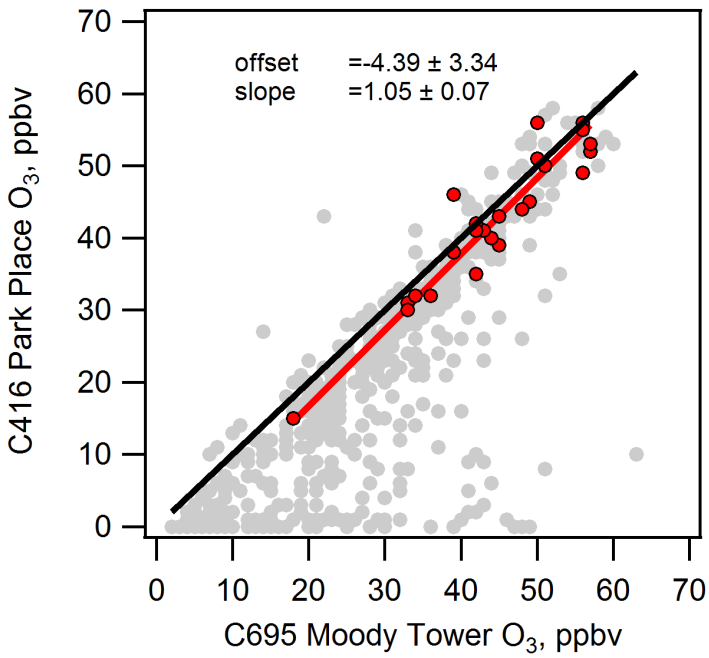

Figure 2-23. Scatter plot of hourly averaged O_3 for C416 and Moody Tower for November 2012. Points for all hours are shown in grey; red points indicate 13:00 CST values.

2.5 CONCLUSIONS

Variations seen in ozone concentrations in an urban area may be driven by several factors, including titration from nearby sources. This variability can complicate the comparison of data between measurement sites. By examining O_x, the sum of $NO_2 + O_3$, some of the variability can be removed. Ambient O_3 near emission sources, such as power plants or roadways, are often titrated to NO_2. This NO_2 can then easily be photolyzed to reform O_3 in the presence of sunlight. In this way O_x is largely conserved and tends to show a flatter diurnal profile than O_3 does.

Measurements at the Moody Tower (70 m) and the Launch Trailer (5 m), separated by approximately ½ mile, show good agreement between O_3 and O_x at both sites when comparing afternoon values. This agreement is largely due to the strong

vertical mixing present in the afternoons and the proximity of the sites. Differences between the two sites are largest at night and in the early morning when vertical mixing is the weakest, sometimes causing a decoupling between the two measurement heights. The relationships seen in the in situ data are supported by measurements of O_3 and NO_2 from the Moody Tower by LP-DOAS. These measurements also show that O_x is conserved over a broader area and range of altitudes.

Analysis of the data from the fall of 2011 and 2012 shows that the titration of O_3 to NO_2 accounts for approximately 50% of the observed differences at night between O_3 measured at the two heights. Since these differences occur in the overnight and early morning hours, variations in O_3 production can be ruled out, leaving dry deposition and other reactions to account for the remainder of the difference. The morning rate of increase in O_x can be significantly different than that for O_3. In some cases, O_3 can increase at ~40 ppbv/hr while O_x remains constant, an indication that in these situations the observed increase in O_3 is due to a change in Ox partitioning.

Finally, significant differences were seen between O_3 measurements at the Moody Tower and some Houston area O_3 monitors during 2010 and 2011when values would be expected to be comparable, in particular the sites operated by the City of Houston. Under the same conditions other monitors operated by the TCEQ agreed well with the Moody Tower, even at greater than expected distances. The differences observed between the City of Houston sites and the Moody Tower appears to have improved when examining the measurements from 2012, possibly indicating that a change in operation method or calibration took place. Loss of O_3 in "dirty" sampling inlets is also another possibility, although City of Houston monitor sample inlets were changed on a 6-12 month cycle.

2.6 REFERENCES

Esteve, W., H. Budzinski, and E. Villenave (2006), Relative rate constants for the heterogeneous reactions of NO2 and OH radicals with polycyclic aromatic hydrocarbons adsorbed on carbonaceous particles. Part 2: PAHs adsorbed on diesel particulate exhaust SRM 1650a, *Atmospheric Environment*, *40*(2), 201-211, doi:10.1016/j.atmosenv.2005.07.053.

Haman, C. L., B. Lefer, and G. A. Morris (2012), Seasonal variability in the diurnal evolution of the boundary layer in a near-coastal urban environment, *Journal of Atmospheric and Oceanic Technology*, *29*(5), 697-710, doi:10.1175/jtech-d-11-00114.1.

Jenkin, M. E. (2004), Analysis of sources and partitioning of oxidant in the UK - Part 1: the NOX-dependence of annual mean concentrations of nitrogen dioxide and ozone, *Atmospheric Environment*, *38*(30), 5117-5129, doi:10.1016/j.atmosenv.2004.05.056.

Luke, W. T., P. Kelley, B. L. Lefer, J. Flynn, B. Rappengluck, M. Leuchner, J. E. Dibb, L. D. Ziemba, C. H. Anderson, and M. Buhr (2010), Measurements of primary trace gases and NO(y) composition in Houston, Texas, *Atmospheric Environment*, *44*(33), 4068-4080, doi:10.1016/j.atmosenv.2009.08.014.

Murphy, J. G., D. A. Day, P. A. Cleary, P. J. Wooldridge, D. B. Millet, A. H. Goldstein, and R. C. Cohen (2007), The weekend effect within and downwind of Sacramento - Part 1: Observations of ozone, nitrogen oxides, and VOC reactivity, *Atmospheric Chemistry and Physics*, *7*(20), 5327-5339.

Parrish, D. D. (2006), Critical evaluation of US on-road vehicle emission inventories, *Atmospheric Environment*, *40*(13), 2288-2300.

Pollack, I. B., B. M. Lerner, and T. B. Ryerson (2010), Evaluation of ultraviolet light-emitting diodes for detection of atmospheric NO2 by photolysis - chemiluminescence, *Journal of Atmospheric Chemistry*, *65*(2-3), 111-125, doi:10.1007/s10874-011-9184-3.

Sarwar, G., H. Simon, P. Bhave, and G. Yarwood (2012), Examining the impact of heterogeneous nitryl chloride production on air quality across the United States, *Atmospheric Chemistry and Physics*, *12*(14), 6455-6473, doi:10.5194/acp-12-6455-2012.

Sather, M. E., E. T. Slonecker, K. G. Kronmiller, D. D. Williams, H. Daughtrey, and J. Mathew (2006), Evaluation of short-term Ogawa passive, photolytic, and federal reference method sampling devices for nitrogen oxides in El Paso and Houston, Texas, *Journal of Environmental Monitoring*, *8*(5), 558-563, doi:10.1039/b601113f.

Shetter, R. E., et al. (2003), Photolysis frequency of NO2: Measurement and modeling during the International Photolysis Frequency Measurement and Modeling

Intercomparison (IPMMI), *Journal of Geophysical Research-Atmospheres*, *108*(D16), 15, doi:10.1029/2002jd002932.

Stutz, J., B. Alicke, R. Ackermann, A. Geyer, A. White, and E. Williams (2004), Vertical profiles of NO3, N2O5, O-3, and NOx in the nocturnal boundary layer: 1. Observations during the Texas Air Quality Study 2000, *Journal of Geophysical Research-Atmospheres*, *109*(D12), doi:10.1029/2003jd004209.

Williams, E. J., F. C. Fehsenfeld, B. T. Jobson, W. C. Kuster, P. D. Goldan, J. Stutz, and W. A. McCleanny (2006), Comparison of ultraviolet absorbance, chemiluminescence, and DOAS instruments for ambient ozone monitoring, *Environmental Science & Technology*, *40*(18), 5755-5762, doi:10.1021/es0523542.

Wong, K. W., H. J. Oh, B. L. Lefer, B. Rappenglueck, and J. Stutz (2011), Vertical profiles of nitrous acid in the nocturnal urban atmosphere of Houston, TX, *Atmospheric Chemistry and Physics*, *11*(8), 3595-3609.

Ziemba, L. D., J. E. Dibb, R. J. Griffin, C. H. Anderson, S. I. Whitlow, B. L. Lefer, B. Rappengluck, and J. Flynn (2010), Heterogeneous conversion of nitric acid to nitrous acid on the surface of primary organic aerosol in an urban atmosphere, *Atmospheric Environment*, *44*(33), 4081-4089, doi:10.1016/j.atmosenv.2008.12.024.

3. A COMPARISON OF O3 PRODUCTION IN HOUSTON AND LOS ANGELES

3.1 INTRODUCTION

Ozone has been linked to impairing lung function, particularly in sensitive groups such as asthmatics, children, and the elderly, and may lead to permanent damage to the lungs with repeated exposure. It is also a strong oxidizer that damages vegetation and crops. EPA estimates show that ozone may be responsible for approximately $500 million in crop damage annually (http://www.epa.gov/oar/oaqps/gooduphigh/bad.html).

The Houston-Galveston-Brazoria (HGB) region of southeast Texas has been designated by the EPA as a marginal non-attainment area of the 75 ppbv 2008 NAAQS for 8-hour ozone with a design value of 84 ppbv. Nearly 5.9 million people reside in the eight counties included in the HGB non-attainment area. In contrast, the Los Angeles-South Coast Air Basin in California is designated as being in extreme non-attainment of the 2008 8-hour ozone standard with a design value of 112 ppbv, the highest in the nation, affecting over 15.7 million people in the four county area (http://www.epa.gov/oaqps001/greenbk/hntc.html).

Tropospheric ozone forms by reactions of nitrogen oxides (NO_x), volatile organic carbon (VOC), and oxygen in the presence of solar radiation. Ozone photochemistry occurs when NO_2 is photolyzed in sunlight. Tropospheric ozone formation is the result of the following reactions:

$$NO_2 + h\nu \rightarrow NO + O(^3P) \qquad \text{(where } h\nu < 420 \text{ nm)} \qquad (3.1)$$

$$O(^3P) + O_2 + M \rightarrow O_3 + M \quad (3.2)$$

Once formed, ozone reacts with NO to regenerate NO_2.

$$O_3 + NO \rightarrow NO_2 + O_2 \quad (3.3)$$

Net ozone production is not possible unless a peroxy radical is present to react with NO to regenerate the NO_2 without destroying an ozone molecule as in reaction 3.

$$RO_2 + NO \rightarrow NO_2 + RO \text{ (where R can be: H, } CH_3, C_2H_5, \text{ etc.)} \quad (3.4)$$

This chapter will present the results of analysis on four intensive measurement projects in Houston, TX and Pasadena, CA. The TexAQS Radical Measurement Project (TRAMP) took place at the Moody Tower in August and September of 2006 as part of the TexAQS 2006 study. This was followed by the Study of Houston Atmospheric Radical Precursors (SHARP) in April and May of 2009 at the same location. In the late summer and fall (August – October) of 2010 a third measurement project was also focused on the Moody Tower (MT2010). The combination of these three campaigns provided data that are used to examine both the seasonal and temporal variability in ozone production in Houston. The fourth campaign examined here is the California Nexus – Research at the Nexus of Air Quality and Climate Change (CalNex) project in May and June 2010. Data from the CalNex ground site in Pasadena, CA allows for a comparison between Houston, with its heavy refining and petrochemical industry influence, to Los Angeles, an area with roughly three times the population of Houston but with fewer refinery and petrochemical emissions.

3.2 METHODS

The TRAMP, SHARP, and MT2010 campaigns took place on the roof of the North Moody Tower on the UH campus, approximately 4 km south of the tall buildings in downtown Houston and between 6-35 km west of the industrialized portion of the Houston ship channel (Figure 3-1), an area that contains a significant portion of the national refining and petrochemical capacity. The North Moody Tower is an 18-story dormitory with a balcony level approximately 60 meters above ground level with a 10 meter sample tower (samples taken from 70 m above ground level).

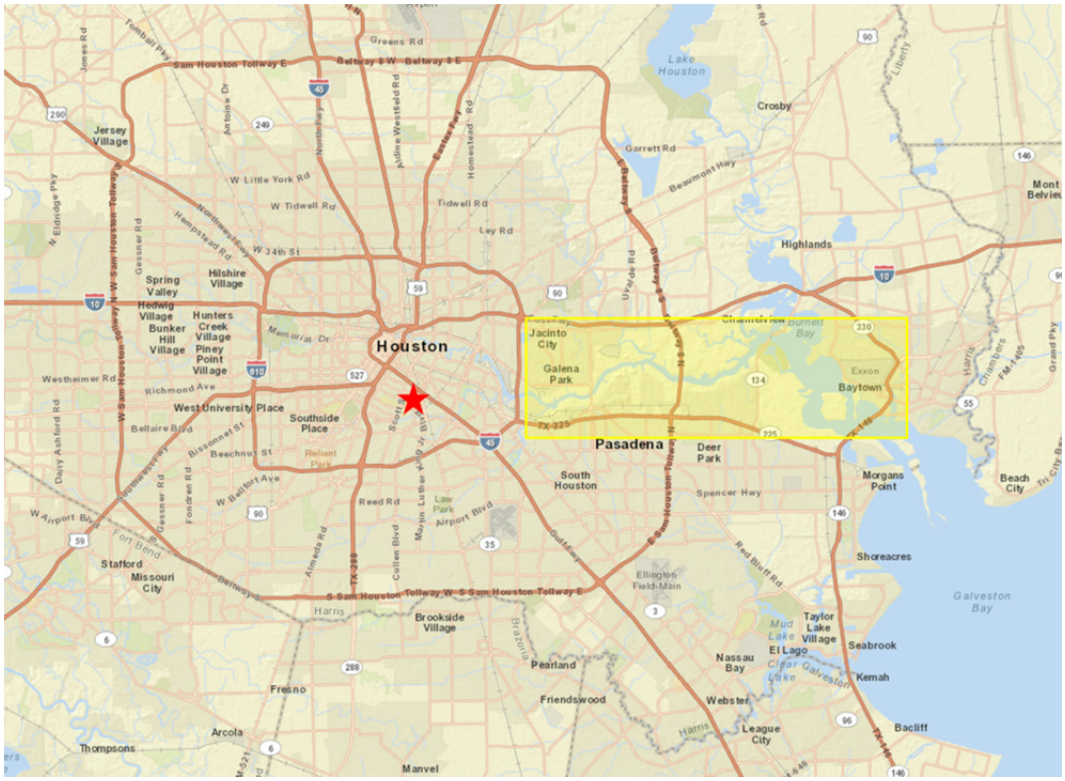

Figure 3-1. Map of the Houston area, the UH campus, indicated with a red star, is located approximately 4km south of downtown Houston. The industrialized portion of the Houston ship channel lies to the east of campus, indicated by the yellow shaded box. Map courtesy TCEQ.

The CalNex Pasadena temporary ground site was located in a parking lot on the northeast corner of the California Institute of Technology campus, approximately 16 km northeast of downtown Los Angeles and 6 km south of the base of the San Gabriel Mountains (Figure 3-2). Temporary office trailers were arranged around two 10 meter sample towers where most of the measurement sample inlets were located.

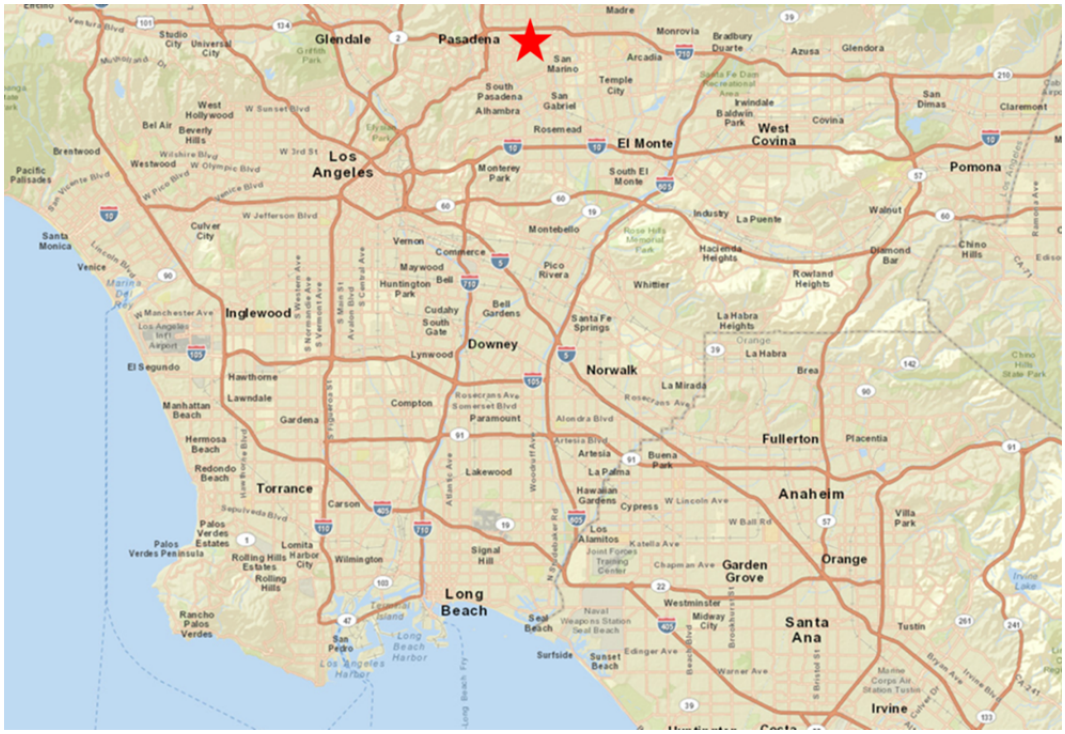

Figure 3-2. Map of the Los Angeles area. The red star indicates the location of the measurement site in Pasadena, CA, approximately 16 km northeast of downtown Los Angeles. Map courtesy TCEQ.

The data presented here are based on both field measurements and the use of a zero-dimensional photochemical box model. The model and measurement methods for each of the campaigns are described below.

3.2.1 Measurements

Trace gasses

Trace gasses were measured by a variety of techniques and groups during each of the four campaigns. Only those gasses used as a model constraint will be described here. Measurements of O_3 during all four campaigns were measured by the UH group using

UV-photometry (Williams et al., 2006). Carbon monoxide (CO) was also measured by the UH group by gas-filter correlation wheel during the three Houston projects (TEI 48i-TLE), and by NOAA using vacuum ultraviolet-fluorescence during the CalNex project (Holloway et al., 2000). Measurements of NO were made by chemiluminescence and NO_2 by chemiluminescence with a photolytic converter (BLC+Chemi) during the Houston projects by either UH or a UH/NOAA collaboration (Luke, et al, 2010). During the CalNex project UH measured NO by chemiluminescence and NOAA measured NO_2 by cavity ring-down spectroscopy (Fuchs et al., 2009). HONO was measured by several techniques including long path differential optical absorption spectroscopy (LP-DOAS) by UCLA in TRAMP and SHARP (Wong et al., 2012), long path absorption photometer (LOPAP) by UH during MT2010 (Heland et al., 2001), and by incoherent broadband cavity enhanced absorption spectrometry by NOAA during CalNex (Washenfelder et al., 2008). Peroxyacetyl nitrate (PAN) was measured by gas chromatograph with electron capture detector (GC-ECD) in Houston by UH (Volz-Thomas, Xueref, & Schmitt, 2002) and thermal desorption chemical ionization mass spectrometer (TD-CIMS) by the University of Calgary during CalNex (Mielke & Osthoff, 2012). Formaldehyde measurements used in this work were made by the UCLA LP-DOAS (TRAMP & SHARP) or by UH using Hanzch reaction (MT2010 & CalNex) (Dasgupta et al., 2005). VOCs were measured by UH during TRAMP and MT2010 by gas chromatograph with flame ionization detector (GC-FID) (Leuchner & Rappenglueck, 2010) and UH and Washington State University during SHARP (GC-FID and proton transfer reaction mass spectrometry (PTR-MS), respectively) (Karl et al., 2003). NOAA measured VOCs during CalNex via gas chromatograph with mass spectrometer (GC-MS) and proton-

transfer ion-trap mass spectrometer (PIT-MS) (Pollack et al., 2012; de Gouw & Warneke, 2007).

Photolysis rates

A 2π steradian zenith viewing scanning actinic flux spectroradiometer (SAFS) (Lefer et al., 2003) was used to measure downwelling actinic flux during each of the four campaigns. The system is comprised of a collection optic mounted on an elevated point near the trace gas inlets with an artificial horizon, fiber optic cable, scanning double monochrometer, PMT, and a data and control system. This system was configured and optimized to measure the light intensity between 280 and 420 or 560 nm, which covered the range of interest for the photolysis frequencies of many compounds including NO_2 and ozone. Wavelength and spectral calibrations were typically performed weekly to correct for shifts in the monochrometer and to track performance of the PMT.

Measured actinic fluxes from the SAFS instrument were coupled with the latest JPL and IUPAC recommended absorption cross sections and quantum yields for the photolysis of NO_2 to calculate the photolysis rate for NO_2 used in the model.

3.2.2 LARC Model

Details on the NASA Langley Research Center (LaRC) time dependent box model can be found in Olson et al. (2006) and Crawford et al. (1999). In general, chemical reactions and kinetics are those recommended by Sander et al. (2006). Non-methane hydrocarbon chemistry is based on the modified condensed scheme in Lurmann

et al. (1986). For this study, the model is run in a time-dependent mode using an assumption of diurnal steady state. The time-dependent mode is useful when observations of moderately-lived HO_x precursor species are missing that cannot be adequately represented by photostationary steady state. A comparison of several model mechanisms, including the LaRC mechanism used here, can be found in Chen, et al. (2010). Overall the LaRC mechanism compared quite well to CB05, RACM, SAPRC-99, SAPRC-07, and MCMv3.1 for HO_2, OH, and O_3 production in Houston. In addition to the standard model chemical constraints of measurements of O_3, CO, NO_x, acetone, methanol, ethanol, formic and acetic acids, and non-methane hydrocarbons, the model is also constrained by measurements of PAN, HCHO, and HONO. Previous work shows that constraining to measurements of H_2O_2 and HNO_3 have little impact on the calculated ozone production rates (Flynn et al., 2010). Input data was averaged or interpolated to 10-minute intervals and removed records that were missing one or more of the constraints mentioned above, as well as limited the data to periods with valid jNO_2 measurements and solar zenith angles $\leq 90^{o}$. Like other zero-dimensional models, the LaRC model does not include advection in the model, but it is considered during the analysis of the results.

The LaRC model produces two output files, one containing the reaction rates for each of the 251 reactions in the model, and another file with modeled gas concentrations. In addition, the second file includes calculated O_3 formation (FO_3), destruction (DO_3), and net production (PO_3), as well as the component rates used to calculate FO_3 and DO_3.

3.3 RESULTS

3.3.1 Campaign results

Table 3-1 below shows the overall start and stop dates, number of days sampled, and the number of hours for which sufficient data was available to run the LaRC model. Additional information regarding the conditions for these projects can be found in Lefer and Rappenglueck (2010), Ren et al., (2013), and Ryerson et al. (2013), for the TRAMP, SHARP, and CalNex campaigns, respectively. For the remainder of this chapter, comparisons figures for the campaigns will be presented with TRAMP in the upper left, SHARP in the upper right, MT2010 in the lower left, and CalNex in the lower right panel. All times are local standard time.

Project	Start Date	Stop Date	Number of days	Number of modeled hours
TRAMP	8/13/2006	10/2/2006	50	512
SHARP	4/15/2009	5/31/2009	46	148
CalNex	5/13/2010	6/16/2010	34	189
MT2010	8/14/2010	10/18/2010	65	350

Table 3-1. Table of campaigns analyzed for the work presented here.

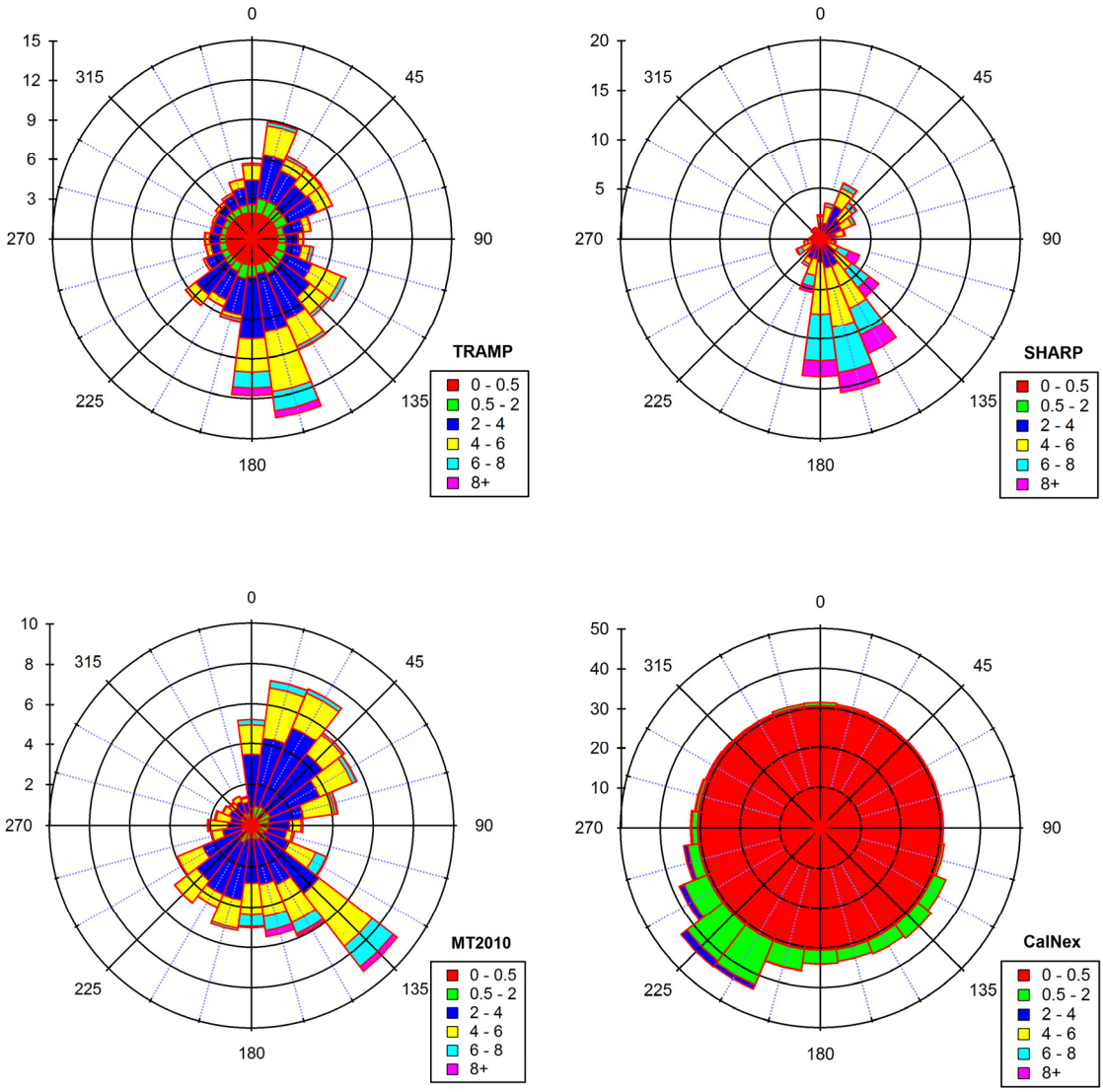

Figure 3-3. Wind roses for TRAMP, SHARP, MT2010, and CalNex. CalNex experienced calm wind conditions approximately 30% of the time.

Wind roses with 15º bins are presented for all four campaigns in Figure 3-3. In Houston, both TRAMP and SHARP were dominated by southerly winds with a secondary mode characterized by northeasterly winds. SHARP also had a greater frequency of higher wind speeds. Winds during MT2010 were divided more evenly between southerly and northeasterly than the other two Houston projects, but the wind speeds were comparable to TRAMP. In all three studies, winds from the northwest were infrequent. In

comparison, CalNex experienced calm winds for ~30% of the campaign. Light southwesterly winds dominated the remainder of the project. Northerly winds were rare during CalNex.

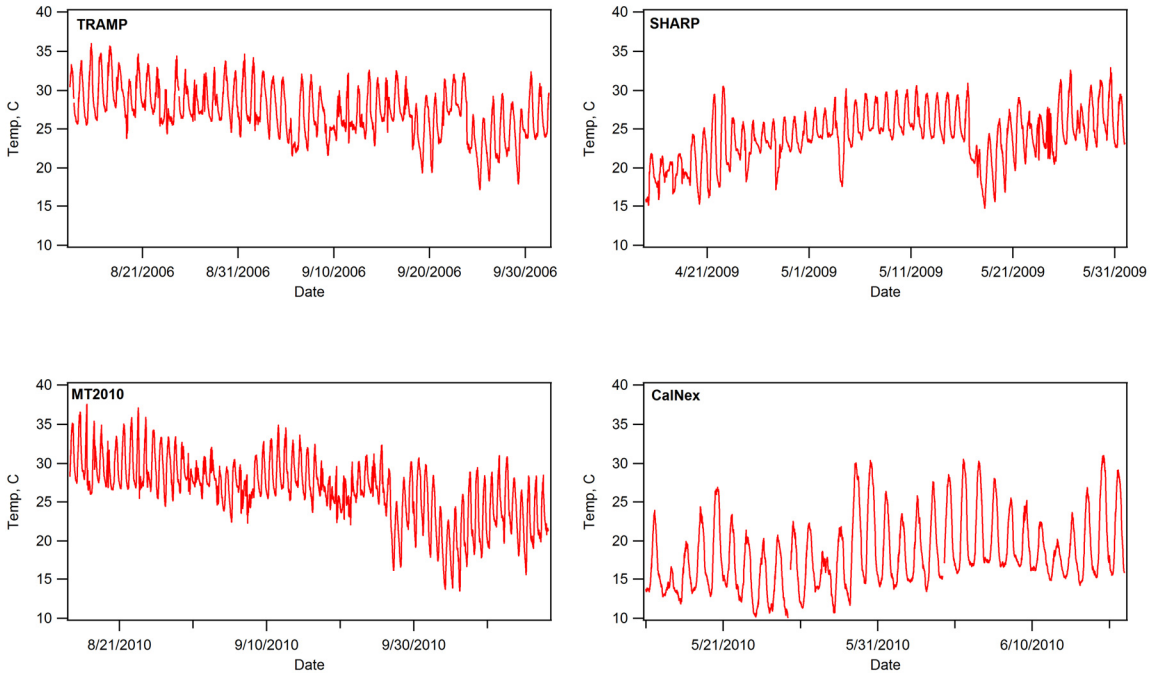

Figure 3-4. Time series of ambient temperature during TRAMP (late summer), SHARP (spring), MT2010 (late summer), and CalNex (late spring).

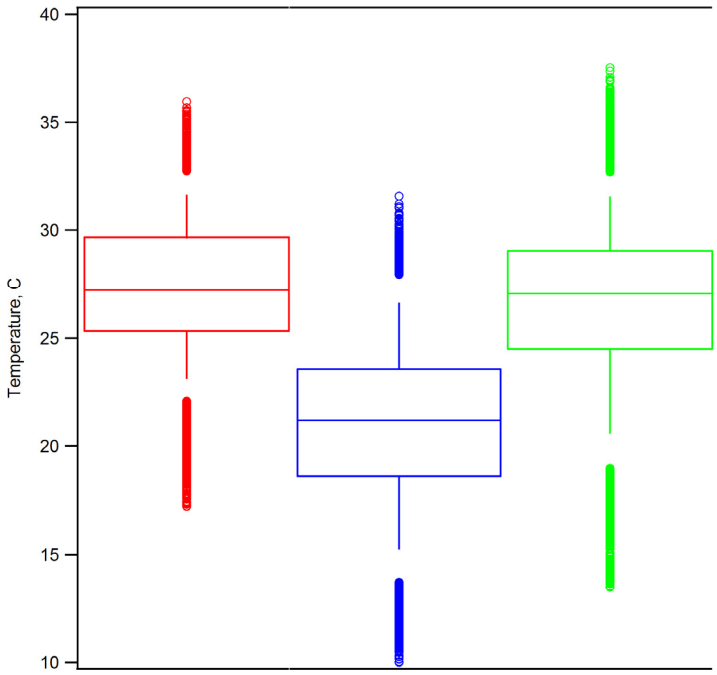

Figure 3-5. Box and whiskers plot for ambient temperature during TRAMP (red), SHARP (blue), and MT2010 (green).

Temperatures were relatively warm during the two late summer campaigns at the Moody Tower (Figure 3-4 and Figure 3-5), while the spring campaign tended to be ~5ºC cooler. The summer 2010 CalNex project was the coolest of all the campaigns, with nighttime lows approaching 10ºC. The ambient temperature time series of the three Houston projects clearly shows multiple cold frontal system passages occurred during each campaign. None of the campaigns saw particularly unusual temperatures for the time of year and location.

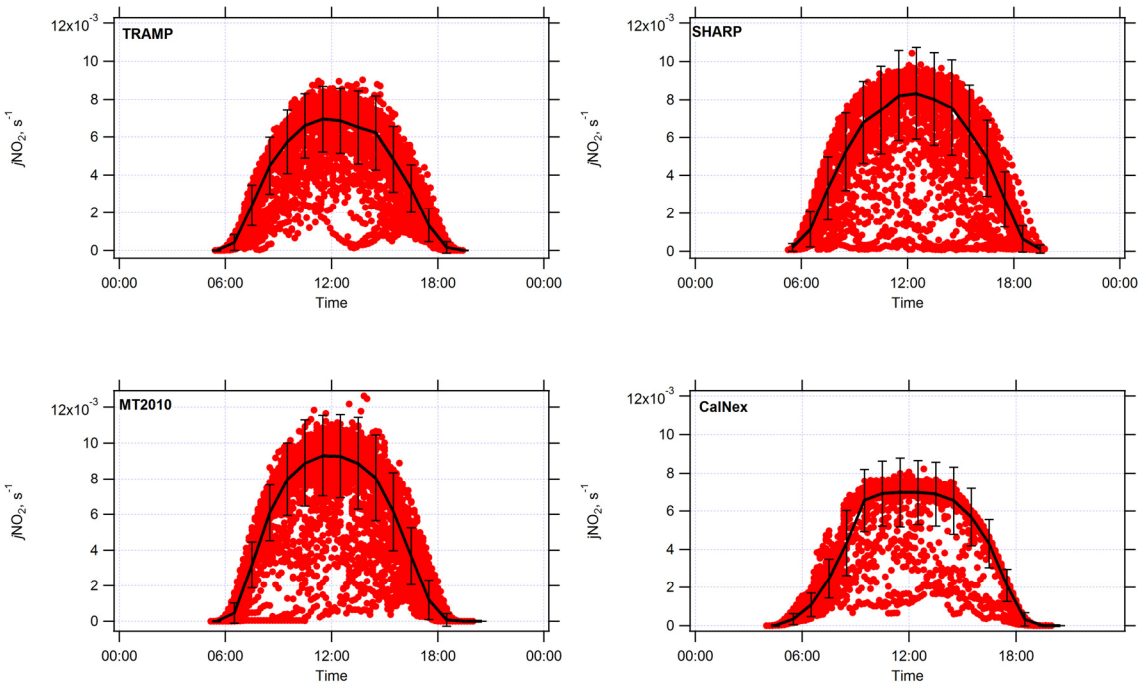

Figure 3-6. Median diurnal profile of jNO_2 ± 1 standard deviation. Individual data points are shown as dots.

Since photochemistry is always photon-limited (Lefer et al., 2003), it is important to consider sky conditions when comparing ozone production from different projects. The median diurnal profiles presented in Figure 3-6 show that CalNex had very few cloudy days, although tall nearby trees taller than the measurement tower to the east of the measurement site cast a shadow on the measurement tower for several hours each morning (Figure 3-7) resulting in the concave shape in the morning profile. Both SHARP and MT2010 had cloudier conditions with several days of heavy overcast conditions. It should be noted that there are significantly more days in the MT2010 project than any other campaign (Table 3-1).

Figure 3-7. Photo of CalNex ground site with trees to the east. The 10m scaffold tower in the center of the trailers was not built at the time the photo was taken.

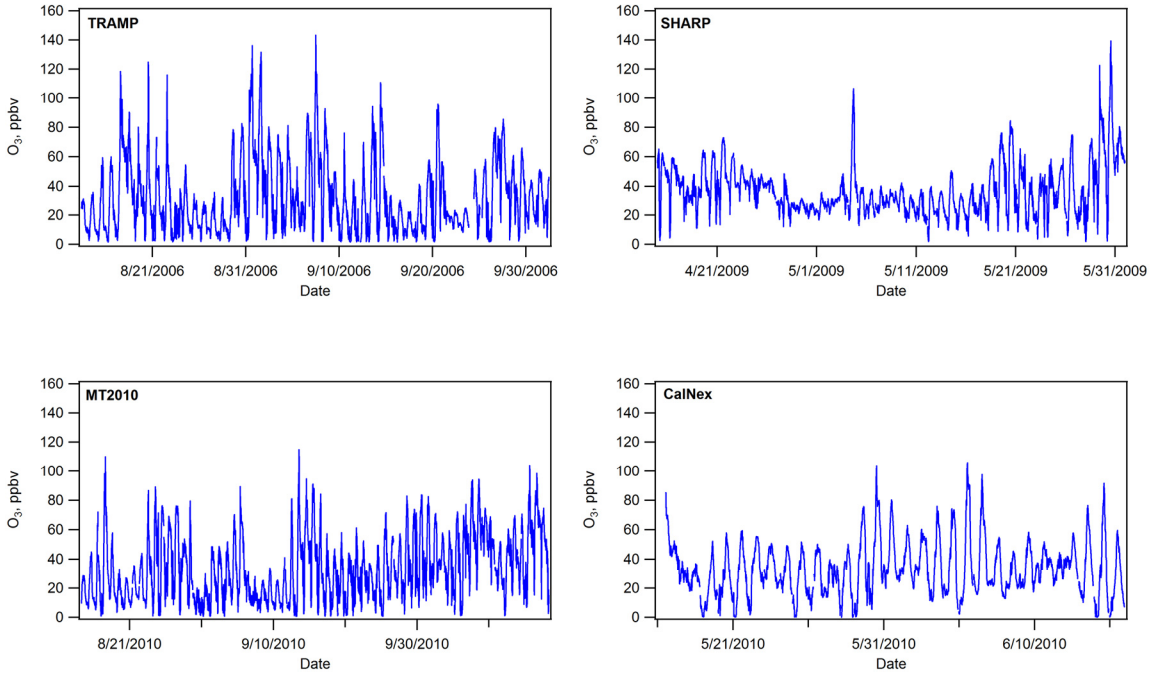

Figure 3-8. Time series of ozone measured at the Moody Tower during the four campaigns.

Figure 3-8 shows the time series of the 10-minute averaged O_3 for each of the campaigns examined in this chapter. Of the four, TRAMP had the highest O_3 with several days exceeding 100 ppbv and a peak value in excess of 140 ppbv. MT2010 experienced several periods of elevated O_3 levels, however only a few days exceeded 100 ppbv.

Unlike the SHARP project, nighttime O_3 was often titrated to near zero in both TRAMP and MT2010. Overall the SHARP measurement period was dominated by relatively clean conditions and higher wind speeds (Figure 3-8 and Figure 3-3) during the first $^2/_3$ of the project but had a period of increasing O_3 in the final days. Ozone levels measured during the CalNex campaign had the lowest peak O_3 value of the four studies, with only two days that exceeded 100 ppbv.

3.4 DISCUSSION

In order to better compare the results from the measurements and model calculations for these four campaigns the data was divided into two modes. The first consists of days with peak eight-hour average O_3 greater than 70 ppbv and the second consists of days with peak eight-hour O_3 less than 50 ppbv, and will be referred to as high and low O_3 days, respectively. Table 2-1 shows the number of high and low O_3 days for each of the four campaigns examined here. The division into days greater than 70 and less than 50 ppbv was selected so as to separate the more photochemically active days from the less active days, and to attempt to have roughly equal number of points in each mode in a project. It should be noted however, that although the balance of high and low days across the projects are roughly equal, with the exception of the SHARP campaign which had many more low O_3 days, the number of days that were able to be modeled was impacted by the availability of data required to constrain the model. Because some projects experienced more instrument difficulties than others, the number of hours that were successfully modeled was quite variable as summarized in Table 3-1 and are apparent in the following figures.

	TRAMP 2006	SHARP 2009	MT2010	CalNex 2010
High days	12	5	12	3
Low days	28	29	32	16

Table 3-2. Number of days of high and low O_3 days for the four campaigns.

3.4.1 Diurnal profiles of O_3 rates

As mentioned previously, one of the model output files includes calculated rates of instantaneous O_3 formation (FO_3), destruction (DO_3), and net production ($PO_3 = FO_3 - DO_3$), as well as the component rates that are summed to create the formation and destruction terms. Median diurnal profiles of these rates were calculated for high and low ozone days and are presented below.

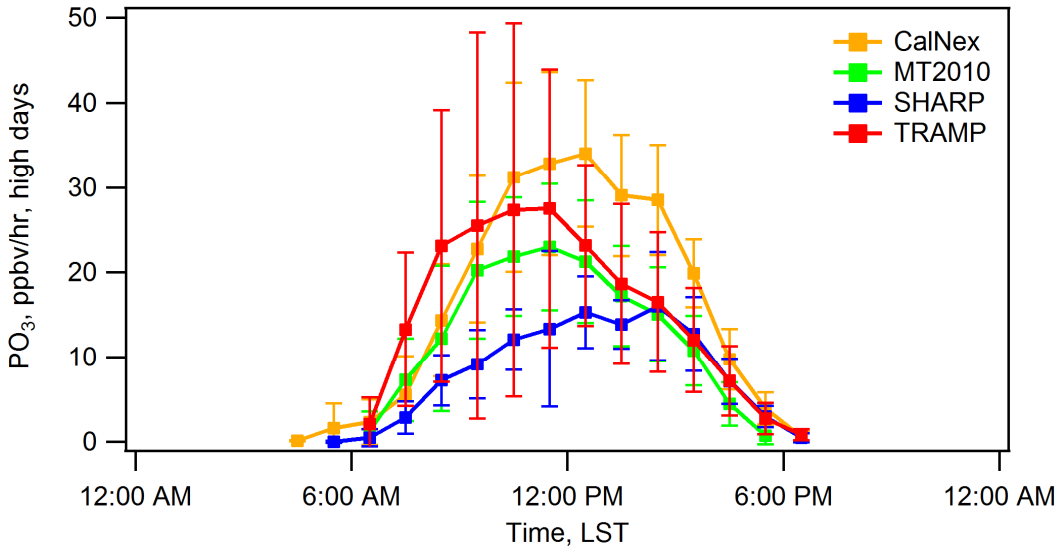

Figure 3-9. PO_3 Diurnal profile, high days.

Both fall campaigns in Houston saw the peak in PO_3 before noon on high O_3 days (Figure 3-9), while the spring Houston project peaks mid-afternoon. In the spring, wind speeds began to increase at sunrise, increasing the rate of boundary layer growth which suppressed PO_3 in the mornings by rapidly diluting O_3 precursors. CalNex summer PO_3 exhibits a more typical pattern peaking around solar noon. The highest median PO_3 values on high O_3 days were found during the CalNex campaign; however, TRAMP had many more high O_3 days, including three days, August 31, September 7, and September 14, with peak PO_3 values between 70 and 120 ppbv/hr. Of the four projects, SHARP had the lowest median PO_3 rate on high O_3 days. It should be noted that there are only three high days in the CalNex profile. When considering the overall campaign averages, TRAMP had the highest PO_3 rates of the four campaigns.

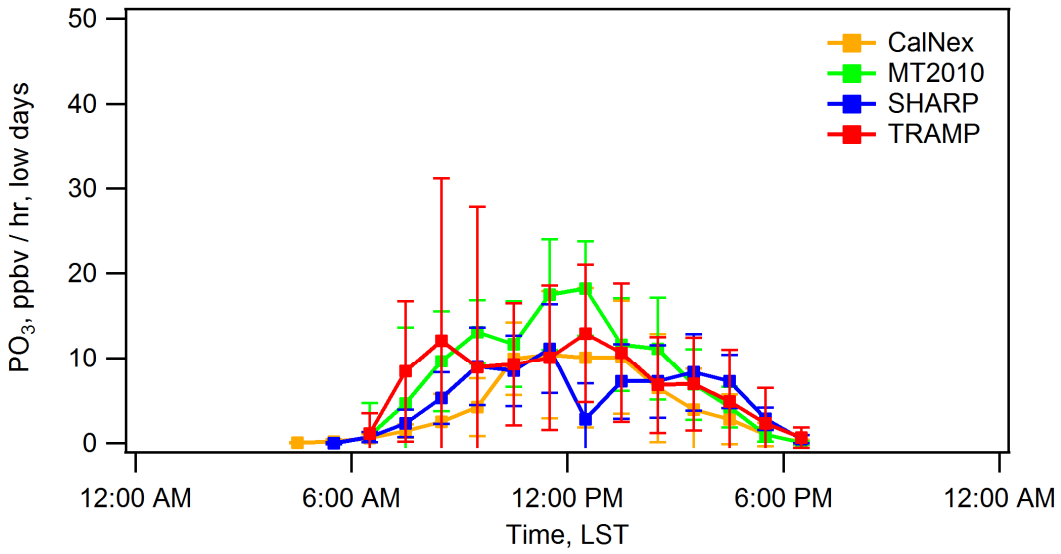

Figure 3-10. PO_3 Diurnal profile, low days.

Figure 3-10 shows that during the TRAMP campaign days it was possible to have very high PO_3, up to 100 ppbv/hr, in the mornings, even on low O_3 days. Unlike the high O_3 days, the median diurnal profile of PO_3 for low days tends to follow jNO_2 for all

campaigns. SHARP does show an unusual dip in the profile around noon that seems to be driven by a couple of overcast days. If there were more points available to model for SHARP, the profile would likely be smoother more like the other three projects. Interestingly, there is only a few ppbv/hr difference between the high and low O_3 days for the MT2010 project.

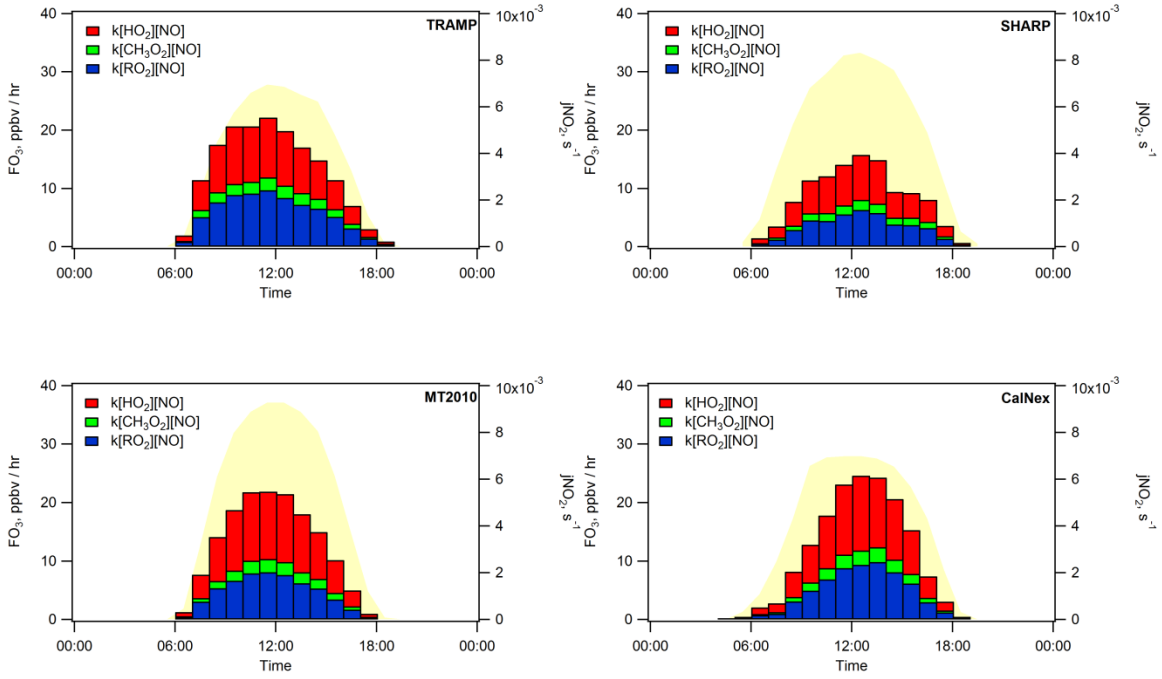

Figure 3-11. Diurnal FO_3 and relative contribution from individual formation rates for all days.

Like the high O_3 day PO_3 profiles, an examination of the TRAMP and MT2010 FO_3 rates and components in Figure 3-11 shows that FO_3 peaks just before noon and with similar values. CalNex reaches slightly greater values and is highest around and just after solar noon. Like CalNex, FO_3 during SHARP peaks around noon. Ozone formation by HO_2 + NO accounts for roughly 50% of the overall FO_3 rates, regardless of time of day or project.

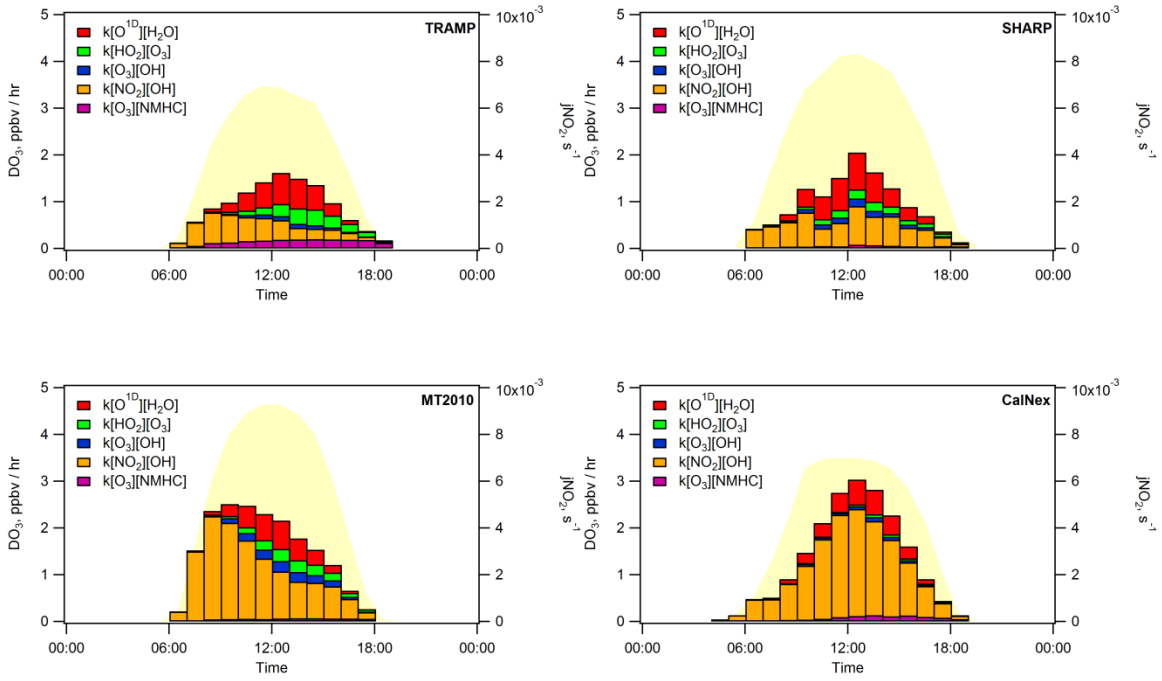

Figure 3-12. Diurnal DO_3 and relative contribution from individual destruction rates for all days.

Unlike the O_3 formation rates in Figure 3-11, the destruction rates shown in Figure 3-12 illustrate that while the DO_3 rates are considerably lower than FO_3, the relative contribution of the individual rate components are more variable. For TRAMP, DO_3 is the lowest of all campaigns and is dominated by HNO_3 formation (NO_2 + OH) in the mornings while losses due to O_3 reactions become more important in the afternoon, potentially indicating excess NO_x in the mornings. The increase in HO_2 + O_3 and O_3 + NMHC losses in the afternoon is greater than losses to HNO_3 formation which may indicate that NO_x is no longer in excess. Destruction rates for SHARP show a much flatter profile with losses to HNO_3 more constant through the day. Reactions of O^1D + H_2O contribute most to the profile shape. CalNex DO_3 was dominated by HNO_3

production during all times, with only O^1D+H_2O playing any significant role. Losses during MT2010 are also dominated by HNO_3 formation and the other DO_3 components are much less important than in TRAMP, even in the afternoon. Reactions of O_3+NMHC during MT2010 are negligible, consistent with a reduction in reactive NMHCs since the TRAMP project.

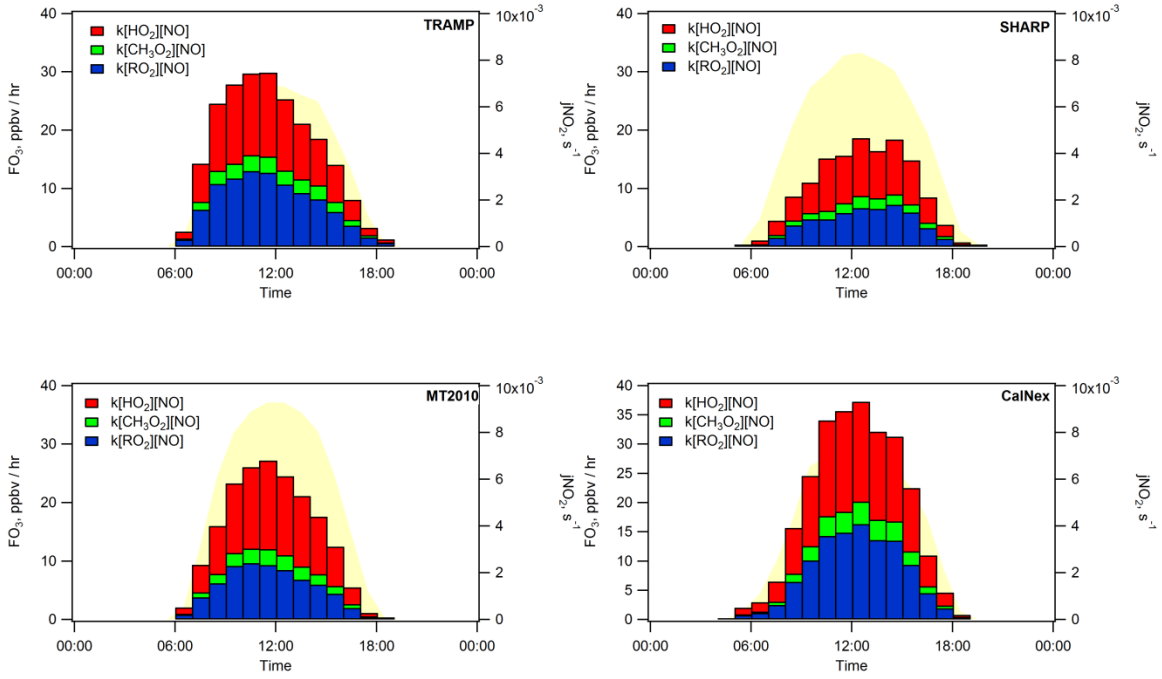

Figure 3-13. Diurnal FO_3 and relative contribution from individual formation rates for high O_3 days.

Separating the data by days with high O_3 finds that of all of the campaigns, CalNex had the highest median rate, greater than 35 ppbv/hr, peaking around noon (Figure 3-13). Both TRAMP and MT2010 had similar peak FO_3 values and shapes peaking before noon, however the relative contribution of HO_2 + NO was greater in MT2010 than in TRAMP. Although the median FO_3 rates were similar between these two projects, MT2010 lacked the extremely high PO_3 rates seen in TRAMP (Figure 3-9). Figure 3-14 shows the DO_3

rates for days with high O_3. The profiles and relative importance of the individual rates are quite similar to the values for all days, but with greater magnitudes. The one notable difference is that the mornings of high O_3 days in SHARP have a significant peak in NO_2 + OH in the 9:00-10:00 hour.

Kleinman et al. (2005) compared PO_3 calculated from in Houston to four other cities and found PO_3 rates of 49 ppbv/hr for the highest 10% of data based on PO_3 Houston during TexAQS 2000. The next highest city examined, Philadelphia, had PO_3 values with a maximum of 25 ppbv/hr. In Houston, clouds and aerosols were found to reduce PO_3 by 17% on average based on measurements from TRAMP (Flynn et al., 2010). In Los Angeles, Griffin et al. (2004) report that peak surface level PO_3 ranged between 33.8 and 47 ppbv/hr and occurred between 11:00 AM-3:00 PM. Their work also points out that the 49 ppbv/hr peak PO_3 found in Kleinman occurred in the ship channel area and that a value closer to 40 ppbv/hr is more representative of the overall Houston metro area. These reported values for Houston and Los Angeles are quite similar to those found in this work.

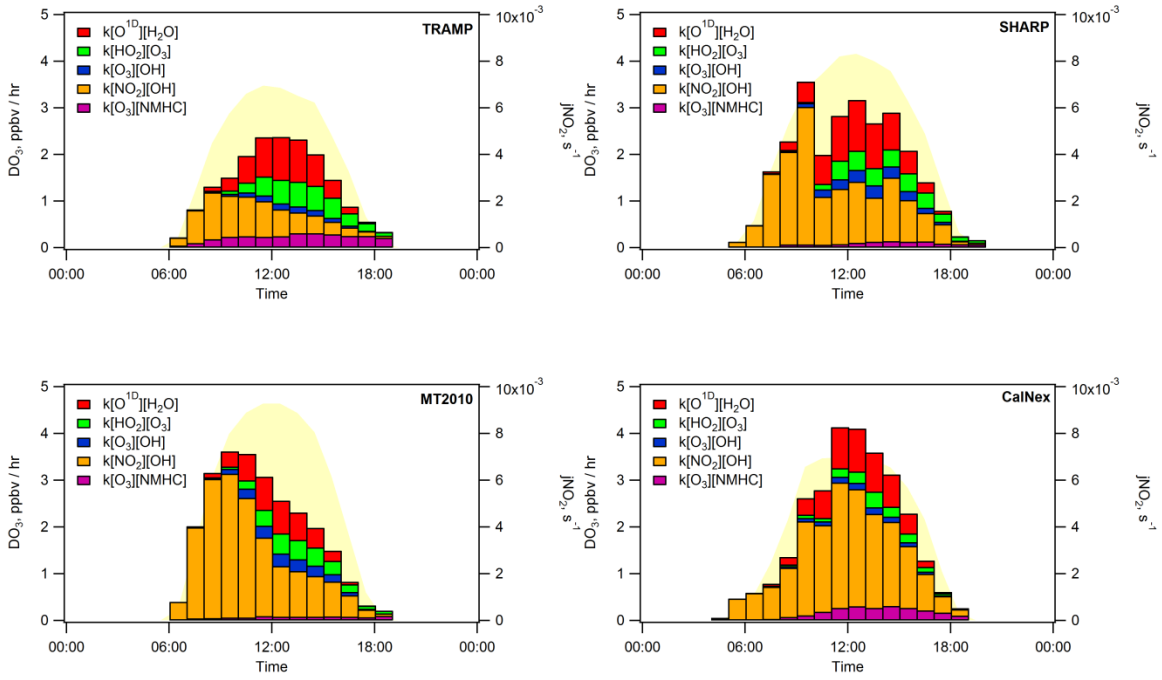

Figure 3-14. Diurnal DO_3 and relative contribution from individual destruction rates for high O_3 days.

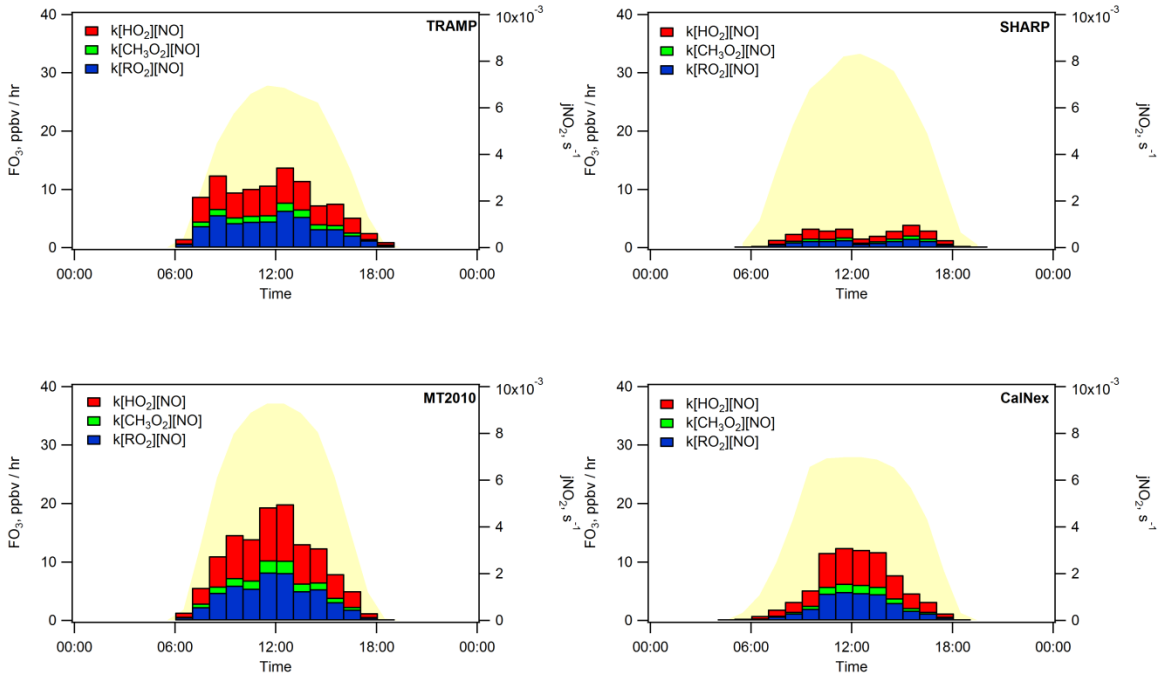

Figure 3-15. Diurnal FO_3 and relative contribution from individual formation rates for low O_3 days.

With the exception of SHARP, O_3 formation rates on low O_3 days can still approach or exceed 15 ppbv/hr in both Houston and Los Angeles (Figure 3-15). Peak rates for SHARP on low O_3 days did not exceed 5 ppbv/hr, a factor of 3-4 lower than on high O_3 days. The FO_3 rates for CalNex were also reduced by a similar factor. DO_3 values shown in Figure 3-16 are also significantly reduced, although while the relative importance contribution of the FO_3 rates are generally consistent between high and low days, the contribution of the individual DO_3 rates to the overall destruction are more variable. Destruction rates on low O_3 days during TRAMP were primarily due to O^1D+H_2O; losses due to either HNO_3 formation or O_3+NMHC reactions were minimal. CalNex losses are almost entirely due to HNO_3 formation and follows the typical photochemical profile such that the loss rate is likely being driven by the availability of OH.

The reduction in importance of O_3+NMHC reactions on high O_3 days in Houston together with the increase in relative importance of NO_2+OH is one indication that VOC emissions have declined and that NOx-saturated conditions are more common, especially in the mornings. Mao et al. (2010) found that during TRAMP, Houston was NO_x-sensitive for most of the day. Ren et al. (2013) found that on high O_3 days during SHARP, Houston was NO_x saturated until midday but became NO_x-sensitive around 9:00 AM on low O_3 days. Both of these findings are consistent with what is shown here.

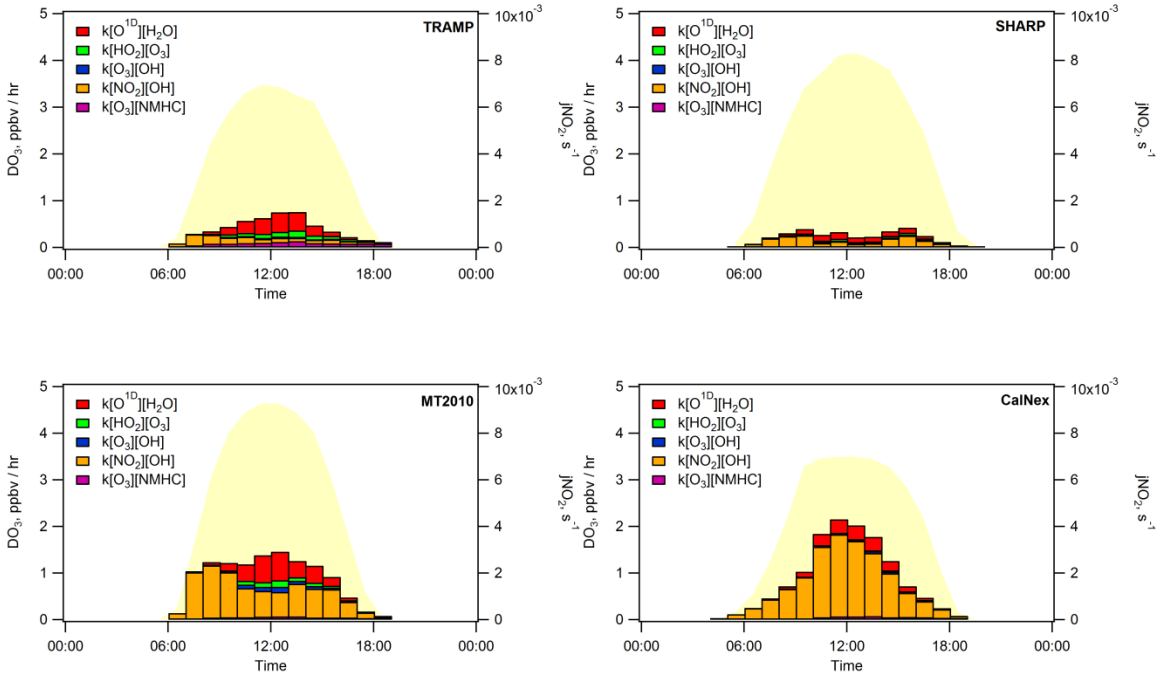

Figure 3-16. Diurnal DO_3 and relative contribution from individual destruction rates for low O_3 days.

3.4.2 PO_3 VS. NO

Figure 3-17 and Figure 3-18 show the sensitivity of PO_3 to NO levels for high and low O_3 days, respectively. These figures can give an indication of the NO_x-sensitivity of

PO_3 during each of these campaigns. For points to the right of the peak, PO_3 is reduced as NO increases, indicating that a NO_x saturated condition exists. NO_x-sensitive conditions exist for points to the left of the peak as PO_3 increases with increasing NO. On high O_3 days for all four of the projects it is more common to have a NO_x-saturated condition in the mornings, possibly from morning rush hour emissions, and transition to a NO_x-sensitive condition later in the day. A deeper boundary layer provides a larger volume which to dilute the evening rush hour resulting in lower NO_x mixing ratios. Low O_3 days show a similar trend; however, it is more common to find a NO_x-sensitive condition in the mornings.

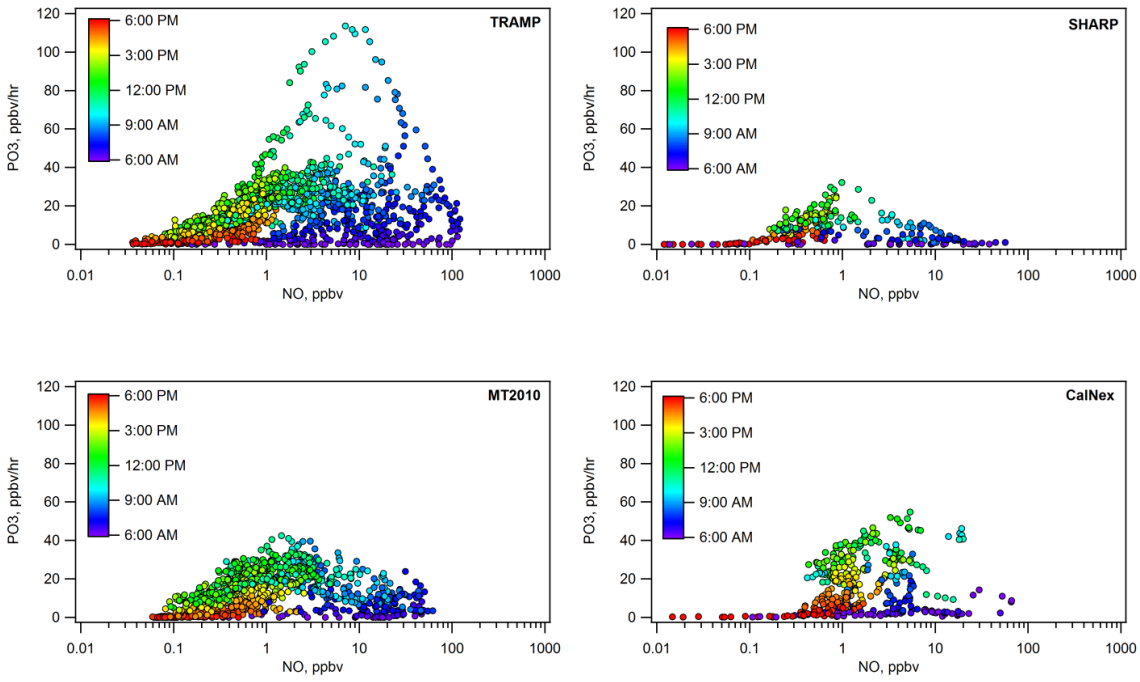

Figure 3-17. PO_3 vs. NO, high O_3 days.

Although the overall shape and diurnal trend is similar for each of the projects, the NO level for peak PO_3 varies for each project. The peak in PO_3 where the transition from

NO_x-sensitive to NO_x-saturated occurs during the TRAMP campaign is ~5 ppbv for most days, however a few days saw the transition point as high as 8-10 ppbv. Both SHARP and MT2010 peaks in PO_3 occur at lower NO levels, generally 1-2 ppbv. This shift towards lower NO levels would indicate that VOC levels at the Moody Tower may have declined over time and the transition to a NO_x-saturated condition occurs at lower NO levels (Murphy et al., 2007).

Work by Carzola et al. (2012) compared measurements of PO_3 using the measurement of O_3 production sensor (MOPS) to calculated and modeled PO_3 during SHARP. In that study the RACM2 modeled PO_3 was lower than both the modeled and calculated values. Given that the LaRC modeled PO_3 was similar to the other models tested in Chen et al. (2010), it is likely that the MOPS and calculated PO_3 would also be greater than the LaRC results presented here.

This NO_x saturated condition is supported by the increase in HNO_3 formation seen in the DO_3 rates discussed in Section 3.4.1. Peak PO_3 on high O_3 days during CalNex occurred around 4-7 ppbv of NO, similar to TRAMP; however, there were fewer points in the NO_x saturated region in the mornings. In large part this is indicative of the transport time required for the Los Angeles urban plume to transport the morning rush hour emissions to the Pasadena measurement site, in contrast with the Moody Tower, which is located much closer to major emission sources. With the exception of two days which have very high PO_3, the NO_x-sensitivity transition point for Houston on low O_3 days falls in the 3-4 ppbv NO range for TRAMP and MT2010, but is closer to 1 ppbv NO for SHARP (Figure 3-18). During CalNex campaign has a well-defined PO_3 profile for low O_3 days with a

peak around 8-10 ppbv NO, significantly higher than the three Houston campaigns presented here.

As with the change in relative importance of O_3+NMHC and NO_2+OH reactions in Section 2.4.1, the changes in the transition between NO_x-sensitive and NO_x-saturated conditions indicates reductions in emissions of VOCs in Houston.

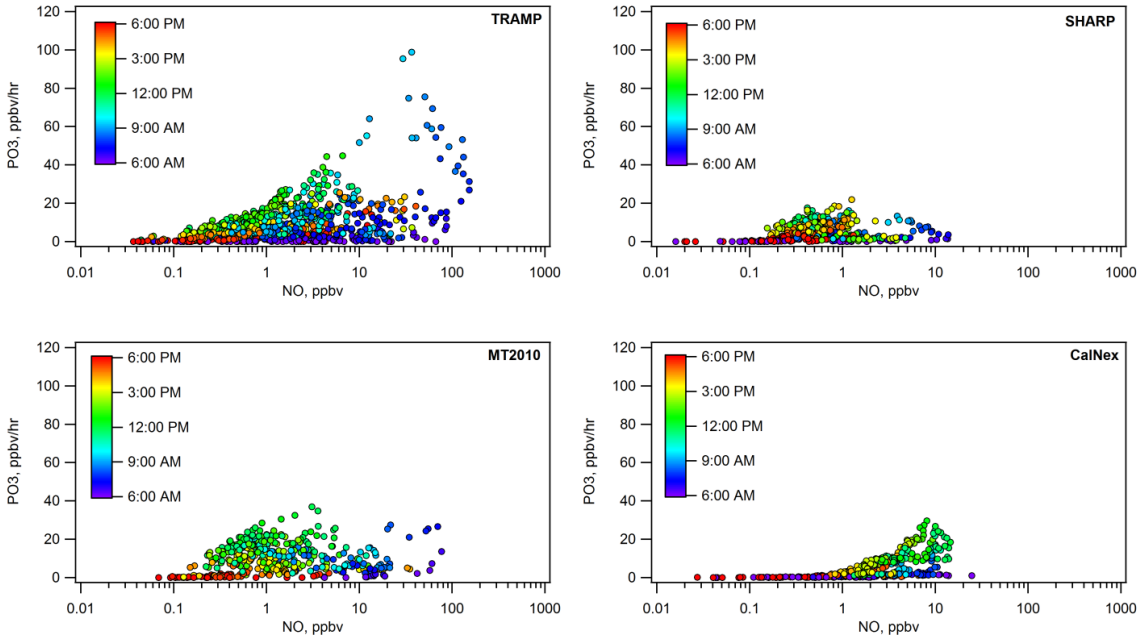

Figure 3-18. PO_3 vs. NO, low O_3 days.

3.4.3 Ozone production efficiency in Houston

NO_z is generally taken to be NO_x consumed during the O_3 production process. The ratio of O_3 to NO_z then is the efficiency of O_3 production per NO_x consumed, known as O_3 production efficiency (OPE) (Griffin et al., 2004). To account for localized titration of O_3 to NO_2, the term O_x is used ($O_x = O_3 + NO_2$) instead of O_3. Figure 3-19

shows O_x vs. NO_z for afternoons on high O_3 days during each of the three Houston campaigns. Both fall campaigns show similar OPEs for the high days while SHARP is higher. The SHARP results may be affected by having a relatively few number of points in that data set compared to the other two campaigns. SHARP only had 5 days with high O_3 and had the poorest coverage of modeled data. It is possible that with additional data points the SHARP OPE may be closer to the other campaigns. It may also be the case that with the increased dilution during SHARP that the VOC/NO_x ratio is more conducive to a higher OPE (Daum, et al., 2003). However, all of these rates are consistent with previous findings of OPE in the Houston urban plume (Griffin et al., 2004, Daum et al., 2003) and lower than those found in petrochemical plumes by Ryerson, et al. (2003).

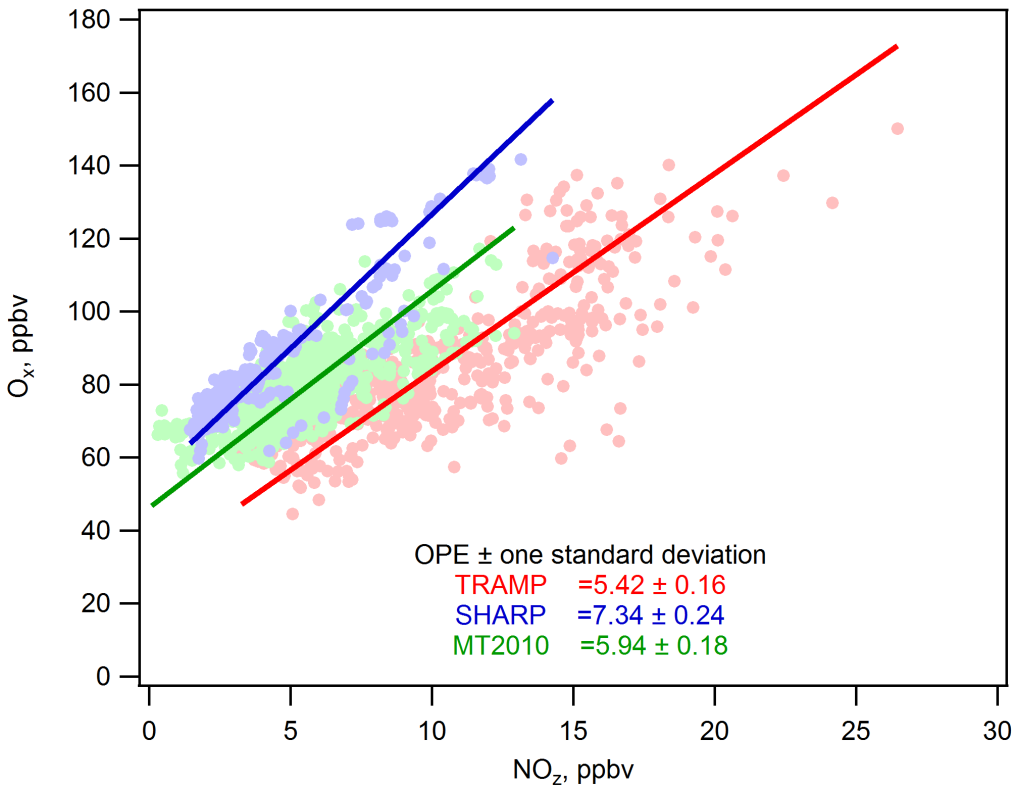

Figure 3-19. O_3 production efficiency for the three Houston campaigns.

3.4.4 VOC reactivity

Reactivity is used as a measure of the total reactivity of VOCs with OH present in the atmosphere. The reactivity presented here is based on the output rate constants from the LaRC model and the concentrations of the VOCs included in the LaRC model input file. The total reactivity was calculated as described in Steiner et al. (2008), where:

$$\text{Reactivity} = R_{ethene+OH}[\text{ethene}] + R_{isoprene+OH}[\text{isoprene}] + R_{alkenes+OH}[\text{alkenes}] + R_{ethane+OH}[\text{ethane}] + R_{propane+OH}[\text{propane}] + R_{alkanes+OH}[\text{alkanes}] + R_{benzene+OH}[\text{benzene}] + R_{aromatics+OH}[\text{aromatics}] + R_{acetone+OH}[\text{acetone}] + R_{formaldehyde+OH}[\text{formaldehyde}] \quad (3.5)$$

Plotting the calculated reactivity by NO_2 is another approach to determining whether a region is NO_x-sensitive or NO_x-saturated. Figure 3-20 shows that the reactivities calculated for each of the campaign are significantly different. Very high calculated reactivities were found for TRAMP, occasionally exceeding 35 s^{-1}, but were not seen in any of the other campaigns. Although high PO_3 primarily occurred at high reactivities during TRAMP it was still possible to find PO_3 values exceeding 40 ppbv/hr at reactivities as low as 10 s^{-1}. Likewise, some reactivities between 30-35 s^{-1} resulted in only moderate PO_3 rates. Compared to TRAMP, the MT2010 campaign saw similar results for reactivities below 10-12 s^{-1}, however there were very few points in this range and none above 14 s^{-1}, a clear indication that the VOC regime was significantly different. Likewise, the SHARP campaign saw extremely low reactivities, never exceeding 5 s^{-1}. These low reactivities coincided with the lowest PO_3 rates out of all four campaigns for all conditions. In Houston, reductions in VOC reactivity would be the most likely

approach to routinely reduce PO_3 rates since it appears that the effects of NO_x reductions may or may not help reduce PO_3.

CalNex results are more similar to the modeling presented by Geddes et al. (2009) where PO_3 isopleths were plotted with reactivity vs. NO_2 for the Toronto area. The resulting figure shows how changes in reactivity and NO_x can affect PO_3. Unlike the Houston projects, the CalNex PO_3 changes in a more predictable fashion with increases in reactivity and NO_2. The majority of points occur with PO_3 of ~20 ppbv/hr or less. From any of these points a reduction in NO_2 without a reduction in reactivity will tend to move towards higher PO_3, while a reduction in reactivity would tend to reduce PO_3, indicating that the conditions during the CalNex campaign were generally NO_x-saturated. Reductions in both NO_2 and VOC reactivity together may not have a significant effect on PO_3.

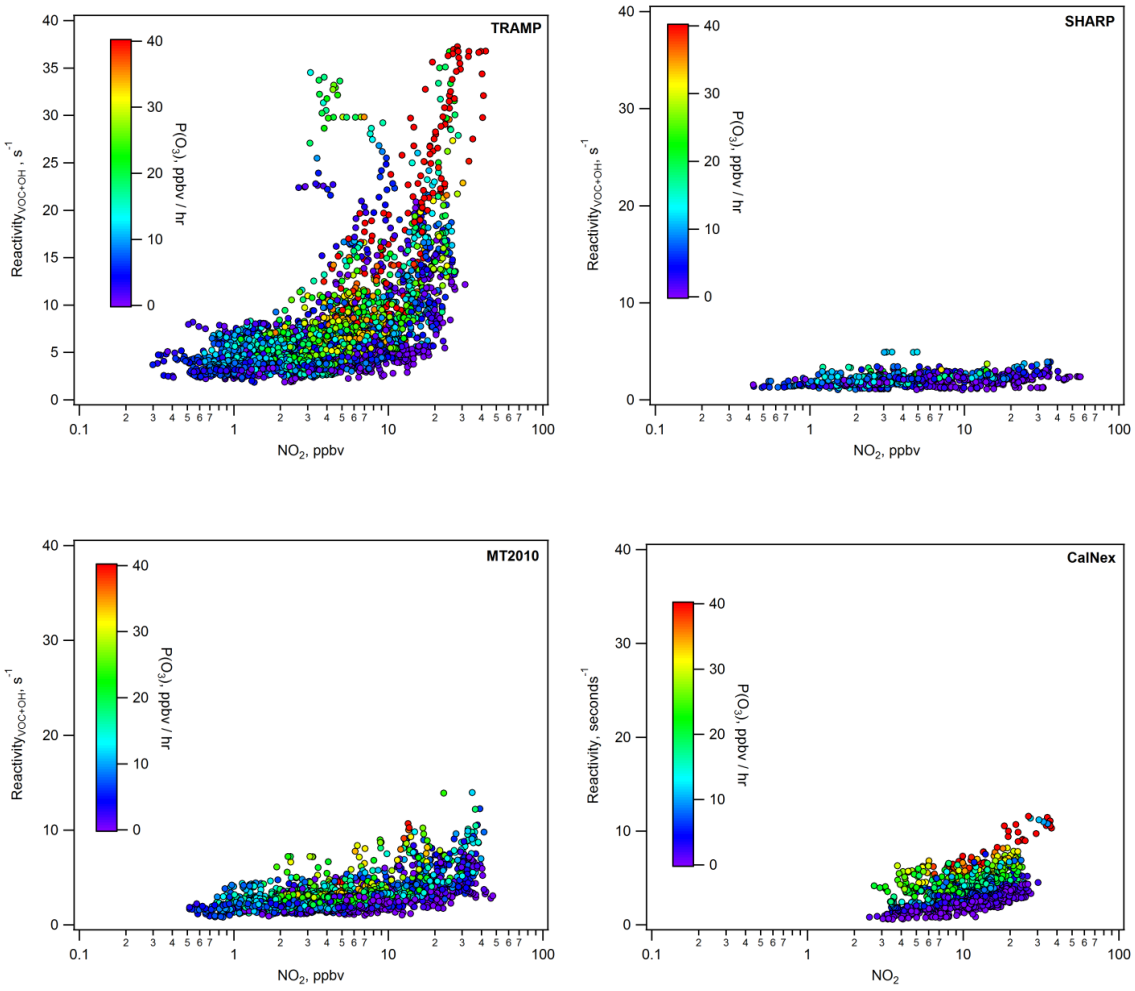

Figure 3-20. VOC reactivity vs NO_2.

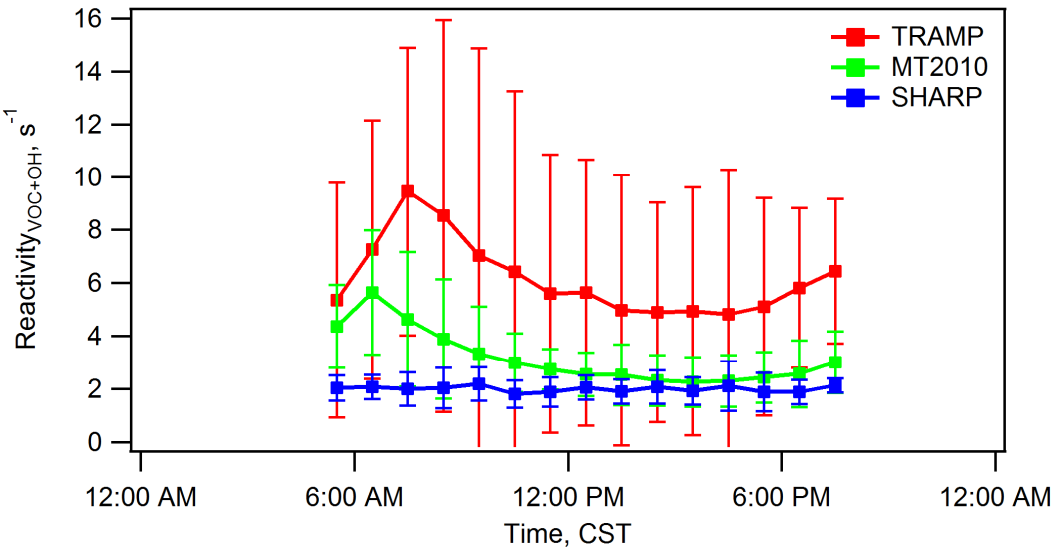

Figure 3-21. VOC reactivity median diurnal profiles for the three Houston campaigns.

Both TRAMP and MT2010 profiles have peaks in reactivity in the morning, roughly coinciding with the morning rush hour and then decreases through the day until late afternoon (Figure 3-21). The majority of the shape of the profile after the morning peak is likely driven by boundary layer heights increasing dilution during the middle of the day. Compared to the two fall campaigns, SHARP reactivity is low and constant throughout the daylight hours. Figure 1-1 shows that between SHARP in 2009 and MT2010 the annual average NO_x and ethylene measurements did not decrease, therefore the other control on ambient levels, meteorology, was responsible for lower NO_x and reactivity during SHARP. Higher wind speeds (Figure 3-23) and persistent southeasterly flow (i.e. winds from the Gulf of Mexico) were the major factors responsible for the lower reactivity and NO_x levels during SHARP. Figure 3-24 shows a histogram of O_3 measurements during TRAMP and MT2010. The MT2010 campaign has a higher incidence of O_3 between 25 and 75 ppbv, but peak O_3 values during TRAMP, although

rare, were higher than MT2010, approaching 150 ppbv. This reduction in peak O_3 levels from TRAMP to MT2010 is also consistent with a reduction in reactivity and PO_3.

Although the emissions between the spring SHARP and fall MT2010 campaigns were not responsible for the difference in measurements, emission reductions do play a significant role in the differences seen between the two fall Houston campaigns, TRAMP and MT2010. Figure 1-1 shows that there was a 37% and 39% reduction in the annual average NO_x and ethylene, respectively, measured between 2006 and 2009. For both fall Houston projects, the temperatures and wind speeds were comparable (Figure 3-23 and Figure 3-5), and although the annual NO_x levels decreased, the measured NO_x at the Moody Tower was the same between the two projects. It should be noted that ethylene emissions in Houston are associated with petrochemical industry emissions (Buzcu and Frasier, 2006) while the strong morning NO_x emissions are more related to mobile emissions based on CO/NO_x ratios (Luke et al., 2010, Parrish et al., 2006). As such, the NOx emissions and ethylene emissions are not necessarily linked and may explain the observed reduction in VOC reactivity yet the measured NOx during TRAMP and MT2010 appear to be unchanged.

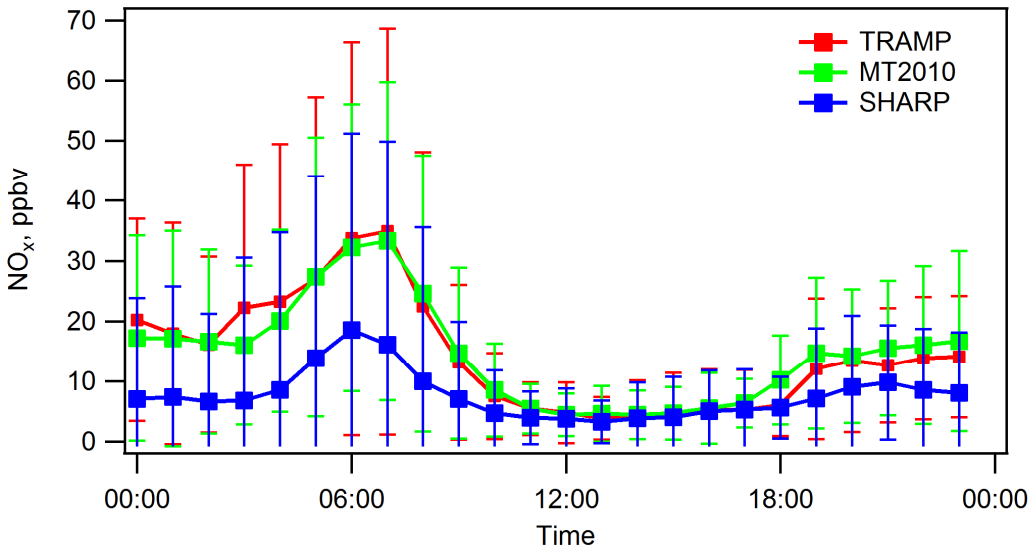

Figure 3-22. Average diurnal profiles of NO_x for the three Houston campaigns.

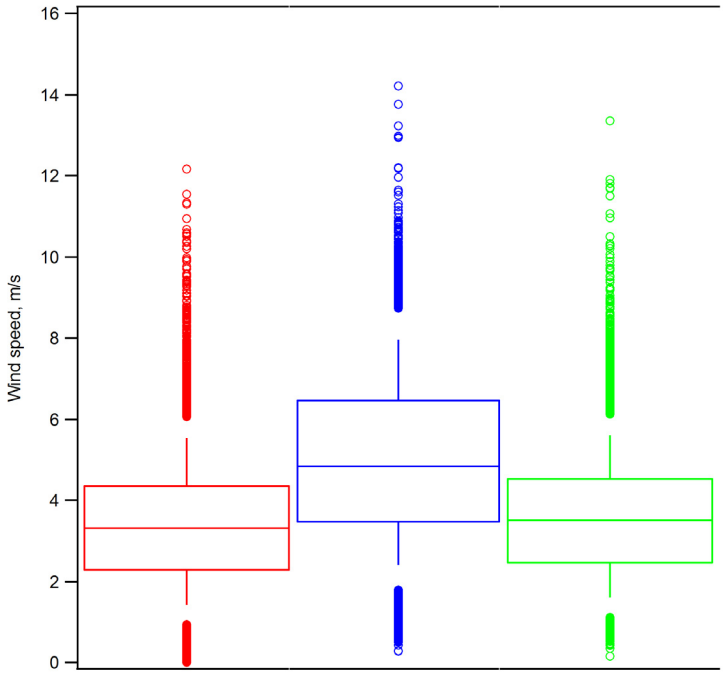

Figure 3-23. Box and whiskers plot for wind speeds during TRAMP (red), SHARP (blue), and MT2010 (green).

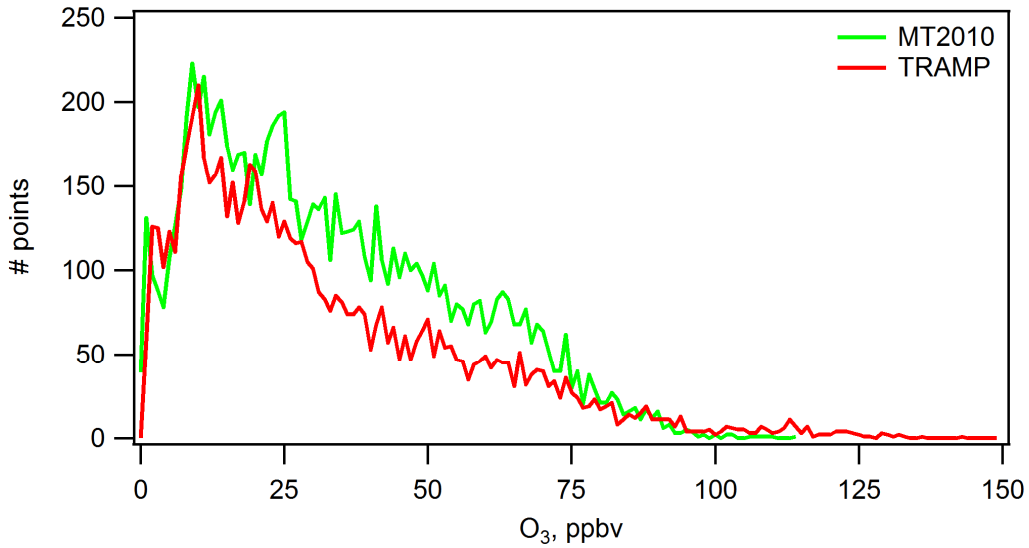

Figure 3-24. Histogram of measured O_3 during TRAMP and MT2010.

The CalNex peak reactivity (not shown) coincides with increased PO_3 and is a relatively broad peak from midday-early afternoon, again illustrating the delay in the Los Angeles area morning rush hour plume reaching the Pasadena measurement site. The reactivity profile also follows the O_3+NMHC losses in DO_3 shown in Section 3.4.1.

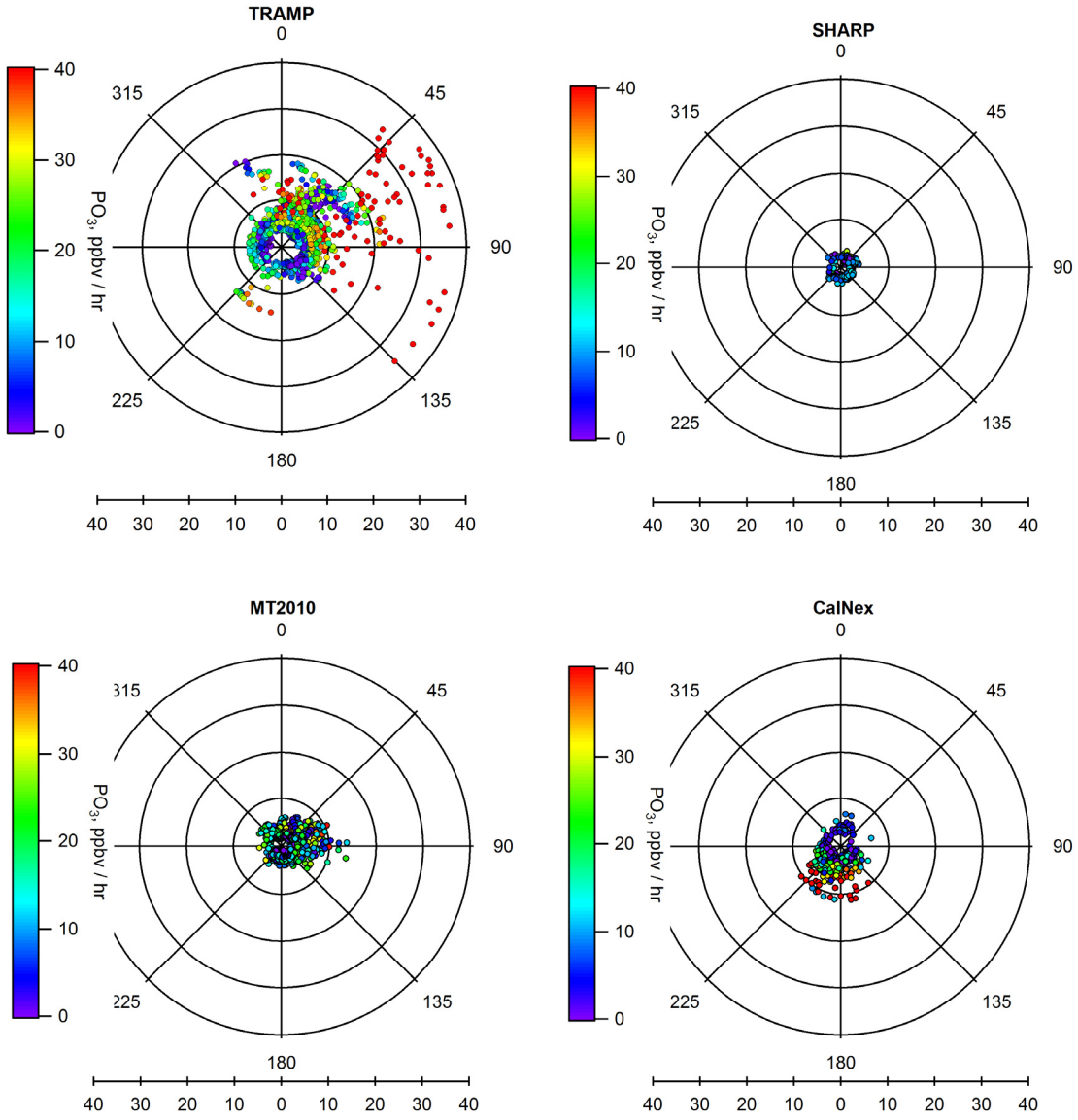

Figure 3-25. VOC reactivity (radius) vs. wind direction, for high O_3 days. Color is by PO_3, with values greater than 40 ppbv /hr shown in red.

Separating the reactivity on high O_3 days and plotting by wind direction reveals the source regions that are associated with the calculated reactivities. Figure 3-25 shows that, unsurprisingly, in Houston the highest reactivities and PO_3 are associated with easterly winds, the direction of the ship channel from the Moody Tower (Figure 3-1) (Luke, et al., 2010, Leuchner and Rappenglueck, 2010, Buzcu and Frasier, 2006).

Westerly winds were associated with much lower reactivities, although some points with significant PO_3 rates can be found in other wind directions. The SHARP data are more evenly distributed with the prevailing wind directions seen during the project and lack any real directionality. The highest reactivities and PO_3 values are associated with southerly winds. The bulk of the points for CalNex are clustered between south and southwesterly winds which was the dominate wind direction during the campaign (Figure 3-3).

3.5 CONCLUSIONS

This chapter presented the results of analysis on four intensive measurement projects that took place in Houston, TX and Pasadena, CA. The three Houston campaigns provided data that was used to examine the temporal variability in ozone production in Houston. Data from the CalNex ground site in Pasadena, CA allowed for a comparison between Houston and Los Angeles.

The two late summer campaigns, TRAMP (2006) and MT2010 (2010), have similar median PO_3 values and profile shapes, peaking ~1-2 hours before noon; however, MT2010 lacks the extremely high PO_3 and reactivity seen during TRAMP. Losses due to O_3+NMHC are highest during the TRAMP campaign and lower in both SHARP and MT2010. Peak PO_3 on high O_3 days has shifted from 5-10 ppbv NO in TRAMP closer to 1-2 ppbv for SHARP and MT2010, an indication that the point at which the system becomes NO_x-saturated is occurring at lower levels than during TRAMP. Together, these factors tend to point to reductions in emissions of VOCs and a shift towards a more NO_x-saturated regime. The diurnal profiles of reactivity peaks in early morning and decreases

through the day during both TRAMP & MT2010 campaigns, but remains flat during SHARP. In Houston, the highest reactivity and PO_3 are associated with easterly winds, indicating the ship channel as the VOC emission source. The spring 2009 SHARP campaign had the lowest reactivity and PO_3 under all conditions when compared to either of the two late summer measurement periods.

Differences between the two fall campaigns show the effect of a reduction in VOC emissions and VOC reactivities over a four-year period and are supported by measurements of ethylene at the TCEQ monitor on Clinton Drive. Comparing the spring 2009 and fall 2010 campaigns finds that although emissions were relatively constant based on annual averages, the measured levels were much lower in the spring. This was most likely due to the strong and persistent southeasterly winds that brought cleaner air masses to the Moody Tower and tended to dilute what emissions may have been present. In Houston, reductions in VOC reactivity would be the most efficient approach to routinely reduce PO_3 rates since it appears that the effects of NO_x reductions may or may not help reduce PO_3.

At the Pasadena ground site during CalNex, PO_3 follows reactivity; peaking mid-day through early afternoon when the morning rush hour plume reaches Pasadena. Compared to Houston, the median PO_3 on high O_3 days was about 5 ppbv higher than TRAMP and MT2010, however O_3 losses by HNO_3 formation accounts for a higher percentage of the overall loss rates than in Houston. The reactivity vs. NO_2 plot would indicate that PO_3 at the Pasadena ground site during the CalNex campaign was NO_x-saturated. The most efficient way to reduce PO_3 in this situation would be to reduce VOC reactivity.

3.6 REFERENCES

Buzcu, B., and M. P. Fraser (2006), Source identification and apportionment of volatile organic compounds in Houston, TX, *Atmospheric Environment*, *40*(13), 2385-2400, doi:10.1016/j.atmosenv.2005.12.020.

Cazorla, M., W. H. Brune, X. Ren, and B. Lefer (2012), Direct measurement of ozone production rates in Houston in 2009 and comparison with two estimation methods, *Atmospheric Chemistry and Physics*, *12*(2), 1203-1212, doi:10.5194/acp-12-1203-2012.

Chen, S. A., X. R. Ren, J. Q. Mao, Z. Chen, W. H. Brune, B. Lefer, B. Rappengluck, J. Flynn, J. Olson, and J. H. Crawford (2010), A comparison of chemical mechanisms based on TRAMP-2006 field data, *Atmospheric Environment*, 44(33), 4116-4125, doi:10.1016/j.atmosenv.2009.05.027.

Crawford, J., et al. (1999), Assessment of upper tropospheric HOx sources over the tropical Pacific based on NASA GTE/PEM data: Net effect on HOx and other photochemical parameters, *Journal of Geophysical Research-Atmospheres, 104*(D13), 16255-16273, doi:10.1029/1999jd900106.

Dasgupta, P. K., J. Z. Li, G. F. Zhang, W. T. Luke, W. A. McClenny, J. Stutz, and A. Fried (2005), Summertime ambient formaldehyde in five US metropolitan areas: Nashville, Atlanta, Houston, Philadelphia, and Tampa, *Environmental Science & Technology, 39*(13), 4767-4783, doi:10.1021/es048327d.

Daum, P. H., L. I. Kleinman, S. R. Springston, L. J. Nunnermacker, Y. N. Lee, J. Weinstein-Lloyd, J. Zheng, and C. M. Berkowitz (2003), A comparative study of O-3 formation in the Houston urban and industrial plumes during the 2000 Texas Air Quality Study, *Journal of Geophysical Research-Atmospheres*, *108*(D23), 18, doi:10.1029/2003jd003552.

de Gouw, J., and C. Warneke (2007), Measurements of volatile organic compounds in the earths atmosphere using proton-transfer-reaction mass spectrometry, *Mass Spectrometry Reviews, 26*(2), 223-257, doi:10.1002/mas.20119.

Flynn, J., et al. (2010), Impact of clouds and aerosols on ozone production in Southeast Texas, *Atmospheric Environment*, *44*(33), 4126-4133, doi:10.1016/j.atmosenv.2009.09.005.

Fuchs, H., W. P. Dube, B. M. Lerner, N. L. Wagner, E. J. Williams, and S. S. Brown (2009), A sensitive and versatile detector for atmospheric NO2 and NOx based on blue diode laser cavity ring-down spectroscopy, *Environmental Science & Technology, 43*(20), 7831-7836, doi:10.1021/es902067h.

Geddes, J. A., J. G. Murphy, and D. K. Wang (2009), Long term changes in nitrogen oxides and volatile organic compounds in Toronto and the challenges facing local ozone control, *Atmospheric Environment*, *43*(21), 3407-3415, doi:10.1016/j.atmosenv.2009.03.053.

Griffin, R. J., M. K. Revelle, and D. Dabdub (2004), Modeling the oxidative capacity of the atmosphere of the south coast air basin of California. 1. Ozone formation metrics, *Environmental Science & Technology*, *38*(3), 746-752, doi:10.1021/es0341283.

Heland, J., J. Kleffmann, R. Kurtenbach, and P. Wiesen (2001), A new instrument to measure gaseous nitrous acid (HONO) in the atmosphere, Environmental Science & Technology, 35(15), 3207-3212, doi:10.1021/es000303t.

Holloway, J. S., R. O. Jakoubek, D. D. Parrish, C. Gerbig, A. Volz-Thomas, S. Schmitgen, A. Fried, B. Wert, B. Henry, and Drummond, Jr. (2000), Airborne intercomparison of vacuum ultraviolet fluorescence and tunable diode laser absorption measurements of tropospheric carbon monoxide, Journal of Geophysical Research-Atmospheres, 105(D19), 24251-24261, doi:10.1029/2000jd900237.

Karl, T., T. Jobson, W. C. Kuster, E. Williams, J. Stutz, R. Shetter, S. R. Hall, P. Goldan, F. Fehsenfeld, and W. Lindinger (2003), Use of proton-transfer-reaction mass spectrometry to characterize volatile organic compound sources at the La Porte super site during the Texas Air Quality Study 2000, *Journal of Geophysical Research-Atmospheres, 108*(D16), doi:10.1029/2002jd003333.

Kleinman, L. I., P. H. Daum, Y. N. Lee, L. J. Nunnermacker, S. R. Springston, J. Weinstein-Lloyd, and J. Rudolph (2005), A comparative study of ozone production in five U.S. metropolitan areas, *Journal of Geophysical Research-Atmospheres*, *110*(D2), 20, doi:10.1029/2004jd005096.

Lefer, B., and B. Rappenglueck (2010), The TexAQS-II radical and aerosol measurement project (TRAMP) Preface, Atmospheric Environment, 44(33), 3997-4004.

Lefer, B. L., R. E. Shetter, S. R. Hall, J. H. Crawford, and J. R. Olson (2003), Impact of clouds and aerosols on photolysis frequencies and photochemistry during TRACE-P: 1. Analysis using radiative transfer and photochemical box models, *Journal of Geophysical Research-Atmospheres, 108*(D21), 22, doi:10.1029/2002jd003171.

Leuchner, M., and B. Rappengluck (2010), VOC source-receptor relationships in Houston during TexAQS-II, *Atmospheric Environment, 44*(33), 4056-4067, doi:10.1016/j.atmosenv.2009.02.029.

Luke, W. T., P. Kelley, B. L. Lefer, J. Flynn, B. Rappengluck, M. Leuchner, J. E. Dibb, L. D. Ziemba, C. H. Anderson, and M. Buhr (2010), Measurements of primary trace gases and NO(y) composition in Houston, Texas, *Atmospheric Environment*, *44*(33), 4068-4080, doi:10.1016/j.atmosenv.2009.08.014.

Lurmann, F. W., A. C. Lloyd, and R. Atkinson, A chemical mechanism for use in long-range transport/acid deposition computer modeling, *Journal of Geophysical Research*, *91*, 10905-10936, 1986.

Mao, J. Q., et al. (2010), Atmospheric oxidation capacity in the summer of Houston 2006: Comparison with summer measurements in other metropolitan studies, *Atmospheric Environment*, *44*(33), 4107-4115, doi:10.1016/j.atmosenv.2009.01.013.

Mielke, L. H., and H. D. Osthoff (2012), On quantitative measurements of peroxycarboxylic nitric anhydride mixing ratios by thermal dissociation chemical ionization mass spectrometry, *International Journal of Mass Spectrometry, 310*, 1-9, doi:10.1016/j.ijms.2011.10.005.

Murphy, J. G., D. A. Day, P. A. Cleary, P. J. Wooldridge, D. B. Millet, A. H. Goldstein, and R. C. Cohen (2007), The weekend effect within and downwind of Sacramento - Part 1: Observations of ozone, nitrogen oxides, and VOC reactivity, *Atmospheric Chemistry and Physics*, *7*(20), 5327-5339.

Olson, J. R., J. H. Crawford, G. Chen, W. H. Brune, I. C. Faloona, D. Tan, H. Harder, and M. Martinez (2006), A reevaluation of airborne HOx observations from NASA field campaigns, *Journal of Geophysical Research-Atmospheres, 111*(D10), 12, doi:10.1029/2005jd006617.

Pollack, I. B., et al. (2012), Airborne and ground-based observations of a weekend effect in ozone, precursors, and oxidation products in the California South Coast Air Basin, *Journal of Geophysical Research-Atmospheres, 117*, doi:10.1029/2011jd016772.

Ren et al., (2013), Atmospheric oxidation chemistry and ozone production: Results from SHARP 2009 in Houston, Texas, *Journal of Geophysical Research-Atmospheres,* in press, doi:10.1002/jgrd.50342.

Ryerson, T. B., et al. (2003), Effect of petrochemical industrial emissions of reactive alkenes and NOx on tropospheric ozone formation in Houston, Texas, *Journal of Geophysical Research-Atmospheres*, *108*(D8), doi:10.1029/2002jd003070.

Ryerson et al. (2013), The 2010 California research at the Nexus of air quality and climate change (CalNex) field study, *Journal of Geophysical Research-Atmospheres*, in press, doi: 10.1002/jgrd.50331

Sander, S., R. R. Friedl, A. R. Ravishankara, D. M. Golden, C. E. Kolb, M. J. Kurylo, M. J. Molina, G. K. Moortgat, H. Keller-Rudek, B. J.Finlayson-Pitts, P. H. Wine, R. E. Huie, V. L. Orkin, Chemical Kinetics and Photochemical Data for Use in Atmospheric Studies Evaluation Number 15, JPL Publication 06-2, 2006

Shetter, R. E., et al. (2003), Photolysis frequency of NO2: Measurement and modeling during the International Photolysis Frequency Measurement and Modeling Intercomparison (IPMMI), *Journal of Geophysical Research-Atmospheres, 108*(D16), 15, doi:10.1029/2002jd002932.

Steiner, A. L., R. C. Cohen, R. A. Harley, S. Tonse, D. B. Millet, G. W. Schade, and A. H. Goldstein (2008), VOC reactivity in central California: comparing an air quality model to ground-based measurements, *Atmospheric Chemistry and Physics*, *8*(2), 351-368.

Volz-Thomas, A., I. Xueref, and R. Schmitt (2002), An automatic gas chromatograph and calibration system for ambient measurements of PAN and PPN, *Environmental Science and Pollution Research*, 72-76.

Washenfelder, R. A., A. O. Langford, H. Fuchs, and S. S. Brown (2008), Measurement of glyoxal using an incoherent broadband cavity enhanced absorption spectrometer, *Atmospheric Chemistry and Physics, 8*(24), 7779-7793.

Williams, E. J., F. C. Fehsenfeld, B. T. Jobson, W. C. Kuster, P. D. Goldan, J. Stutz, and W. A. McCleanny (2006), Comparison of ultraviolet absorbance, chemiluminescence, and DOAS instruments for ambient ozone monitoring, *Environmental Science & Technology, 40*(18), 5755-5762, doi:10.1021/es0523542.

Wong, K. W., C. Tsai, B. Lefer, C. Haman, N. Grossberg, W. H. Brune, X. Ren, W. Luke, and J. Stutz (2012), Daytime HONO vertical gradients during SHARP 2009 in Houston, TX, *Atmospheric Chemistry and Physics, 12*(2), 635-652, doi:10.5194/acp-12-635-2012.

Ziemba, L. D., J. E. Dibb, R. J. Griffin, C. H. Anderson, S. I. Whitlow, B. L. Lefer, B. Rappengluck, and J. Flynn (2010), Heterogeneous conversion of nitric acid to nitrous acid on the surface of primary organic aerosol in an urban atmosphere, *Atmospheric Environment*, *44*(33), 4081-4089, doi:10.1016/j.atmosenv.2008.12.024.

4. NO_Y BUDGET AT THE PASADENA GROUND SITE DURING THE CALNEX-PASADENA FIELD CAMPAIGN

4.1 INTRODUCTION

Tropospheric O_3 forms by reactions of nitrogen oxides (NO_x = NO + NO_2), volatile organic carbon (VOC), and oxygen in the presence of solar radiation. O_3 photochemistry occurs when NO_2 is photolyzed in sunlight. Net O_3 production is not possible unless a peroxy radical is present to react with NO to regenerate the NO_2 without destroying O_3. Total reactive nitrogen (NOy) is the sum of NO_x and its' oxidation products including HNO_3, PAN, PPN, HONO, NO_3, N_2O_5, and aerosol nitrate. These species, collectively known as NO_z (NO_y-NO_x) are generally considered to be the NO_x consumed in the O_3 formation process since they do not directly participate in O_3 formation and can act as a sink for NO_x (e.g. PAN and HNO_3). Because NO_y is composed of numerous species it can be quite difficult to measure all of them continuously. Bulk NO_y is measured more often by using a catalytic converter to reduce NO_2 and NO_z species to NO for measurement with a chemiluminescence detector. Many commercial instruments used in regulatory monitoring applications also use these same converters to measure NO_x. However, NO_x tends to be overestimated because many NO_z species are also converted to NO in the converter. This is particularly true during the daytime when photochemically produced NO_z species are highest. Depending on the operating conditions and history of the converter NH_3 may also be an interference (Sather et al., 2006, Fitz et al., 2003, Geddes, 2013, Dunlea, et al., 2007,Williams et al., 1997, Xue et al., 2011). One solution is to use UV light to convert NO_2 to NO by photolysis

instead of the catalytic converter in a commercial instrument. Unfortunately, depending on the wavelength and intensity of light selected, there can be compromises in conversion efficiency and selectivity. While shorter wavelengths and higher intensities convert a greater fraction of NO_2 to NO, additional interferences from partial conversion of HONO, $BrONO_2$, and $ClNO_2$ can be problematic. Alternately, longer wavelength and lower power converters more selectively convert NO_2, but they also have lower conversion efficiencies and can still suffer interferences from HONO, although these interferences tend to be smaller (Pollack et al., 2010, Fuchs et al., 2010).

Measurements in polluted urban areas, such as Los Angeles and Houston, with many emission sources show that the high levels of NO_y are dominated by NO_x in comparison to measurements of more remote regions (Talbot et al, 1999, Schultz et al., 2000). During these projects measurements over the North Atlantic and South Pacific found much more photochemically aged air which is primarily composed of NO_z. Attempts to measure many of the NO_z species in addition to NO and NO_2 found that the sum of these components often did not equal the bulk NO_y measurement leading to the conclusion that some component(s) of NO_z were not measured (Williams et al., 1997, Day et al., 2003). More recently several field campaigns measured additional NO_z components and have found better agreement between measured NO_y and the sum of NO_y components (Osthoff et al., submitted 2013, Luke et al., 2010, Pollack et al., 2012).

CalNex, an intensive field campaign involving numerous ground sites across California, as well as several aircraft and the R/V Atlantis, took place during May and June 2010. One of the ground sites was located on the California Institute of Technology

campus in Pasadena, CA (Figure 4-1). Additional details and the overall objectives of this campaign are described in Ryerson, et al. (in press). Many of the major components of NO_y were measured during the campaign, and in some cases duplicate measurements of the same species were made using different techniques. This chapter will present the results of the analysis of the NO_y measurements, a comparison of two techniques for measuring NO_2, and will show the effects that different data classification methods can have on data analysis and conclusions.

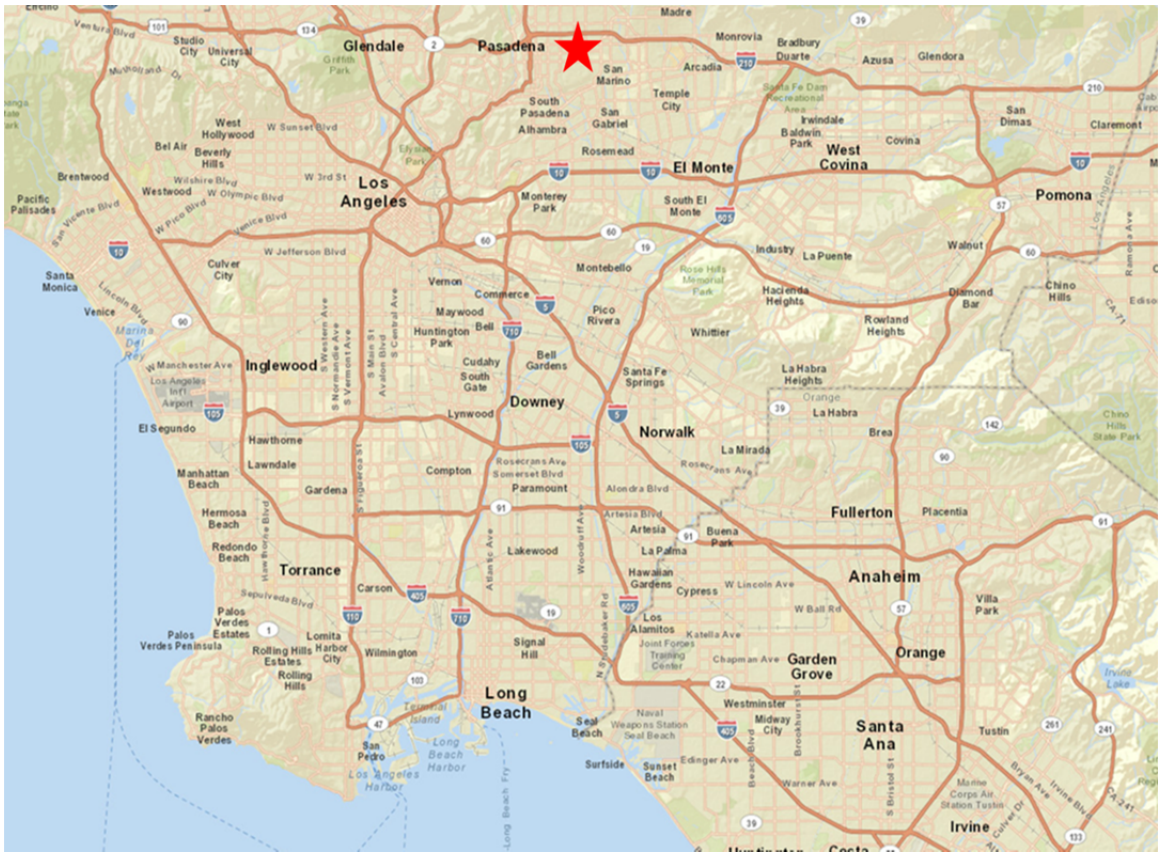

Figure 4-1. Map of the Los Angeles area. The location of the CalNex ground site is indicated with a red star.

4.2 METHODS

The CalNex ground site was located in a parking lot on the northeast side of the California Institute of Technology in Pasadena, CA, approximately 16 km northeast of downtown Los Angeles. Measurements were collected between May 15 and June 16, 2010. A detailed overview of the sampling location and conditions during the CalNex campaign can be found in Ryerson, et al. (2013). Most sample inlets were located on the top level of a 10 m walk-up scaffold; however, some sample inlets lengths prohibited sampling from the tower and were raised from the individual trailers. All samples used in this work were collected nominally within a 15 m radius of the scaffold tower, with the exception of NO3, which was only sampled by long-path DOAS.

Two TEI 42c-TL (NO_x and NO_y) and one 42i-TL (NO) analyzers were operated in NO mode with 10s averaging times. These instruments used pre-reactor zeros to determine instrument baselines at least once per hour for the two 42c instruments and once per sample interval in the case of the 42i-TL analyzer.

A custom inlet system was designed and built specifically for the CalNex campaign. The basic flow diagram is shown in Figure 4-2. The inlet consisted of a fiberglass enclosure which housed power supplies, a USB hub, solenoid valves, molybdenum NO_y converter, photolytic NO_2 converter, HNO_3 permeation oven, LabJack UE9-Pro and relay board, temperature controllers, plug strip, and cooling fan. Inlets extended ~1.5" below the bottom of the enclosure and used the grid support portion of a 47mm PFA filter holder to prevent most rain and bugs from entering the sample lines. A 45-foot length of 2" non-metallic liquid tight flexible conduit was used as an umbilical to

run the power, data, and gas lines to and from the inlet. The conduit protected the gas and data lines from the elements and darkened the sample lines to prevent further photochemistry from occurring in the sample lines.

The inlet tube of a new molybdenum NO_y converter cartridge was shortened so that only ~1.5" of stainless steel (SS) tubing extended beyond the heated cartridge. The cartridge was heated to 300ºC. This heated the SS fittings used to connect the converter to a ¾" long piece of 0.065" ID PFA Teflon tubing to ~125ºC by conduction. The Teflon tubing connected the Mo converter to a ¼" PTFE Teflon cross, where one port was used as the sample inlet, and one for NO/NO_x. The fourth port on the cross was used for calibrations. Upon exiting the converter the sample passed through a SS frit and glass capillary before traveling down the umbilical to the instrument.

The NO/NO_x sample was passed through a 2 μm Teflon filter before splitting with a PFA tee into separate NO and NOx sample lines. The NO sample passed through a glass capillary to set the flow rate and pressure. The NO_x sample passed through a UV-LED photolytic converter (Blue-Light Converter (BLC), Air Quality Design, Wheat Ridge, CO) before passing through a glass capillary. Using the BLC to measure NOx avoids many of the problems associated with using a molybdenum converter as it is much more selective and has only a small interference from HONO (Sather, et al., 2006, Dunlea, et al., 2007, Fuchs, et al., 2010, Pollack et al., 2011). O_3 and SO_2 were also sampled though parallel sample inlets housed in the same enclosure. Measurements of NO_z species are discussed in Osthoff, et al., (submitted 2013) and references therein.

Calibrations were conducted by blending zero air with NO and NO_2 gas standards from Scott-Marrin Inc. (Riverside, CA) with a TEI 146i gas dilution system. These blends were then fed through the calibration port on the Teflon cross, allowing calibrations through the entire sample line including any filters, with the exception of 1.5-2" at the very tip of the inlet. A 2-way valve connected to the calibration line immediately prior to the cross allowed the connection of a vacuum line to prevent sampling residual calibration gasses during ambient measurements. This valve was closed during calibrations. Additionally, N_2 was used as a carrier gas providing continuous flow through a homemade HNO_3 permeation oven (permeation tube purchased from Kin-Tec, La Marque, TX). A 3-way valve was used to selectively add the HNO_3 in N_2 to a zero air flow before a 120 cc mixing volume prior to being added to the sample inlet. A 3-way valve between the mixing volume and sample inlet was used to bypass calibration gasses and allow equilibration of as much of the lines as possible prior to calibration in order to expedite the calibrations. Exhaust gasses from calibration bypasses were routed back down to the instrument rack where they were passed through a scrubber. During calibrations, excess calibration gas was allowed to overflow from the inlet.

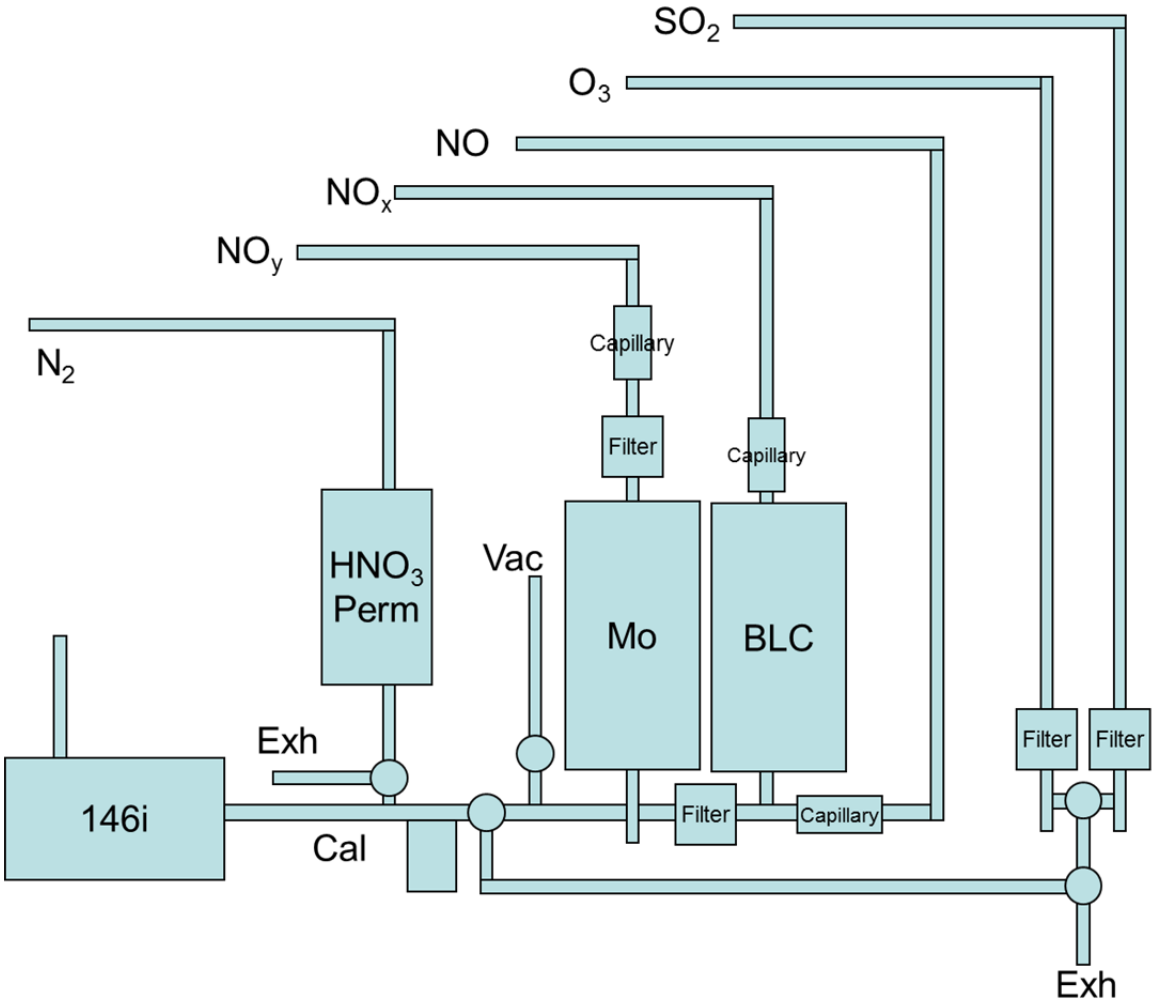

Figure 4-2. Simplified flow schematic of the inlet design for NO, NO_x, NO_y, O_3, and SO_2 used during the CalNex campaign.

4.3 RESULTS

This section will present a comparison of three different methods of measuring NO_2. Differential optical absorption spectroscopy (DOAS) was used to measure path averaged mixing ratios of NO_2 along four light paths at different altitudes. Cavity ring-down spectroscopy (CRDS) and a photolytic converter followed by chemiluminescence (BLC+Chemi) were used to measure in situ NO_2 at the CalNex ground site Pasadena. A

comparison of NOy to the sum of the measured NO_y components, along with a comparison of the sum of NO_z species and NO_y-NO_x will also be presented.

4.3.1 NO_2 comparison – cavity ring-down spectroscopy vs. photolytic converter & chemiluminescence

The two in situ measurements of NO_2 were expanded to 1s and then averaged over the DOAS start-stop sample times for the lowest light path (35-78 m above ground level). The DOAS sample interval was dependent on atmospheric transmission, and the cycle time between the four light paths, resulting in 575 CRDS and 390 BLC-Chemi records out of a possible 779, shown in Figure 4-3. Comparison of the three NO_2 measurements showed that the DOAS data was consistently higher than CRDS (NOAA) and BLC+Chemi (UH) (Figure 4-4). Because the DOAS NO_2 is a path average over which crossed a major interstate, only the two collocated in situ NO_2 measurements from the 10 m scaffold were included in this work. Calibration standards were shared between the UH and NOAA groups to ensure comparability of the data.

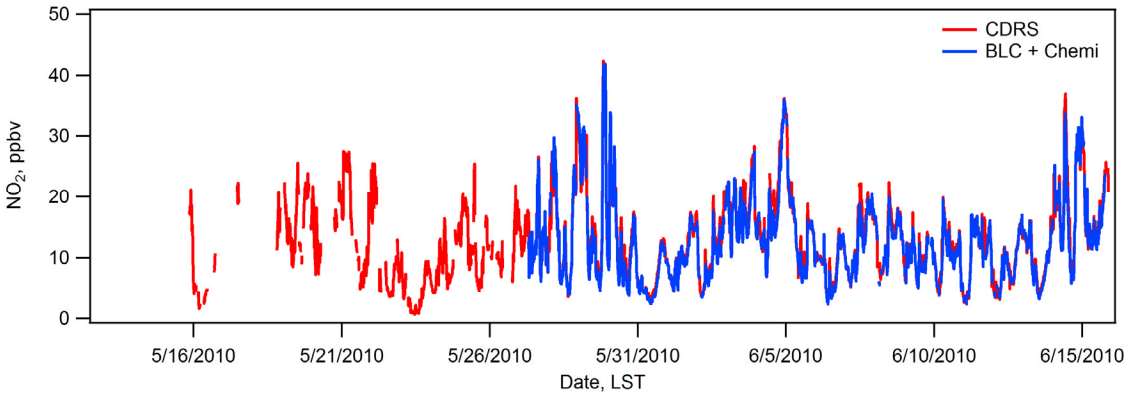

Figure 4-3. Time series plot of 10-minute averaged NO_2 data for CRDS (red) and BLC + Chemiluminescence (blue).

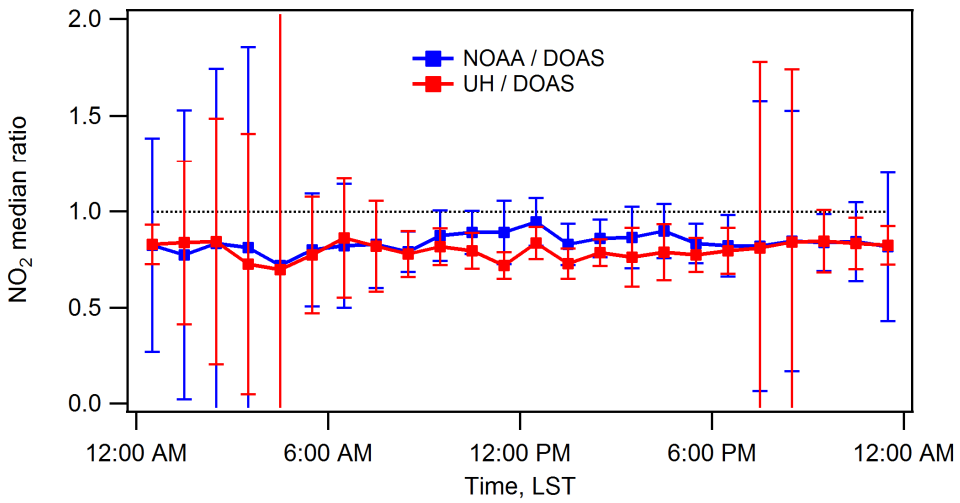

Figure 4-4. Comparison of CRDS and BLC+Chemi NO_2 to LP-DOAS.

A small leak in the UH NO_x sample line after the BLC was discovered on May 27 that was affecting the calibration of the instrument. While the leak was small, it changed each time the inlet enclosure was opened for adjustments to various components and/or filter changes. This resulted in several changes to the calibration and apparent conversion efficiency during the first 10 days of the campaign. Data from this period were not reported.

Tests with the NOAA HONO calibration source during CalNex revealed that the BLC used for the NO_x channel also converted ~7% of HONO. The BLC-Chemi NO_2 data used in this work has been corrected for this interference using HONO measured by incoherent broad-band cavity enhanced absorption spectroscopy (IBBCEAS) which was collocated with the NO_2 measurements and had better temporal coverage than the other HONO measurements collected at the ground site. Previous work has found similar levels of HONO conversion using the BLC (Fuchs, et al., 2010). However, Pollack, et al.

(2010) found that of the LED based photolytic converters used in their study, the BLC was the most selective for only converting NO_2 to NO. It should be noted that this selectivity is at the sacrifice of conversion efficiency. Increases in light output do increase NO_2 conversion efficiency but also increase the HONO interference, up to ~13% for some LED photolytic converters.

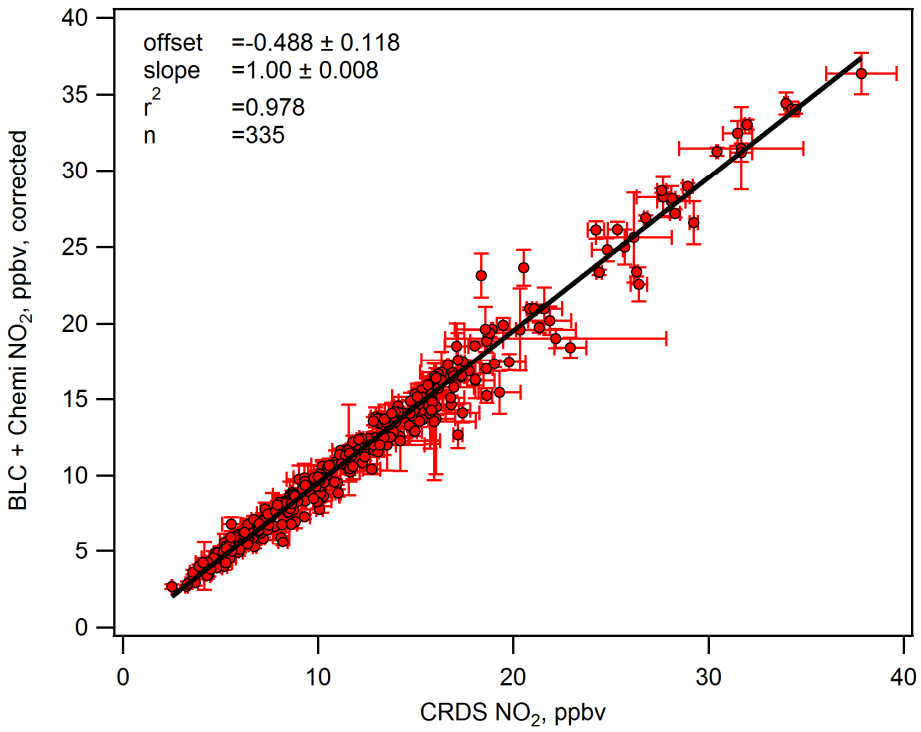

Figure 4-5. NO_2 measured with BLC + Chemiluminescence vs. CRDS. Error bars represent 1σ standard deviation of the averaged data. Black line represents the linear fit with orthogonal distance regression.

Figure 4-5 shows that there is excellent agreement between the BLC+Chemi and CRDS NO_2 measured during CalNex, with the BLC+Chemi NO_2 data biased 0.488 ± 0.118 ppbv low. The uncertainty for CRDS NO_2 is reported as 3%, and 6% for NO_2 by BLC+Chemi.

The diurnal profile of BLC+Chemi - CRDS and BLC+Chemi/CRDS (Figure 4-6) shows that the CRDS method agreed very well at night but reported slightly higher NO_2 values during the daytime than did the BLC+Chemi. Histograms of the relative distribution of the differences in the measurements and ratios show peaks centered on zero and one, respectively. The agreement between the BLC+Chemi NO_2 and CRDS NO_2 has been previously documented, however it should be noted that the CRDS instrument measures trace gas absorption at 532 nm, a region of the visible spectrum where NO_2 strongly absorbs and O_3 weakly absorbs. CRDS NO_2 measurements therefore have greater uncertainty during periods with large O_3/NO_2 ratios (Fuchs et al., 2010). This O_3 interference in the CRDS NO_2 may be responsible for the differences in NO_2 measurements during CalNex as shown in Figure 4-7. It is also possible that $NO + O_3$ reactions within the sample chamber could produce additional NO_2 and cause the observed interference.

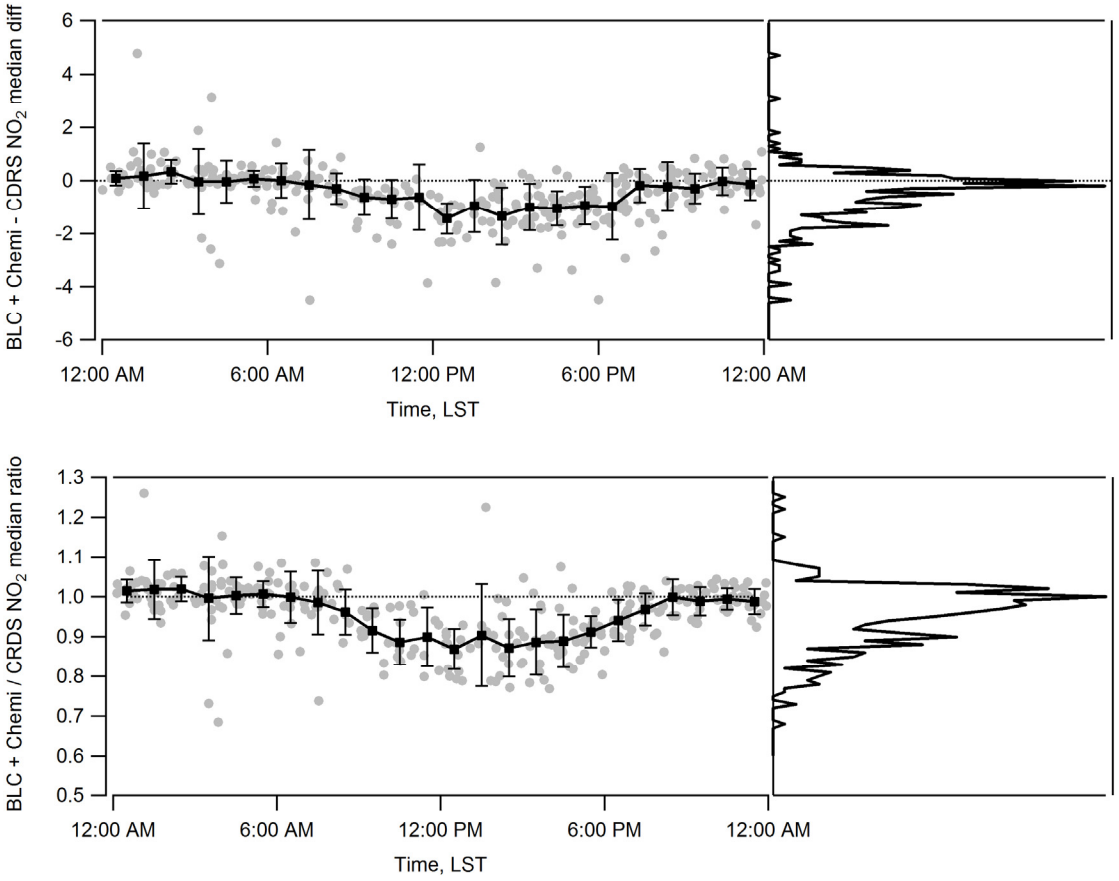

Figure 4-6. Upper panel: Median diurnal profile of the difference in NO_2 measurements ± 1σ. Lower panel: Median diurnal profile of the ratio of BLC+Chemi to CRDS NO_2. For both plots the black line represents the median value, error bars are ± 1 standard deviation) grey dots represent individual values and the black line in the right panels represent the relative histogram of the difference and ratio.

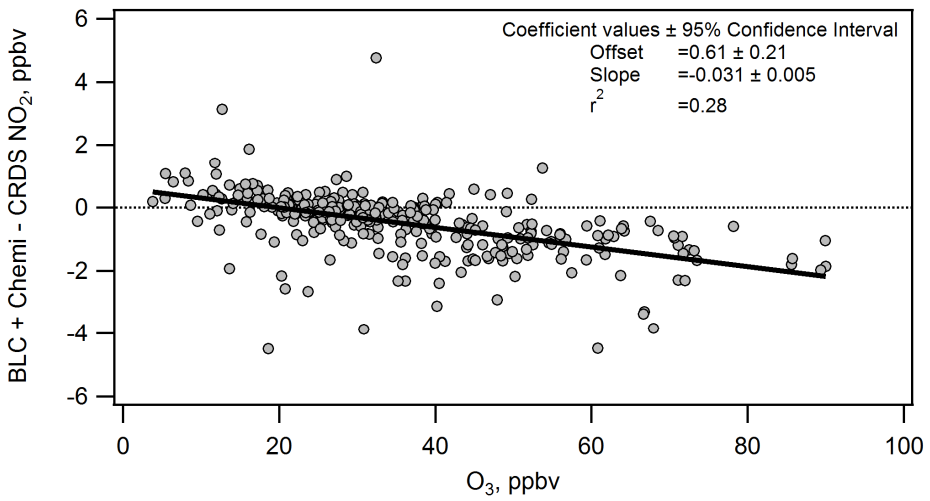

Figure 4-7. Difference in BLC+Chemi and CRDS NO_2 measurement as a function of O_3.

4.3.2 NO_y – measured vs. sum

Measurements of NO_y are compared to the sum of the individual NO_y species. For the purposes of this chapter NO_y sum was calculated as the sum of the individual NO_y species measured at the ground site where:

$$NO_y \text{ sum} = NO + NO_2 + HNO_3 + PAN + PPN + 2N_2O_5 + NO_3 + HONO$$

$$+ ClNO_2 + \text{sub-micron aerosol nitrates (alkyl-, methyl-, and ethylnitrate)} \qquad (4.1)$$

NO_y sum was only calculated for those points where concurrent measurements of each of the components were available with the exception of PPN, N_2O_5, NO_3, and HONO during daylight hours (Figure 4-8). Because daytime mixing ratios of these gasses are relatively low (typically few hundreds of pptv) compared to total NO_y (several tens of ppbv) missing or below detection limit periods for these species were treated as zero in order to calculate a value for NO_y sum. This approach results in 1862 10-minute measurements of NO_y sum, compared to 4037 for measured NO_y.

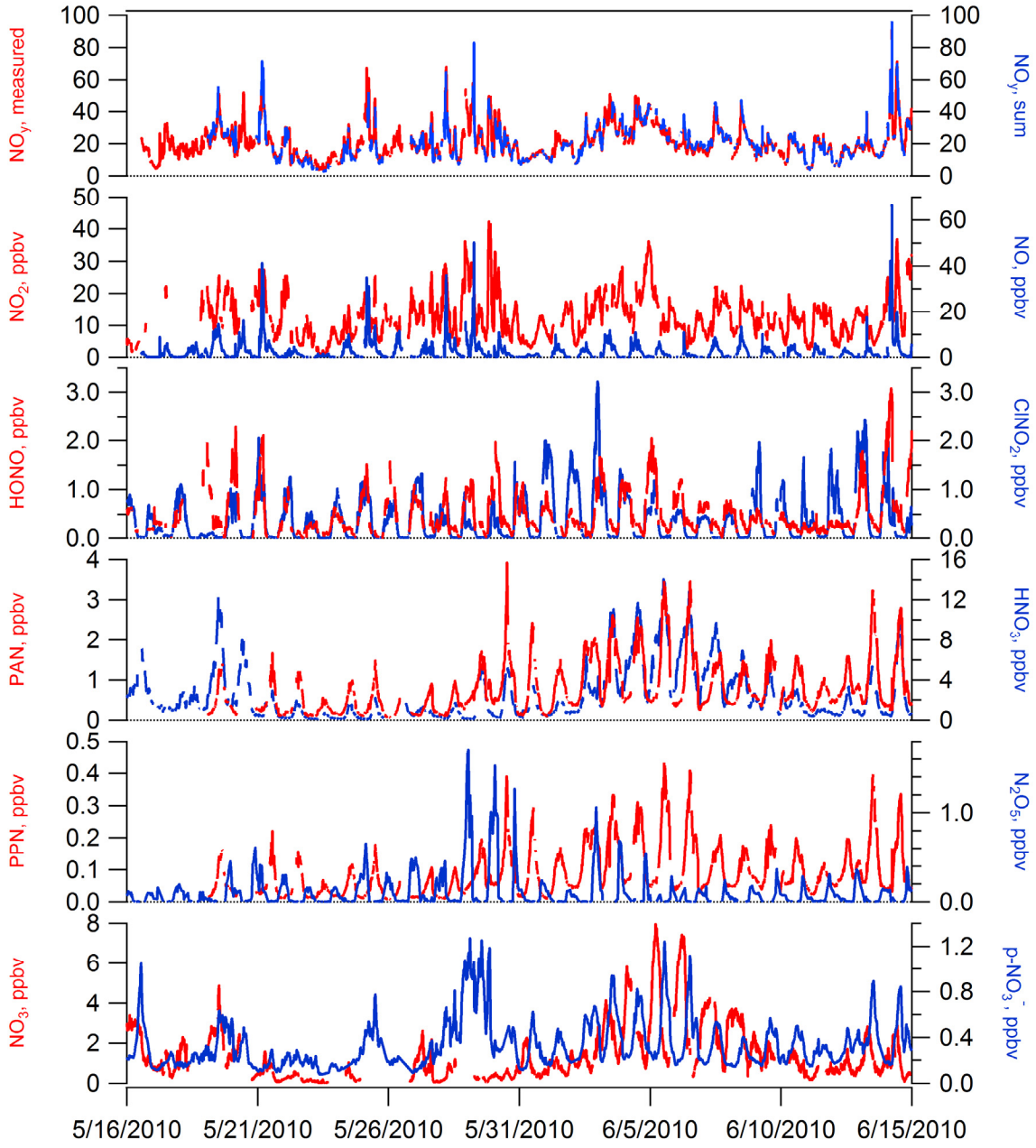

Figure 4-8. Time series of NO_y, NO_y sum, and NO_y components during CalNex.

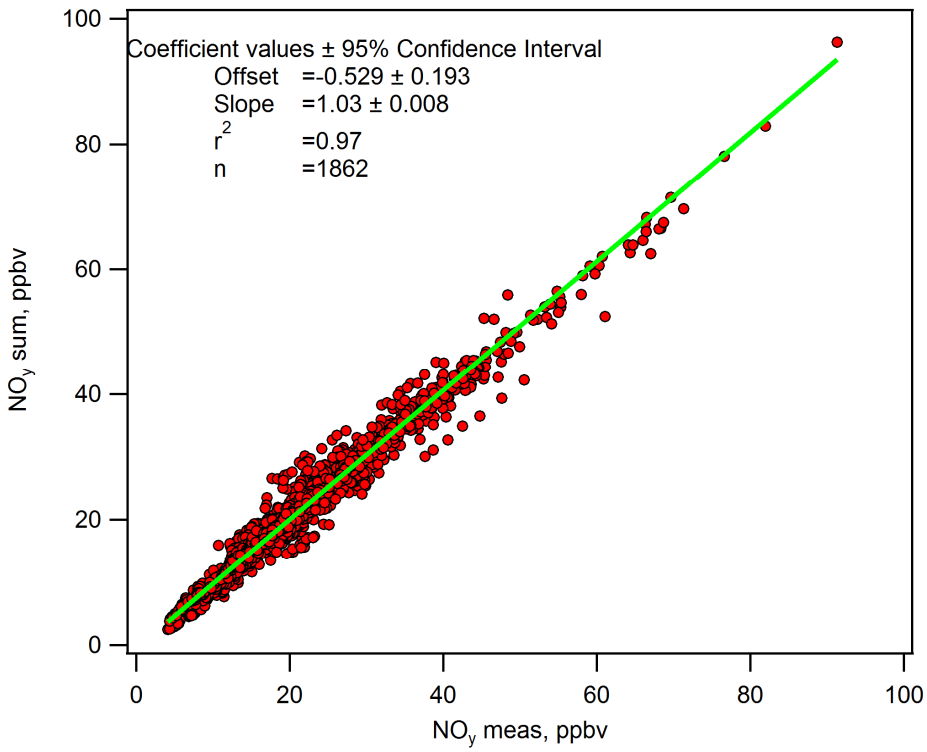

Figure 4-9. Calculated NO_y sum vs. NO_y measured. Green line represents linear orthogonal distance regression fit.

Figure 4-9 shows the good overall agreement between NO_y sum and NO_y measured (slope 1.03 ± 0.008 at 95% confidence level, r^2 0.97). These results are similar to those found in other urban areas when many of the NO_y components were measured. Luke et al. (2010) found that the sum of NO_x, HNO_3, PANs, HONO, and aerosol nitrates accounted for 97% ± 16% ($r^2 > 0.99$) of the measured NO_y during the day and 99% ± 16% ($r^2 > 0.99$) during the night at the Moody Tower in Houston during the TRAMP 2006 campaign. Rural measurements at the University of California – Blodgett Forest Research Station in 2000 and 2001 found the agreement between measured NO_y and the sum of NO_x, HNO_3, and peroxy and alkyl nitrates to be 0.98 ± 0.007 ($r^2 = 0.66$) with most of the NO_y measurements less than 5 ppbv (Day et al., 2003). Measurements on a

mountain peak in rural China showed that the sum of NO_x, PAN, HNO_3, and NO_3 accounted for slightly more than measured NO_y (slope 1.07) with an r^2 of 0.97 (Xue et al., 2011). Talbot et al. (1999) found very low NO_y levels in the remote atmosphere between 8 and 12.5 km over the North Atlantic during the fall of 1997. A mixture of measured and modeled NO_y species for that project agreed to within 99% of the measured NO_y.

NO_y measurements made with a commercial molybdenum converter cartridge have been studied in the past and reported in several publications. Fitz, et al. (2003) reported that while NH_3 conversion in different commercial molybdenum converters varied between 0-26%, NH_3 conversion was more dependent on the age and use of the converter rather than temperature, with older converters tending to convert more NH_3 than newer ones. Williams et al. (1997) found similar results with lower NH_3 conversion efficiencies at higher temperatures than were employed on the ground during CalNex. A similar inlet design to that used during CalNex was used during TRAMP 2006, and laboratory tests found NH_3 conversion to be insignificant (Luke et al., 2010). Xue et al. (2011) report that tests conducted on several converters like those used at the CalNex ground site may still exhibit a temperature dependent NH_3 conversion efficiency even in new converters, with a high of 38% conversion at 350ºC and ~11% at 325ºC. These temperatures are higher than those employed in the NO_y measurements reported here. Geddes (2013) found that NH_3 conversion is not linear with temperature (30% conversion at 300ºC and 70% at 340ºC) and presents a detailed investigation into NH_3 and other nitrogen species conversion in commercial molybdenum NO_y converters.

Recent work by Pollack et al. (2012) compared the NO_y measurements from the CalNex ground site to the sum of NO_x, HNO_3, and PAN on the P-3B aircraft after finding that there were only minimal differences between NO_y sum and measured NO_y. Measurements of NO_y on the P-3B using a 300ºC gold tube and chemiluminescence detector (Ryerson et al., 1999) were not available for all flights and showed the effects of a known interference with NH_3 and aerosol nitrate that lead to over-reporting NO_y, especially at NH_3 levels of ~10 ppbv or greater.

In contrast with the P-3B data, ground level NO_y measurements, which were made with a new molybdenum converter at 300ºC, do not show any significant interference by NH_3 as seen in Figure 4-10 where the difference and ratio between NO_y measured and NO_y sum are distributed normally about zero and one, respectively. Additionally, the largest differences between NO_y measured and NO_y sum tend to occur at relatively low NO_y levels.

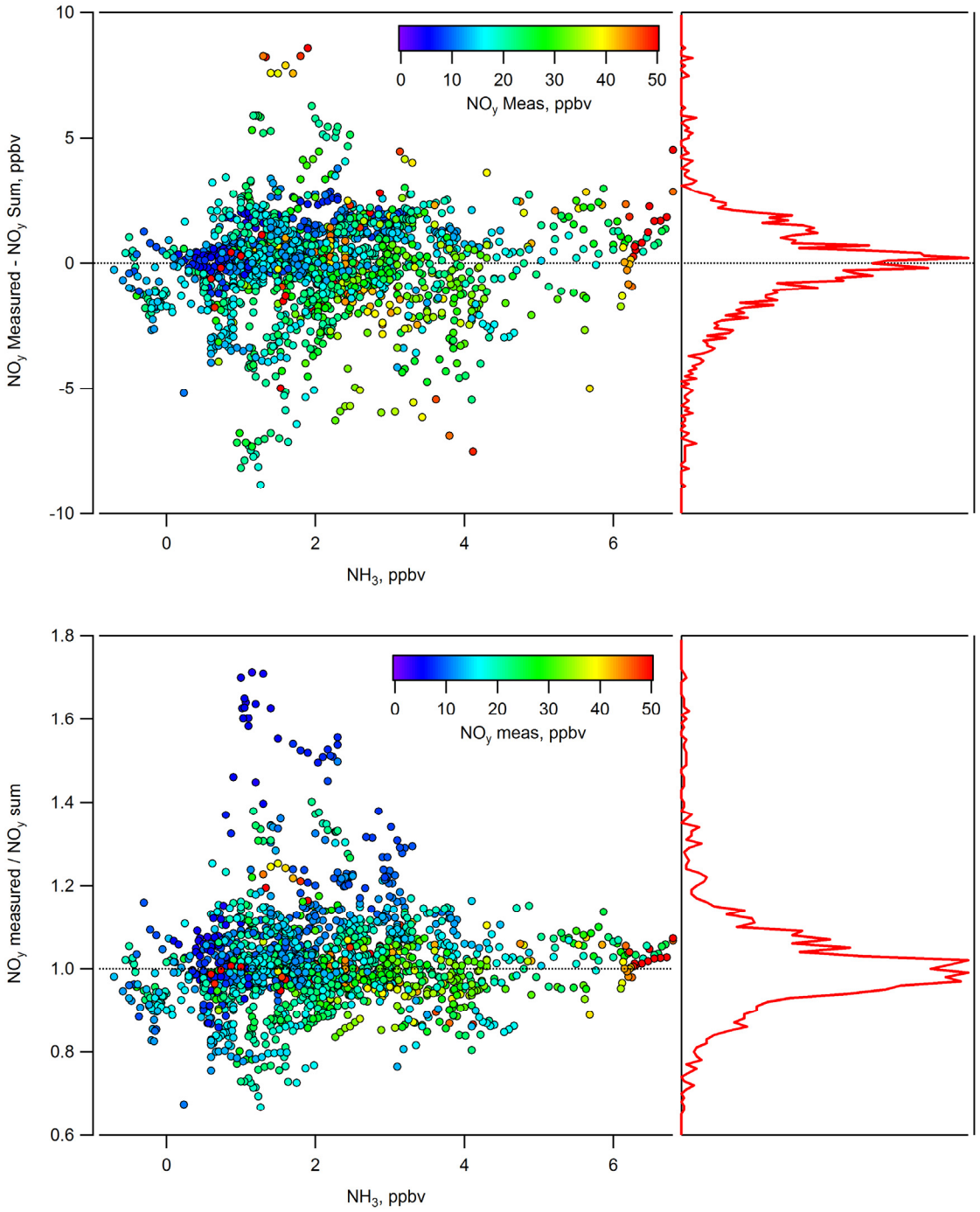

Figure 4-10. Upper Panel: Difference between NO_y measured and NO_y sum vs. measured NH_3. Lower Panel: Ratio of NO_y measured to NO_y sum vs NH_3. Both Panels: relative histogram of point distribution is shown in the right-hand panel.

4.3.3 NO_y-NO_x vs. NO_z sum

Separating NO_z (NO_y-NO_x, alternately referred to as NO_z measured) and NO_z sum (sum of HNO_3, PAN, PPN, $2N_2O_5$, NO_3, HONO, $ClNO_2$, and pNO_3) by day and night shows good correlation, $r^2 = 0.83$ and 0.70, respectively, with similar slopes, however there is roughly 1 ppbv difference in the offset and an apparent overestimation of NO_z sum (Figure 4-11). As NO_z sum is a composite of 10 individual measurements, the combined uncertainty is 58.7% for the major NOz components compared to NO_y-NO_x (8.25%). These NO_y-NO_x data were calculated using the NO_2 measured by CRDS; however, if BLC+Chemi NO_2 is used in the calculation differences appear between day and night measurements. Figure 4-12 shows the relationship between the two NO_z datasets when BLC+Chemi NO_2 is used. While the nighttime regression remains essentially unchanged, the daytime slope is much closer to 1 and the offset is improved as well. This result is consistent with the findings shown in Figure 4-6 where the two NO_2 methods agree during the night but have larger differences during the day. Because of the sampling issues with the BLC+Chemi inlet at the beginning of the measurement campaign and the resulting lack of coverage, the remainder of this section will use NO_2 from the CRDS instrument to calculate NO_y-NO_x values.

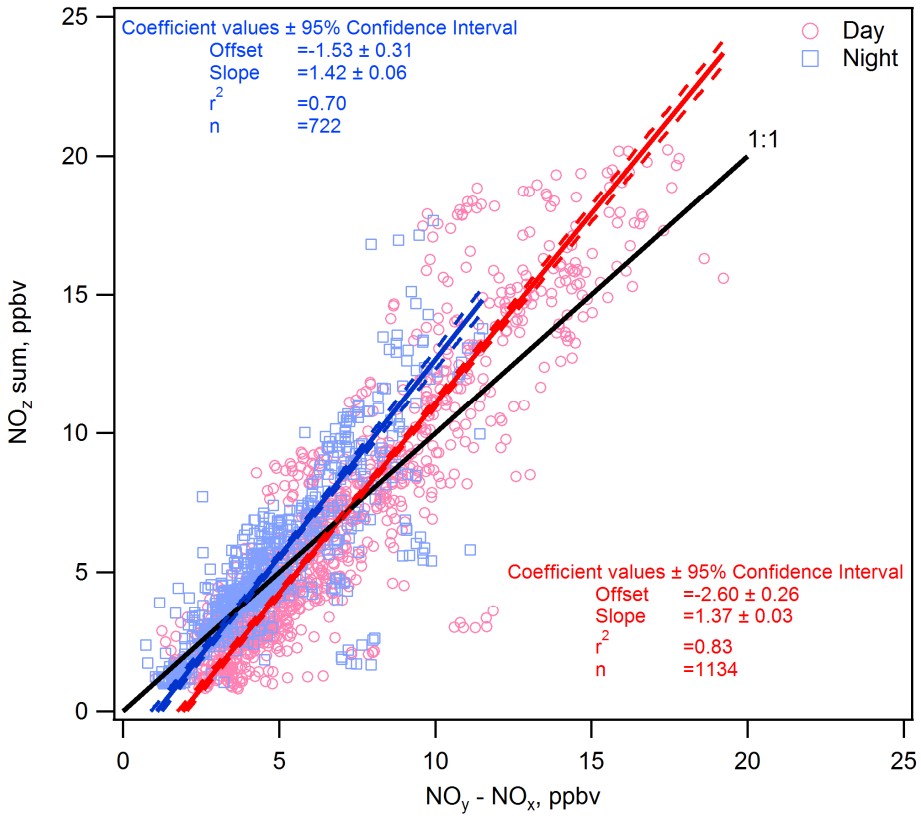

Figure 4-11. NO_z sum vs $NO_y - NO_x$ for day (red) and night (blue) using CRDS NO_2 in NO_x calculation. Solid lines represent ODR linear fit; dashed lines indicate the 95% confidence bands.

Several studies showed "missing" NO_y, for example, analysis of NO_z species from the P-3B during the TexAQS 2000 study found that the sum of HNO_3, PAN, and PPN accounted for 90% of NO_y-NO_x (Neuman et al., 2002). Results from the data collected at the Moody Tower during the TRAMP campaign had excellent agreement between NO_z sum and NO_y-NO_x (slope 0.99, r^2 0.85 for day; slope 0.89, r^2 0.69 at night) when using the sum of HNO_3, PANs, HONO, and pNO_3^- to calculate NO_z sum (Luke, et al., 2010).

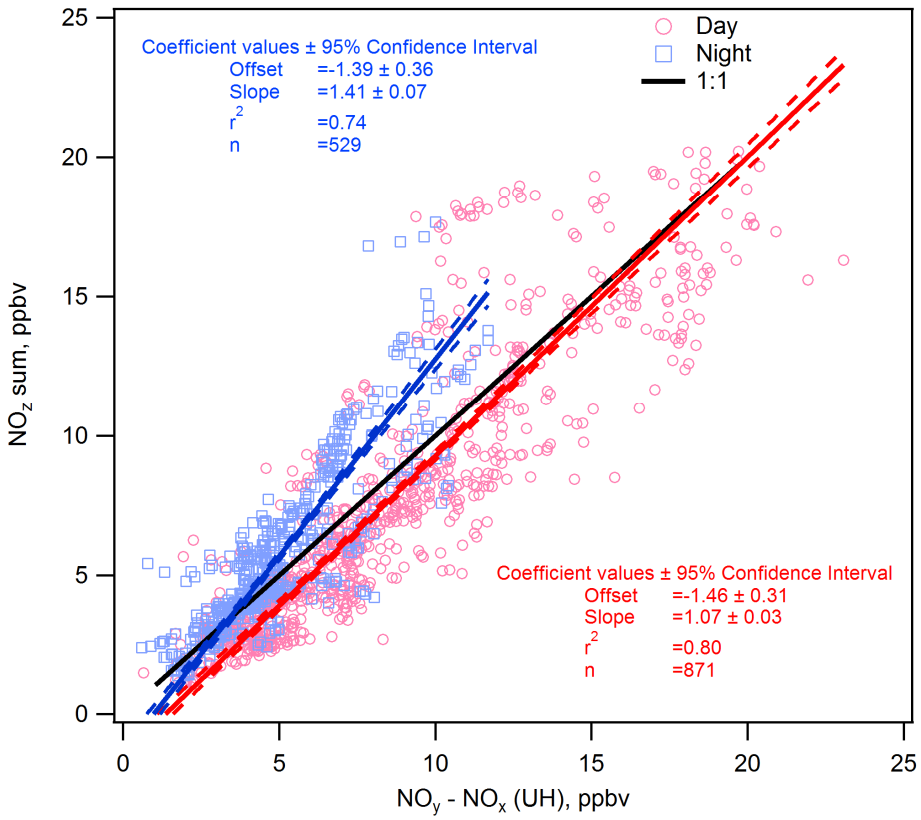

Figure 4-12. NO_z sum vs $NO_y - NO_x$ for day (red) and night (blue) using BLC + Chemi NO_2 in NO_x calculation.

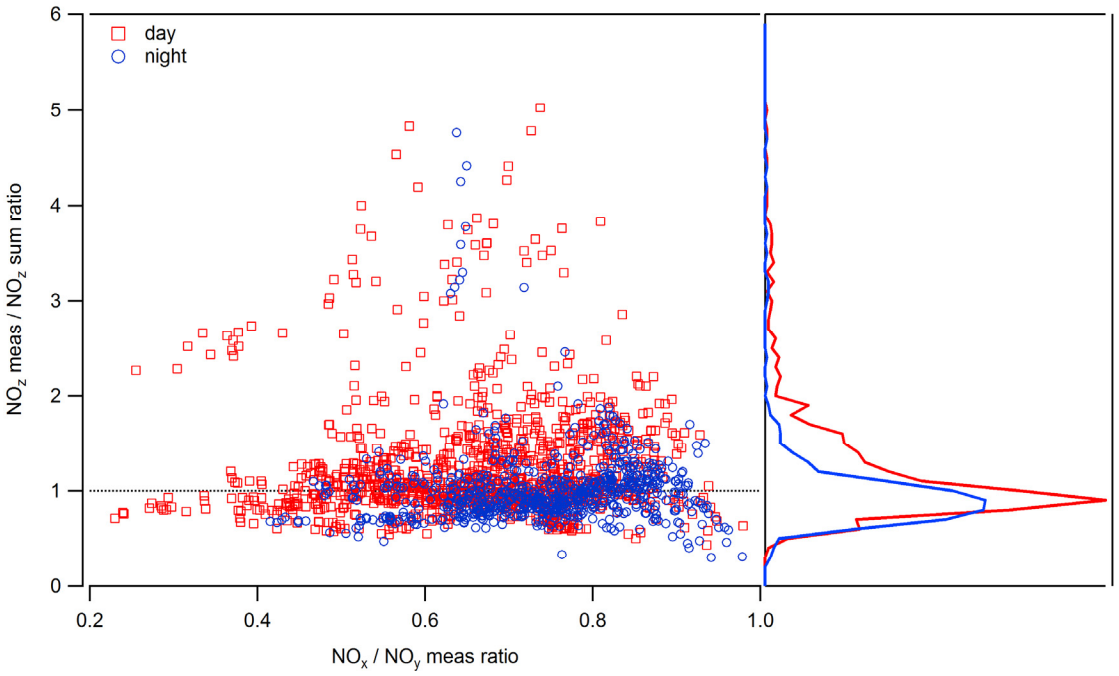

Figure 4-13. Ratio of NO_z measured (NO_y - NO_x) / NO_z sum vs NO_x/NO_y for day (red) and night (blue). Histogram for data distribution in right panel.

Plotting the NO_z measured/NO_z sum ratio against the NO_x/NO_y ratio can show whether there is a NO_z dependence on the photochemical age of the air mass. Figure 4-13 shows that the NO_z ratio does not seem to be affected by photochemical age during day or night. The distribution of the data are nominally centered on 1 for both day and night, indicating that there are no significant measurement artifacts impacting the majority of the NO_z ratios in either the day or night. The NO_z ratios greater than 2 tend to fall between May 22-25 and can be seen as differences in NO_y measured and NO_y sum in Figure 4-8. The histogram of day and night ratios does show a slight difference between day and night, which was also seen in the offsets in Figure 4-11. Plotting the NO_y-NO_x/NO_z sum ratio as a diurnal profile (Figure 4-14) along with the median profile of jNO_2 shows the clear trend indicating that there likely is undetermined interference in one or more of the measurements.

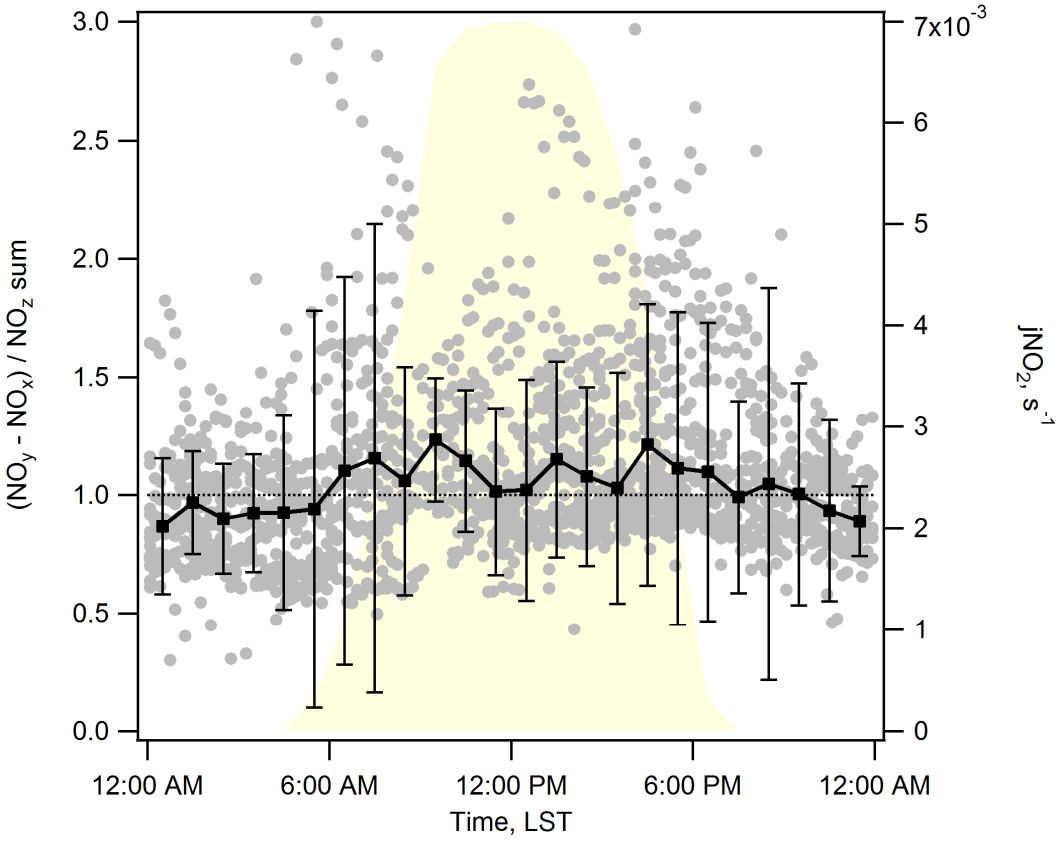

Figure 4-14. Average diurnal profile of $(NO_y\text{-}NO_x)/NO_z$ shows difference between day and night. Median jNO_2 is shown in pale yellow.

4.3.4 Average diurnal profiles of NO_y and NO_z species

The NO profile on intermediate and low days are quite similar throughout the day, but on the highest O_3 days NO is much lower during the day (Figure 4-15). NO_2 has a very similar profile on intermediate and low days, but is lowest on the highest O_3 days (Figure 4-16). Comparison of the CRDS (upper panel) and BLC+Chemi (lower panel) are similar on high and intermediate days but do show some differences on low O_3 days, most notably in the 3:00-9:00 AM and midday periods.

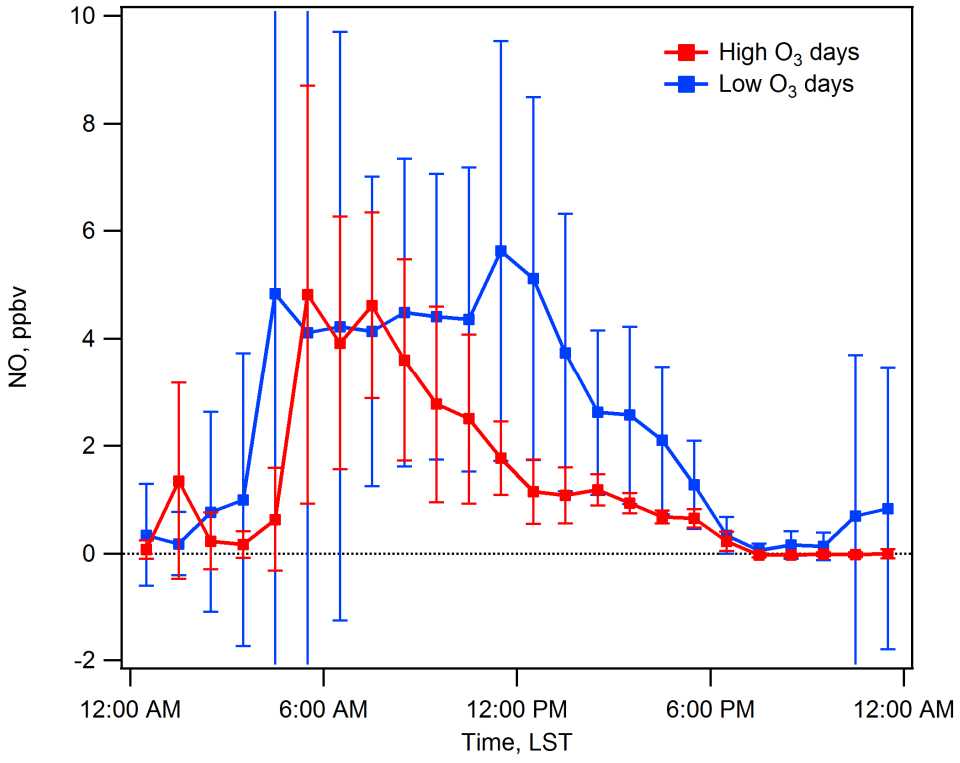

Figure 4-15. Average diurnal profile of NO on high and low O_3 days.

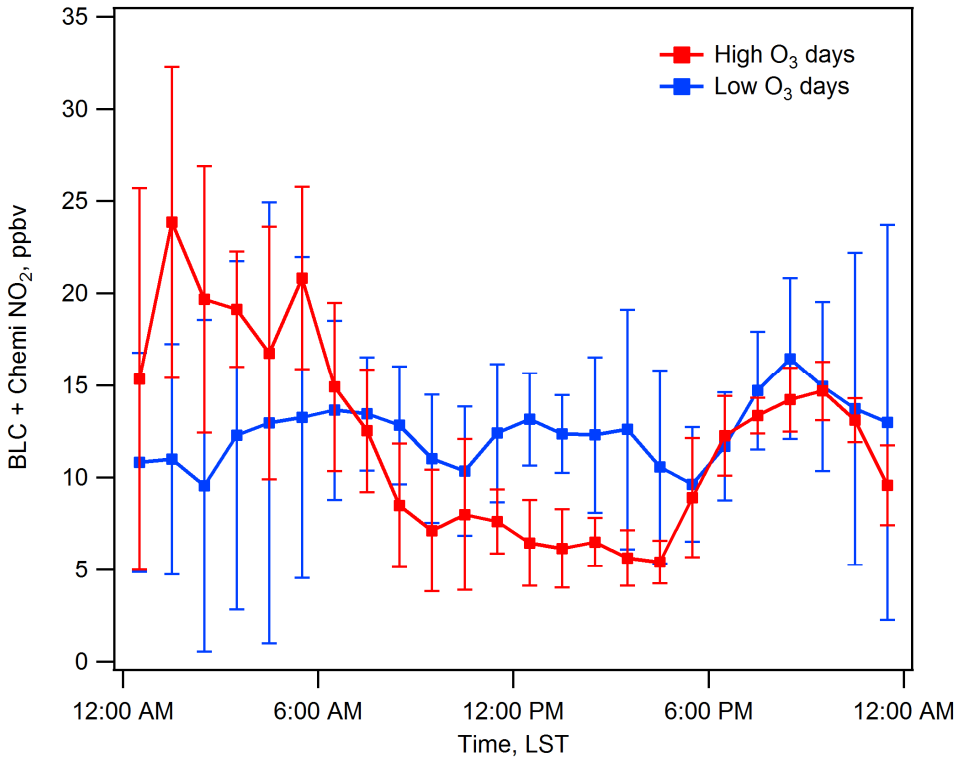

Figure 4-16. Average diurnal profile of BLC + Chemi NO_2 on high and low O_3 days.

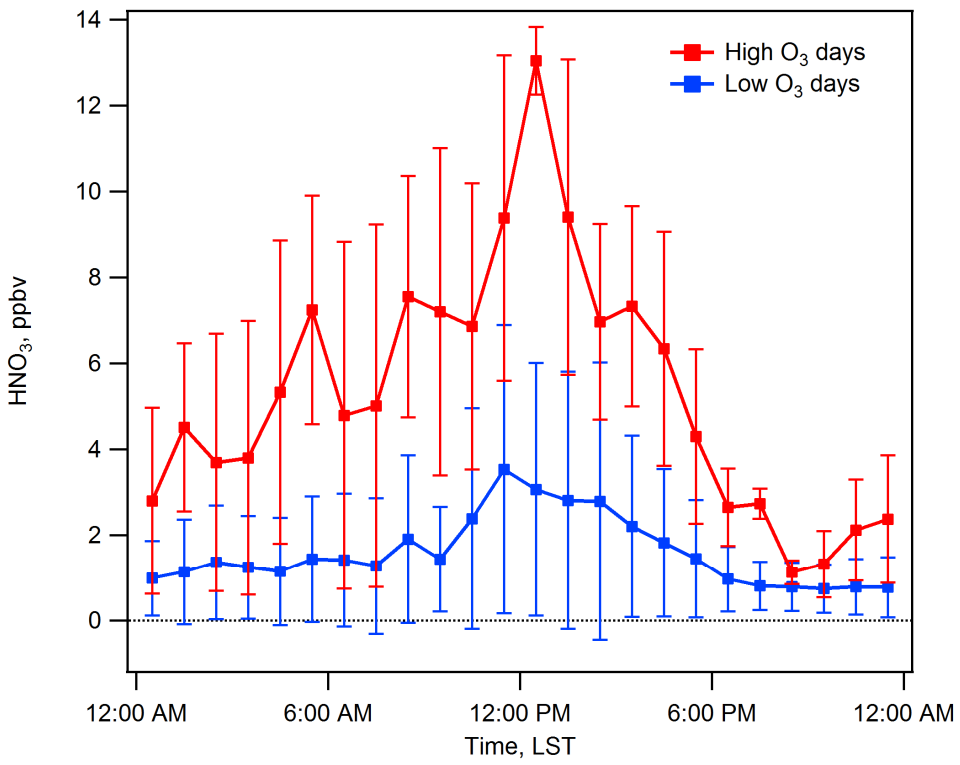

Figure 4-17. Average diurnal profile of HNO_3 on high and low O_3 days.

Both HNO_3 and PAN are key components of daytime NO_z and are formed photochemically during O_3 production. The average diurnal profile of HNO_3 shown in Figure 4-17 can comprise as much as 9-10 ppbv or 56% of median NO_y during midday on high O_3 days. The profiles for the three conditions for HNO_3 and PAN (Figure 4-18) follow the same relative diurnal profile as O_3 (Figure 4-25). The increased HNO_3 on high O_3 days is consistent with the dominant DO_3 feature seen on high O_3 days where HNO_3 formation rates approach 3 ppbv/hr.

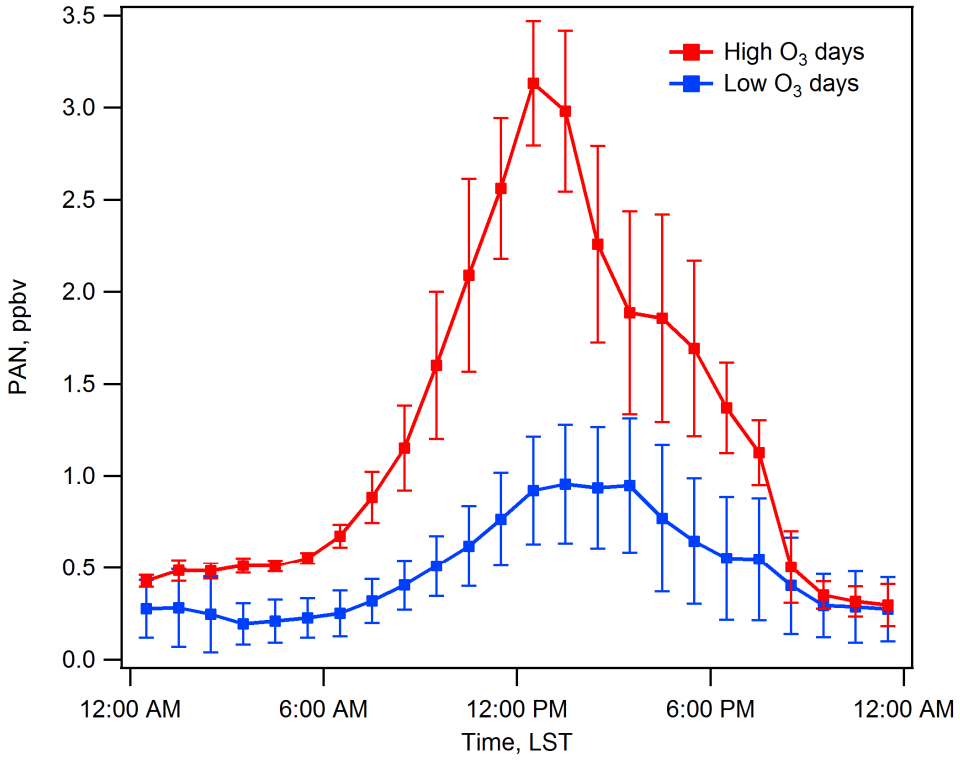

Figure 4-18. Average diurnal profile of PAN on high and low O_3 days.

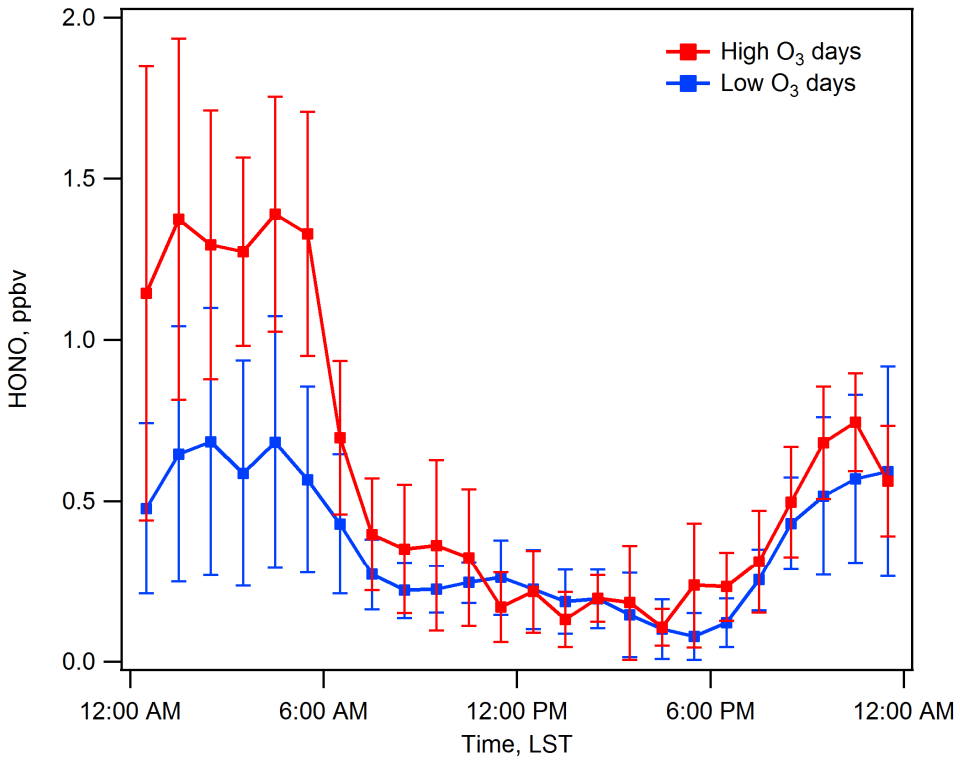

Figure 4-19. Average diurnal profile of HONO on high and low O_3 days.

HONO is easily photolyzed around sunrise and is an important source of OH radicals in the morning. Figure 4-19 shows that all three diurnal profiles for HONO show lower levels (typically 100-300 pptv) of HONO during daytime because of photolysis, with much greater mixing ratios (nominally 0.5-1.5 ppbv) at night. On high O_3 days HONO is ~2.5 times greater than on low O_3 days in the midnight to 6:00 AM timeframe.

4.4 DISCUSSION

4.4.1 NO_z differences

Figure 4-12 shows that the sum of the individual NO_z components adds to ~40% more than the calculated difference between NO_y and NO_x, especially at night. During the day the agreement is much better. The overall combined uncertainty for the sum of individual NO_z components is approximately 59% and is larger than the difference between the two NO_z values. During the day NO_z accounts for a higher fraction of NO_y than in the evenings (Figure 4-20, upper panel), and is dominated by HNO_3 (lower panel). HNO_3 is contributes less to the total NO_z at night while other species such as HONO, $ClNO_2$, and NO_3 that play minor roles during the day are more significant at night. Because daytime NO_z is primarily one component there are fewer opportunities for measurement errors to compound into larger values. At night both the absolute value and relative contribution of NO_z is smaller and is comprised of more species of relatively equal proportions. Because of this the opportunity for errors are greater (i.e. sum of multiple small numbers with large uncertainties) and likely explains the differences between the day and night NO_z agreement.

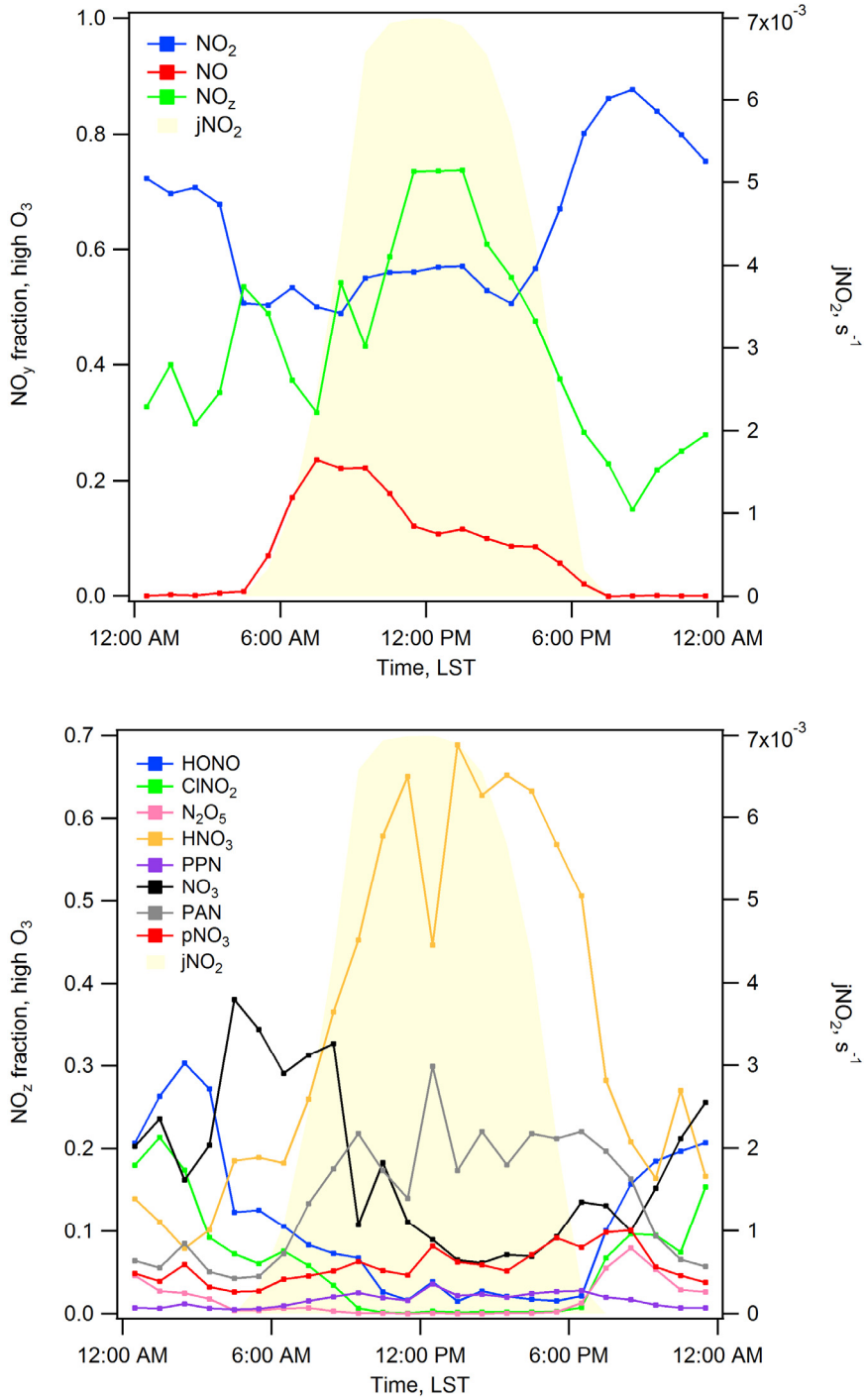

Figure 4-20. Median fraction of NO_y (upper panel) and NO_z (lower panel) for high O_3 days during CalNex.

4.4.2 Differences in classification methods

The data were separated based on the peak O_3 values for each day and by weekdays and weekends (Figure 4-21). The high days were defined as days with peak 8-hour averaged $O_3 \geq 70$ ppbv (3 days) while low days had 8-hour averaged $O_3 < 50$ ppbv (16 days). May 16th was excluded from the analysis because data was not reported for the full day. The sensitivity of O_3 production due to changes in emissions on weekdays and weekends were examined by Pollack et al. (2012) and found that on average O_3 was 22 ± 6 ppbv higher on weekends than on weekdays, while NO_y tended to be ~52% greater on weekdays. Memorial Day (Monday, May 31) was excluded from their analysis, but it was included with the weekend data for this work since it was not a regular business day for most people (Figure 4-21, upper stripe), giving 9 weekend days and 20 weekdays.

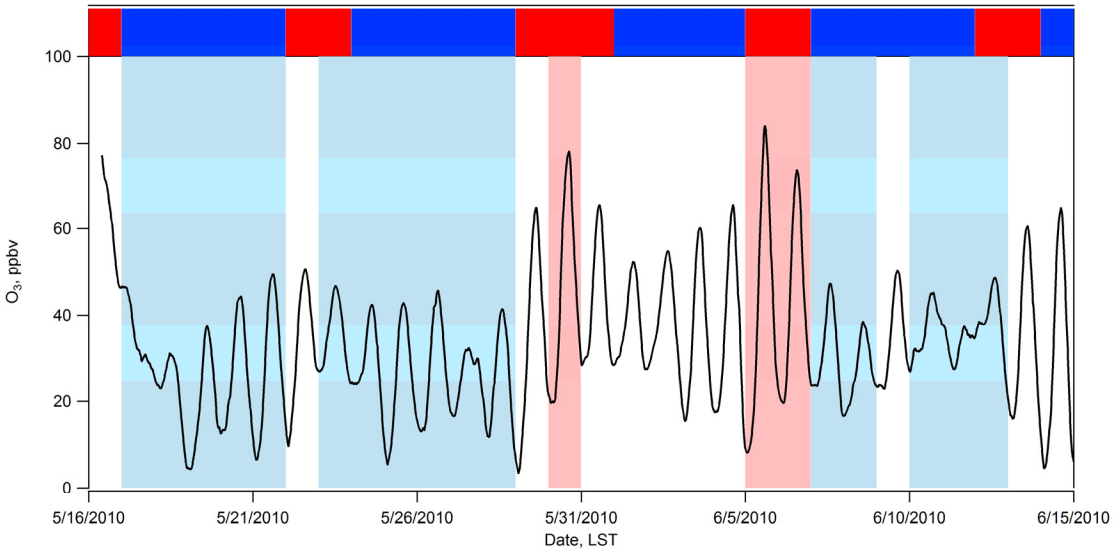

Figure 4-21. Time series of 8-hour averaged O_3. Background shading indicates high (pink) and low O_3 days (light blue). The upper stripe of the graph indicates weekdays (dark blue) and weekends including Memorial Day (red).

In general, most, but not all high O_3 days fell on weekends in the middle of the project. Additionally, there were low and intermediate days on weekends and high O_3 days on weekdays. Classifying days by measured O_3 levels incorporates several factors in the results such as meteorology, emissions, and solar radiation. Classifying days based only by weekdays and weekends can capture patterns in vehicle emissions but ignores other important controls on ambient O_3 levels. The relationship between wind speed and peak O_3 values is shown in Figure 4-22 where the average 1-hour peak O_3 values are plotted against the corresponding wind speeds binned by 0.5 m/s. This figure shows that during CalNex, peak O_3 decreased with increasing wind speeds above 1.5 m/s. The two days with the lowers wind speeds were also affected by overcast conditions which reduced jNO$_2$, and therefore O_3 production, by 50% or more compared to clear sky conditions. By grouping days based on measured O_3 rather than the day of week, these effects can be accounted for. This difference is illustrated in Figure 4-23 where wind speeds are plotted against measured O_3 for the two approaches for classification of the type of day. The upper panel shows that wind speeds above 3 m/s are exclusively associated with low O_3 days and the highest O_3 measurements are only found with wind speeds less than 2 m/s. If the days are classified by weekdays and weekends as in Pollack et al. (2012), the weekends can include low O_3 days with relatively high wind speeds, and high O_3 days with low wind speeds are included in the weekday classification. This highlights the need to understand the benefits and limitations of the types of classification applied when interpreting the results.

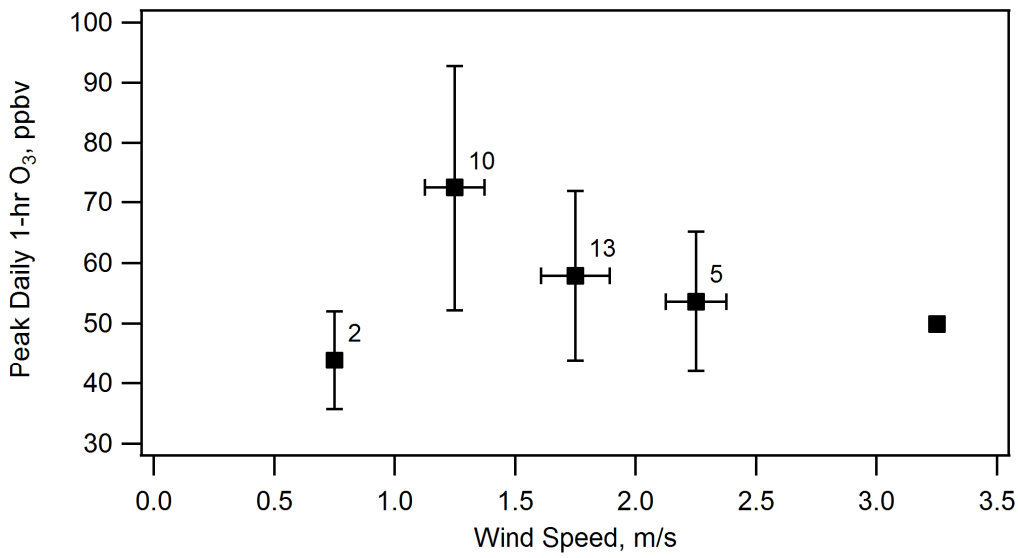

Figure 4-22. Average peak 1-hour O_3 vs. wind speeds binned by 0.5 m/s. Error bars show 1 standard deviation. Values with each point indicate the number of days in each bin.

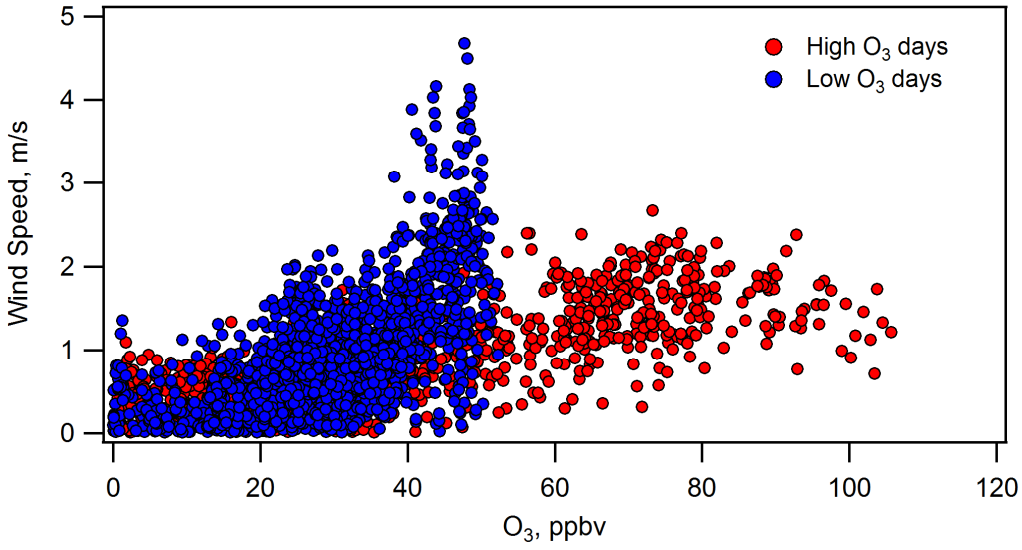

Figure 4-23. Wind speeds vs. O_3 10-minute averages for high and low O_3 days.

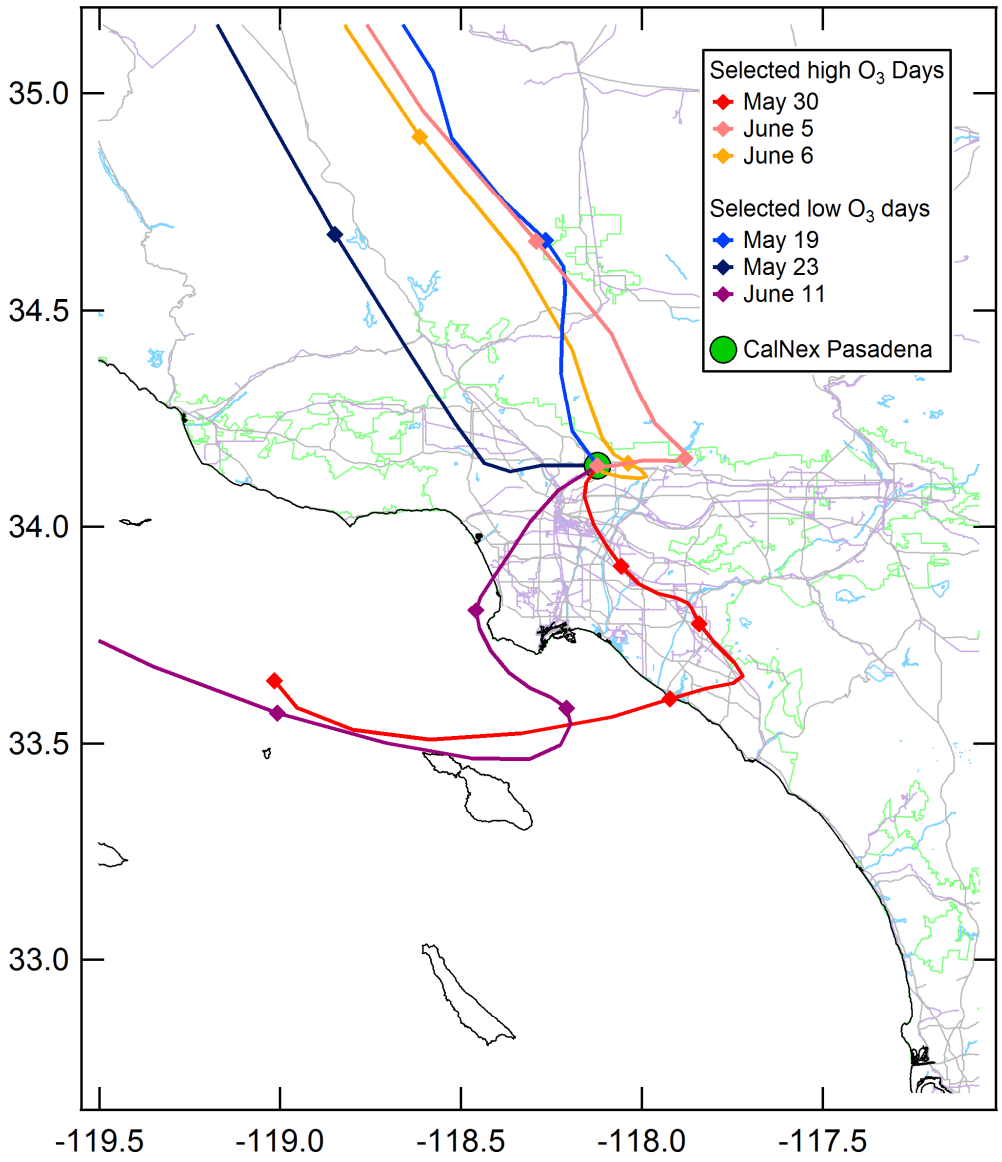

Figure 4-24. 24-hour HYSPLIT back trajectories beginning at noon local time for three low and high O_3 days. Markers are shown every 6 hours prior to noon.

Back trajectories for three high and low O_3 days are shown in Figure 4-24. On the high O_3 days all of the air masses that reached the Pasadena ground site were over the LA basin urban area for at least the previous 6 hours and only travel ~8-27 km during that period. On low O_3 days the air masses travel significantly faster and consequently

covered greater distance in the six hours prior to reaching the measurement site (49-89 km). This is consistent with the dependence of O_3 on wind speeds shown in Figure 4-22 and Figure 4-23. Additional trajectory modeling reported by Neuman, et al. (2012) found that on the last day of measurements, May 16, also a high O_3 day, recirculation of air over the LA basin for several days resulted in stagnated conditions allowing pollutants to build in the region.

The average diurnal profiles of O_3 for both classification methods are shown in Figure 4-25. The highest O_3 days have peak values approaching 100 ppbv while low O_3 days are roughly half that. The weekend peak O_3 levels are closer to 80 ppbv. Although O_3 levels during the late evenings are similar, the 12:00-6:00 AM time period shows that O_3 is lower on high O_3 days. This is likely a change in partitioning of O_x since NO_2 is higher on high O_3 days.

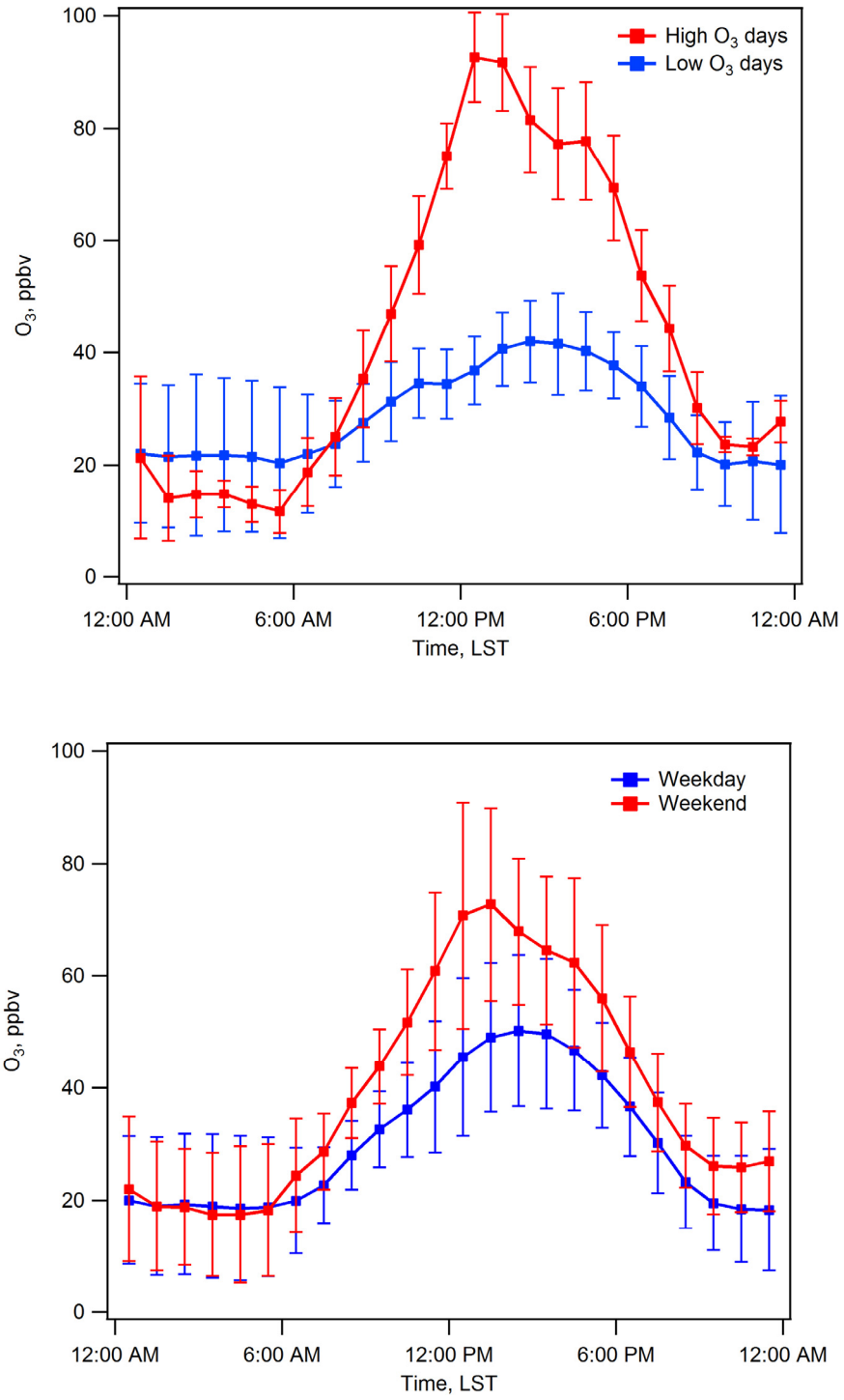

Figure 4-25. Upper Panel: Average diurnal profile of O_3 on high and low O_3 days. Lower Panel: Average diurnal profile of O_3 on 20 weekdays and 9 weekend days. Memorial Day was included in the weekend profile.

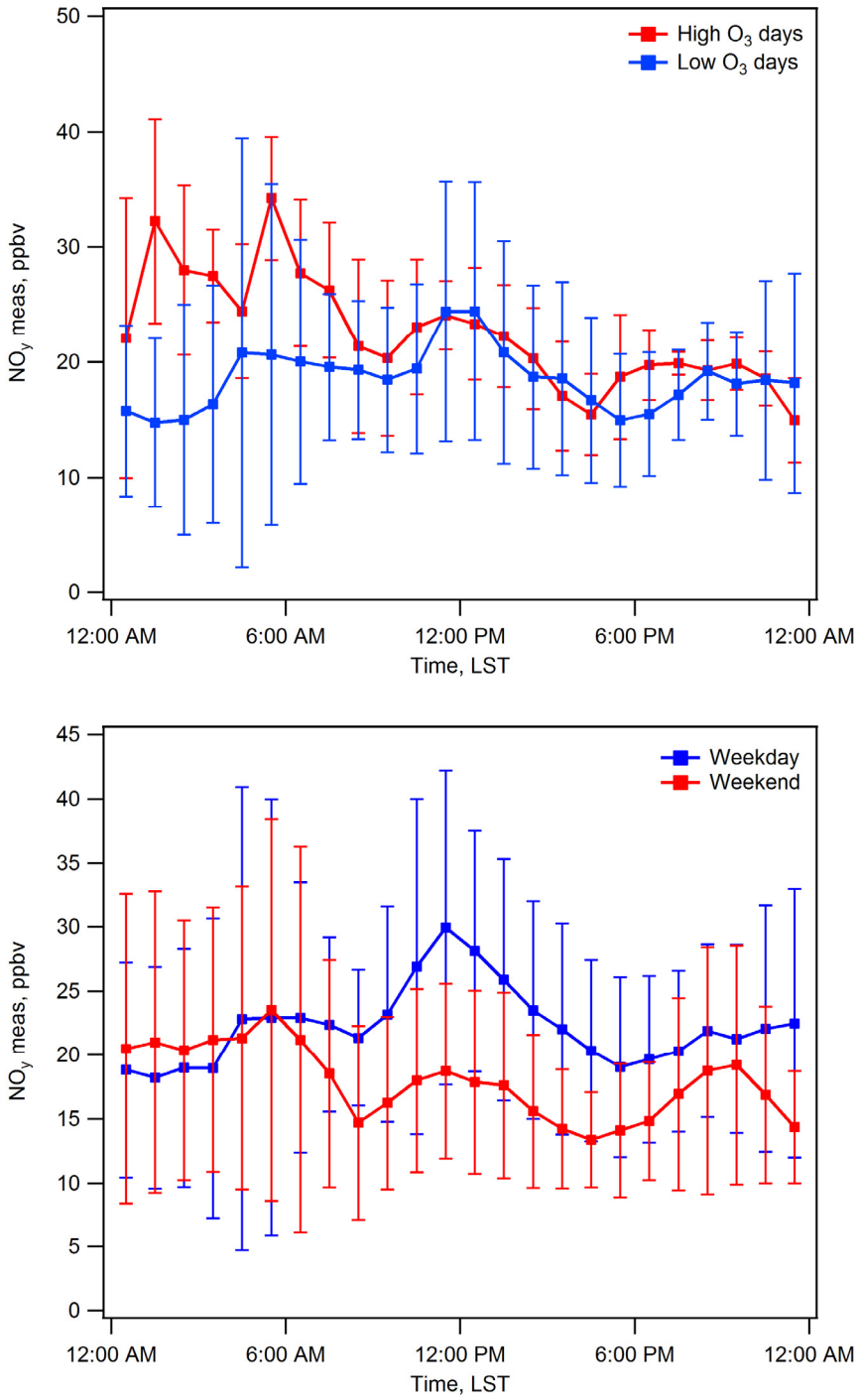

Figure 4-26. Upper Panel: Average diurnal profile of NO_y on high and low O_3 days. Lower Panel: Average diurnal profile of NO_y on weekdays and weekends. Memorial Day was included in the weekend profile.

Differences in the classification approach are also evident in the average

measured NO_y diurnal profiles shown in Figure 4-26. Midday differences in NO_y

between high and low O_3 days are less clear than when divided by weekdays and weekends. For each of the classifications, all days show an increase in NO_y during the middle of the day that is likely related to morning emissions from the LA basin being transported to Pasadena later in the day. In this way Pasadena acts as a receptor site for processed air from the LA basin.

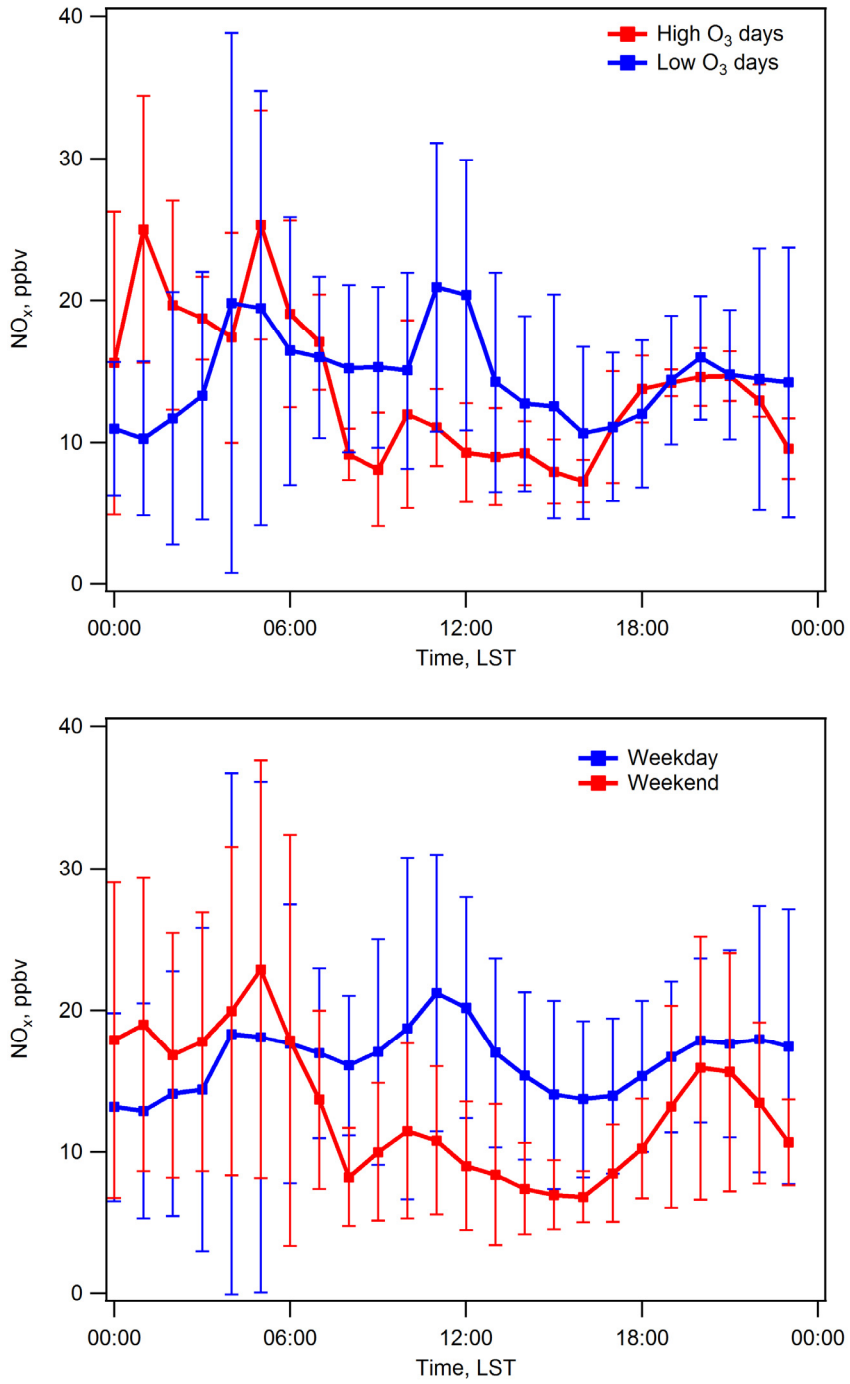

Figure 4-27. Upper Panel: Average diurnal profile of NO_x on high and low O_3 days. Lower Panel: Average diurnal profile of NO_x on weekdays and weekends. Memorial Day was included in the weekend profile.

The NO_x profile for high/low days generally agrees with the weekday/weekend split. Given that NO_y differences are less clear, elevated NO_z on high O_3 days is

responsible for the relative uniformity of NO_y when separating days by O_3 levels (Figure 4-27). However, there are still significant differences in NO_x when comparing the classification method. On weekdays and weekends, NO_x accounts for approximately $^2/_3$ of NO_y at midday. Using O_3 to classify the day type finds that on low O_3 days, NO_y is composed almost entirely of of NO_x at midday and on the three highest O_3 days NO_x comprises only $\sim^1/_3$ of NO_y, indicating that the air masses sampled on high O_3 days is much more photochemically processed prior to reaching the Pasadena ground site.

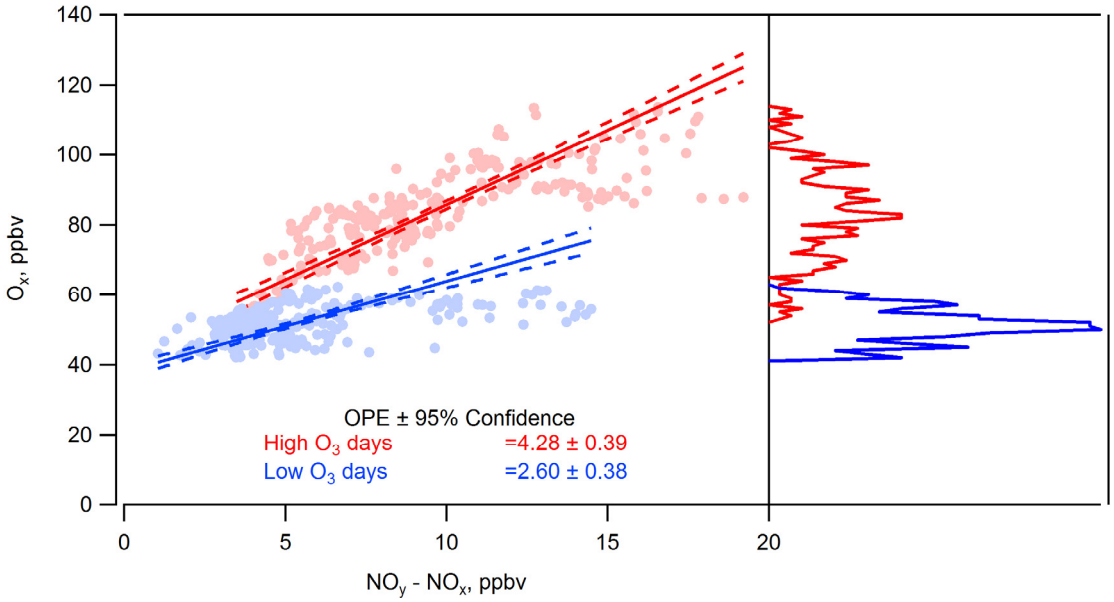

Figure 4-28. O_3 production efficiency for afternoons during CalNex using different classifications. The right portion of the figure shows the distribution of data points for each classification method.

Ozone production efficiency (OPE) is a measure of the amount of O_3 produced per NO_x consumed. There are significant differences in the calculated OPE depending on the classification method as seen in Figure 4-28 for data between noon and 6:00 PM LST. As expected, when classifying based on O_3 level, the days with the highest O_3 also have the highest OPE (4.28 ± 0.39) and the low O_3 days have the lowest OPE (2.60 ± 0.38).

OPEs calculated for data separated by weekdays and weekends again find different results, 4.59 ± 0.33 and 5.69 ± 0.31, respectively. These are consistent with the Pollack's findings that the weekend OPE is greater than on weekdays. The weekday OPE is higher than the highest OPE when classifying by O_3 level. Because not all weekends are high O_3 days, data points from low O_3 weekend days shifts the low end of the fit towards lower O_3 values while the high points remain somewhat unchanged, resulting in a steeper slope (higher OPE). Similarly, because some weekdays do have high O_3, the slope of the fit is pulled higher because of these points, again resulting in a higher OPE. The inclusion of low O_3 on weekends and high O_3 on weekdays is easily seen in the distribution of data points in the right portions of Figure 4-28 where the weekday-weekend distributions cover broader ranges of O_3 than does the distributions based on peak O_3 levels. Since classifying by peak O_3 separates the high and low O_3 conditions by definition, a clearer picture of the actual OPE can be found for these periods.

4.5 CONCLUSIONS

This chapter presented the results and analysis of NO_y and numerous NO_y species from the CalNex campaign in Pasadena, CA during May and June 2010. Collocated measurements of NO_2 by both BLC+Chemi and CRDS agreed very well (slope 1.00 ± 0.008, r^2 0.978) but there were some unresolved differences during daylight hours that may be related to O_3 interferences with the CRDS method.

Measurements of NO_y and calculated NO_y sum also agree well (slope 1.03 ± 0.008, r^2 0.97) and are comparable to recent measurements where similar NO_y species

were measured. Potential interferences by NH_3 conversion in the molybdenum NO_y converter did not appear to have a significant impact, which may be related to the operating temperature of 300ºC and that a new converter was used in these measurements.

Agreement between NO_z sum and NO_y-NO_x is not as good (slope 1.42 for night and 1.07 during the day) as for NO_2 and NO_y when using BLC+Chemi NO_2, but in both cases were less than the combined uncertainty of NO_z sum. The difference between day and night NO_z agreements is likely due to daytime NO_z having larger absolute values and being dominated by just one species, HNO_3, as compared to nighttime when NO_z levels are lower and comprised of several smaller components, increasing the opportunity for measurement errors to compound and become more significant. Findings during TRAMP using similar NO_z species found better agreement, especially during the day. For this study the NO_z agreement during the day and night was found not to be dependent on the photochemical age of the air mass.

Finally, it is important to consider the method for classifying days for analysis because classifications can ignore important factors that impact ambient O_3 levels, such as wind speeds. Results differ when dividing conditions by weekdays and weekends compared to classification based on measured peak O_3 levels. Splitting days into weekdays and weekends can be used to differentiate days primarily based on mobile emissions, and in doing so finds that NO_x levels are lower on weekends and are correlated with higher O_3. However, classification of days by peak O_3 finds that not all days with high O_3 occur on weekends, and not all weekends have high O_3. Back trajectories on high O_3 days show

that the air mass spent at least six hours over the LA basin prior to reaching the site, while the air mass travelled much further in the last 6 hours on low O_3 days. The distances traveled are consistent with the finding that increases in wind speed above 1.5 m/s were correlated with lower peak O_3 levels.

The calculated OPE also showed a dependence on the classification method used. OPEs classified by peak daily O_3 ranged between 4.28 ± 0.39 on the highest three days and 2.60 ± 0.38 for the low O_3 days. These differences stem from the fact that high and low O_3 conditions are both found on weekdays and weekends.

4.6 REFERENCES

Day, D. A., M. B. Dillon, P. J. Wooldridge, J. A. Thornton, R. S. Rosen, E. C. Wood, and R. C. Cohen (2003), On alkyl nitrates, O-3, and the "missing NOy", *Journal of Geophysical Research-Atmospheres*, *108*(D16), 10, doi:10.1029/2003jd003685.

Dunlea, E. J., et al. (2007), Evaluation of nitrogen dioxide chemiluminescence monitors in a polluted urban environment, *Atmospheric Chemistry and Physics*, *7*(10), 2691-2704.

Fitz, D. R., K. Bumiller, and A. Lashgari (2003), Measurement of NOY during the SCOS97-NARSTO, *Atmospheric Environment*, *37*, S119-S134, doi:10.1016/s1352-2310(03)00385-6.

Fuchs, H., et al. (2010), Intercomparison of measurements of NO2 concentrations in the atmosphere simulation chamber SAPHIR during the NO3Comp campaign, *Atmospheric Measurement Techniques*, *3*(1), 21-37.

Geddes, J. A., J. G. Murphy, and D. K. Wang (2009), Long term changes in nitrogen oxides and volatile organic compounds in Toronto and the challenges facing local ozone control, *Atmospheric Environment*, *43*(21), 3407-3415, doi:10.1016/j.atmosenv.2009.03.053.

Luke, W. T., P. Kelley, B. L. Lefer, J. Flynn, B. Rappengluck, M. Leuchner, J. E. Dibb, L. D. Ziemba, C. H. Anderson, and M. Buhr (2010), Measurements of primary trace gases and NO(y) composition in Houston, Texas, *Atmospheric Environment*, *44*(33), 4068-4080, doi:10.1016/j.atmosenv.2009.08.014.

Neuman, J. A., et al. (2002), Fast-response airborne in situ measurements of HNO3 during the Texas 2000 Air Quality Study, *Journal of Geophysical Research-Atmospheres*, *107*(D20), doi:10.1029/2001jd001437.

Neuman, J. A., et al. (2012), Observations of ozone transport from the free troposphere to the Los Angeles basin, *Journal of Geophysical Research-Atmospheres*, *117*, doi:10.1029/2011jd016919.

Pollack, I. B., B. M. Lerner, and T. B. Ryerson (2010), Evaluation of ultraviolet light-emitting diodes for detection of atmospheric NO2 by photolysis - chemiluminescence, *Journal of Atmospheric Chemistry*, *65*(2-3), 111-125, doi:10.1007/s10874-011-9184-3.

Pollack, I. B., et al. (2012), Airborne and ground-based observations of a weekend effect in ozone, precursors, and oxidation products in the California South Coast Air Basin, *Journal of Geophysical Research-Atmospheres*, *117*, doi:10.1029/2011jd016772.

Ryerson, T. B., L. G. Huey, K. Knapp, J. A. Neuman, D. D. Parrish, D. T. Sueper, and F. C. Fehsenfeld (1999), Design and initial characterization of an inlet for gas-phase NOy

measurements from aircraft, *Journal of Geophysical Research-Atmospheres*, *104*(D5), 5483-5492, doi:10.1029/1998jd100087.

Ryerson et al. (2013), The 2010 California research at the Nexus of air quality and climate change (CalNex) field study, *Journal of Geophysical Research-Atmospheres*, in press, doi: 10.1002/jgrd.50331

Sather, M. E., E. T. Slonecker, K. G. Kronmiller, D. D. Williams, H. Daughtrey, and J. Mathew (2006), Evaluation of short-term Ogawa passive, photolytic, and federal reference method sampling devices for nitrogen oxides in El Paso and Houston, Texas, *Journal of Environmental Monitoring*, *8*(5), 558-563, doi:10.1039/b601113f.

Schultz, M. G., D. J. Jacob, J. D. Bradshaw, S. T. Sandholm, J. E. Dibb, R. W. Talbot, and H. B. Singh (2000), Chemical NOx budget in the upper troposphere over the tropical South Pacific, *Journal of Geophysical Research-Atmospheres*, *105*(D5), 6669-6679, doi:10.1029/1999jd900994.

Williams, E. J., J. M. Roberts, K. Baumann, S. B. Bertman, S. Buhr, R. B. Norton, and F. C. Fehsenfeld (1997), Variations in NOy composition at Idaho Hill, Colorado, *Journal of Geophysical Research-Atmospheres*, *102*(D5), 6297-6314, doi:10.1029/96jd03252.

Xue, L. K., et al. (2011), Source of surface ozone and reactive nitrogen speciation at Mount Waliguan in western China: New insights from the 2006 summer study, *Journal of Geophysical Research-Atmospheres*, *116*, doi:10.1029/2010jd014735.

5. GENERAL CONCLUSIONS

This work presented the results and analysis of measurements collected during several field campaigns in Houston, TX between 2006 and 2012, as well as in Pasadena, CA (CalNex) in the summer of 2010.

Measurements at the Moody Tower and the Launch Trailer show good agreement between O_3 and O_x at both sites during the afternoon. This agreement is largely due to the strong vertical mixing present in the afternoons and the close proximity of the sites. Differences between the two sites are largest at night and in the early morning when vertical mixing is weakest, sometimes causing a decoupling between the two measurement heights. The relationships seen in the in situ data are supported by measurements of O_3 and NO_2 from the Moody Tower by LP-DOAS which also show that O_x is conserved over broad area and range of altitudes. Titration of O_3 to NO_2 accounts for approximately 50% of the observed differences at night between O_3 measured at the two heights. Since these differences occur in the overnight and early morning hours, variations in O_3 production can be ruled out, leaving dry deposition and other reactions to account for the remainder of the difference. The morning rate of increase in O_x can be significantly different than that for O_3. In some cases, O_3 can increase at ~40 ppbv/hr while O_x remains constant, an indication that in these situations the observed increase in O_3 is due to a change in Ox partitioning.

Additionally, significant differences were seen between O_3 measurements at the Moody Tower and some Houston area O_3 monitors during 2010 and 2011when values would be expected to be comparable, in particular the City of Houston sites. Under the

same conditions other monitors operated by the TCEQ agreed well with the Moody Tower, even at greater distances. The differences observed between the City of Houston sites and the Moody Tower appears to have improved when examining the measurements from 2012, possibly indicating that a change in operation method or calibration took place.

Two late summer campaigns in Houston, TRAMP (2006) & MT2010 (2010), have similar median PO_3 values and profile shapes, peaking ~1-2 hours before noon, however MT2010 lacks the extremely high PO_3 and reactivity seen during TRAMP. Losses due to O_3+NMHC are highest during the TRAMP campaign and lower in both SHARP and MT2010. Peak PO_3 on high O_3 days has shifted from 5-10 ppbv NO in TRAMP closer to 1-2 ppbv for SHARP and MT2010, an indication that the point at which the system becomes NO_x-saturated is occurring at lower levels than during TRAMP. Together, these factors tend to point to reductions in emissions of VOCs and a shift towards a more NO_x-saturated regime. The diurnal profiles of reactivity peak in early morning and decreases through the day during both TRAMP & MT2010 but remains flat during SHARP. In Houston, the highest reactivity and PO_3 are associated with easterly winds, indicating the ship channel as the VOC emission source. The spring 2009 SHARP campaign had the lowest reactivity and PO_3 under all conditions when compared to either of the two late summer measurement periods.

At the Pasadena ground site during CalNex, PO_3 follows reactivity, peaking mid-day through early afternoon when the morning rush hour plume reaches Pasadena. Compared to Houston, the median PO_3 on high O_3 days was about 5 ppbv higher than TRAMP and

MT2010, however O_3 losses by HNO_3 formation accounts for a higher percentage of the overall loss rates than in Houston. The reactivity vs. NO_2 plot would indicate that PO_3 at the Pasadena ground site during the CalNex campaign was NO_x-saturated. The most efficient way to reduce PO_3 in Houston and Los Angeles would be to reduce VOC reactivity.

During the CalNex campaign in Pasadena, collocated measurements of NO_2 by both BLC+Chemi and CRDS agreed very well (slope 1.00 ± 0.008, r^2 0.978) but there were some unresolved differences during daylight hours that may be related to O_3 interferences with the CRDS method. Measurements of NOy and calculated NOy sum also agreed well (slope 1.03 ± 0.008, r^2 0.97) and were comparable to recent measurements where similar NOy species were measured. Potential interferences by NH_3 conversion in the molybdenum NOy converter did not appear to have a significant impact which may be related to the operating temperature of 300ºC and that new converter was used in these measurements. Agreement between NOz sum and NOy-NOx was not as good (slope 1.42 for night and 1.37 during the day) as for NO_2 and NOy when using CRDS measured NO_2. Because of the daytime differences in NO_2, NOy-NOx values were dependent on the choice of NO_2 measurement method. Using BLC+Chemi NO_2, the daytime NOz agreement with NOy-NOx improved ~30%. Findings during TRAMP using similar NOz species found better agreement, especially during the day. The NOz agreement during the day and night was found not to be dependent on the photochemical age of the air mass.

Finally, it is important to consider the method for classifying days during analysis because some methods can ignore important factors that impact ambient O_3 levels such as wind speeds. Different results were found when dividing conditions by weekdays and weekends compared to classification of days based on measured peak O_3 levels. Splitting days into weekdays and weekends can be used to differentiate days primarily based on mobile emissions and in doing so finds that NOx levels are lower on weekends and are correlated with higher O_3. Comparing this classification approach to separating days by the peak O_3 finds that not all days with high O_3 occur on weekends. Back trajectories on high O_3 days show that the air mass spent at least six hours over the LA basin prior to reaching the site. On low O_3 days the air masses traveled much further and generally from cleaner source regions. This is consistent with the finding that increases in wind speed above 1.5 m/s were correlated with lower peak O_3 levels. The calculated OPE also showed a dependence on the classification method used. OPEs classified by peak daily O_3 ranged between 4.28 ± 0.39 on the highest three days and 2.60 ± 0.38 for the low O_3 days. Separating the days instead by weekday and weekend finds OPEs of 5.69 ± 0.31 and 4.59 ± 0.33, respectively. These differences stem from the fact that there high and low O_3 conditions are both found on weekdays and weekends.

The findings presented here have broader impacts on society and the environment. The sensitivity of O_3 production to changes in VOCs and VOC reactivity can be used by regulators to show the effectiveness of existing reductions, and as a basis for further reductions. Additionally, the close coupling between NO_2 and O_3 shows the need to measure both species to have a more complete picture of photochemical conditions.

6. COMPLETE REFERENCES

Buzcu, B., and M. P. Fraser (2006), Source identification and apportionment of volatile organic compounds in Houston, TX, *Atmospheric Environment*, *40*(13), 2385-2400, doi:10.1016/j.atmosenv.2005.12.020.

Chen, S. A., X. R. Ren, J. Q. Mao, Z. Chen, W. H. Brune, B. Lefer, B. Rappengluck, J. Flynn, J. Olson, and J. H. Crawford (2010), A comparison of chemical mechanisms based on TRAMP-2006 field data, *Atmospheric Environment, 44*(33), 4116-4125, doi:10.1016/j.atmosenv.2009.05.027.

Crawford, J., et al. (1999), Assessment of upper tropospheric HOx sources over the tropical Pacific based on NASA GTE/PEM data: Net effect on HOx and other photochemical parameters, *Journal of Geophysical Research-Atmospheres, 104*(D13), 16255-16273, doi:10.1029/1999jd900106.

Dasgupta, P. K., J. Z. Li, G. F. Zhang, W. T. Luke, W. A. McClenny, J. Stutz, and A. Fried (2005), Summertime ambient formaldehyde in five US metropolitan areas: Nashville, Atlanta, Houston, Philadelphia, and Tampa, *Environmental Science & Technology, 39*(13), 4767-4783, doi:10.1021/es048327d.

Day, D. A., M. B. Dillon, P. J. Wooldridge, J. A. Thornton, R. S. Rosen, E. C. Wood, and R. C. Cohen (2003), On alkyl nitrates, O-3, and the "missing NOy", *Journal of Geophysical Research-Atmospheres*, *108*(D16), 10, doi:10.1029/2003jd003685.

de Gouw, J., and C. Warneke (2007), Measurements of volatile organic compounds in the earths atmosphere using proton-transfer-reaction mass spectrometry, *Mass Spectrometry Reviews, 26*(2), 223-257, doi:10.1002/mas.20119.

Dunlea, E. J., et al. (2007), Evaluation of nitrogen dioxide chemiluminescence monitors in a polluted urban environment, *Atmospheric Chemistry and Physics*, *7*(10), 2691-2704.

Esteve, W., H. Budzinski, and E. Villenave (2006), Relative rate constants for the heterogeneous reactions of NO2 and OH radicals with polycyclic aromatic hydrocarbons adsorbed on carbonaceous particles. Part 2: PAHs adsorbed on diesel particulate exhaust SRM 1650a, *Atmospheric Environment*, *40*(2), 201-211, doi:10.1016/j.atmosenv.2005.07.053.

Fitz, D. R., K. Bumiller, and A. Lashgari (2003), Measurement of NOY during the SCOS97-NARSTO, *Atmospheric Environment*, *37*, S119-S134, doi:10.1016/s1352-2310(03)00385-6.

Flynn, J., et al. (2010), Impact of clouds and aerosols on ozone production in Southeast Texas, *Atmospheric Environment*, *44*(33), 4126-4133, doi:10.1016/j.atmosenv.2009.09.005.

Fuchs, H., W. P. Dube, B. M. Lerner, N. L. Wagner, E. J. Williams, and S. S. Brown (2009), A sensitive and versatile detector for atmospheric NO2 and NOx based on blue diode laser cavity ring-down spectroscopy, *Environmental Science & Technology, 43*(20), 7831-7836, doi:10.1021/es902067h.

Fuchs, H., et al. (2010), Intercomparison of measurements of NO2 concentrations in the atmosphere simulation chamber SAPHIR during the NO3Comp campaign, *Atmospheric Measurement Techniques*, *3*(1), 21-37.

Geddes, J. A., J. G. Murphy, and D. K. Wang (2009), Long term changes in nitrogen oxides and volatile organic compounds in Toronto and the challenges facing local ozone control, *Atmospheric Environment*, *43*(21), 3407-3415, doi:10.1016/j.atmosenv.2009.03.053.

Geddes, J. A., Observations of reactive nitrogen oxides: From urban ground level ozone production to biosphere-atmosphere exchange in downwind forest environments, Dissertation, University of Toronto, 2013.

Haman, C. L., B. Lefer, and G. A. Morris (2012), Seasonal variability in the diurnal evolution of the boundary layer in a near-coastal urban environment, *Journal of Atmospheric and Oceanic Technology*, *29*(5), 697-710, doi:10.1175/jtech-d-11-00114.1.

Heland, J., J. Kleffmann, R. Kurtenbach, and P. Wiesen (2001), A new instrument to measure gaseous nitrous acid (HONO) in the atmosphere, *Environmental Science & Technology, 35*(15), 3207-3212, doi:10.1021/es000303t.

Holloway, J. S., R. O. Jakoubek, D. D. Parrish, C. Gerbig, A. Volz-Thomas, S. Schmitgen, A. Fried, B. Wert, B. Henry, and Drummond, Jr. (2000), Airborne intercomparison of vacuum ultraviolet fluorescence and tunable diode laser absorption measurements of tropospheric carbon monoxide, *Journal of Geophysical Research-Atmospheres, 105*(D19), 24251-24261, doi:10.1029/2000jd900237.

Jenkin, M. E. (2004), Analysis of sources and partitioning of oxidant in the UK - Part 1: the NOX-dependence of annual mean concentrations of nitrogen dioxide and ozone, *Atmospheric Environment*, *38*(30), 5117-5129, doi:10.1016/j.atmosenv.2004.05.056.

Karl, T., T. Jobson, W. C. Kuster, E. Williams, J. Stutz, R. Shetter, S. R. Hall, P. Goldan, F. Fehsenfeld, and W. Lindinger (2003), Use of proton-transfer-reaction mass spectrometry to characterize volatile organic compound sources at the La Porte super site during the Texas Air Quality Study 2000, *Journal of Geophysical Research-Atmospheres, 108*(D16), doi:10.1029/2002jd003333.

Lefer, B., and B. Rappenglueck (2010), The TexAQS-II radical and aerosol measurement project (TRAMP) Preface, *Atmospheric Environment, 44*(33), 3997-4004.

Lefer, B. L., R. E. Shetter, S. R. Hall, J. H. Crawford, and J. R. Olson (2003), Impact of clouds and aerosols on photolysis frequencies and photochemistry during TRACE-P: 1. Analysis using radiative transfer and photochemical box models, *Journal of Geophysical Research-Atmospheres, 108*(D21), 22, doi:10.1029/2002jd003171.

Leuchner, M., and B. Rappengluck (2010), VOC source-receptor relationships in Houston during TexAQS-II, *Atmospheric Environment, 44*(33), 4056-4067, doi:10.1016/j.atmosenv.2009.02.029.

Luke, W. T., P. Kelley, B. L. Lefer, J. Flynn, B. Rappengluck, M. Leuchner, J. E. Dibb, L. D. Ziemba, C. H. Anderson, and M. Buhr (2010), Measurements of primary trace gases and NO(y) composition in Houston, Texas, *Atmospheric Environment*, *44*(33), 4068-4080, doi:10.1016/j.atmosenv.2009.08.014.

Lurmann, F. W., A. C. Lloyd, and R. Atkinson, A chemical mechanism for use in long-range transport/acid deposition computer modeling, *Journal of Geophysical Research*, *91*, 10905-10936, 1986.

Mielke, L. H., and H. D. Osthoff (2012), On quantitative measurements of peroxycarboxylic nitric anhydride mixing ratios by thermal dissociation chemical ionization mass spectrometry, *International Journal of Mass Spectrometry, 310*, 1-9, doi:10.1016/j.ijms.2011.10.005.

Murphy, J. G., D. A. Day, P. A. Cleary, P. J. Wooldridge, D. B. Millet, A. H. Goldstein, and R. C. Cohen (2007), The weekend effect within and downwind of Sacramento - Part 1: Observations of ozone, nitrogen oxides, and VOC reactivity, *Atmospheric Chemistry and Physics*, *7*(20), 5327-5339.

Neuman, J. A., et al. (2002), Fast-response airborne in situ measurements of HNO3 during the Texas 2000 Air Quality Study, *Journal of Geophysical Research-Atmospheres*, *107*(D20), doi:10.1029/2001jd001437.

Neuman, J. A., et al. (2012), Observations of ozone transport from the free troposphere to the Los Angeles basin, *Journal of Geophysical Research-Atmospheres*, *117*, doi:10.1029/2011jd016919.

Olson, J. R., J. H. Crawford, G. Chen, W. H. Brune, I. C. Faloona, D. Tan, H. Harder, and M. Martinez (2006), A reevaluation of airborne HOx observations from NASA field campaigns, *Journal of Geophysical Research-Atmospheres, 111*(D10), 12, doi:10.1029/2005jd006617.

Parrish, D. D. (2006), Critical evaluation of US on-road vehicle emission inventories, *Atmospheric Environment*, *40*(13), 2288-2300.

Pollack, I. B., B. M. Lerner, and T. B. Ryerson (2010), Evaluation of ultraviolet light-emitting diodes for detection of atmospheric NO2 by photolysis - chemiluminescence, *Journal of Atmospheric Chemistry*, *65*(2-3), 111-125, doi:10.1007/s10874-011-9184-3.

Pollack, I. B., et al. (2012), Airborne and ground-based observations of a weekend effect in ozone, precursors, and oxidation products in the California South Coast Air Basin, *Journal of Geophysical Research-Atmospheres, 117*, doi:10.1029/2011jd016772.

Ren et al., (2013), Atmospheric oxidation chemistry and ozone production: Results from SHARP 2009 in Houston, Texas, *Journal of Geophysical Research-Atmospheres,* in press, doi:10.1002/jgrd.50342.

Ryerson, T. B., L. G. Huey, K. Knapp, J. A. Neuman, D. D. Parrish, D. T. Sueper, and F. C. Fehsenfeld (1999), Design and initial characterization of an inlet for gas-phase NOy measurements from aircraft, *Journal of Geophysical Research-Atmospheres*, *104*(D5), 5483-5492, doi:10.1029/1998jd100087.

Ryerson, T. B., et al. (2003), Effect of petrochemical industrial emissions of reactive alkenes and NOx on tropospheric ozone formation in Houston, Texas, *Journal of Geophysical Research-Atmospheres*, *108*(D8), doi:10.1029/2002jd003070.

Ryerson et al. (2013), The 2010 California research at the Nexus of air quality and climate change (CalNex) field study, *Journal of Geophysical Research-Atmospheres*, in press, doi: 10.1002/jgrd.50331

Sander, S., R. R. Friedl, A. R. Ravishankara, D. M. Golden, C. E. Kolb, M. J. Kurylo, M. J. Molina, G. K. Moortgat, H. Keller-Rudek, B. J.Finlayson-Pitts, P. H. Wine, R. E. Huie, V. L. Orkin, Chemical Kinetics and Photochemical Data for Use in Atmospheric Studies Evaluation Number 15, JPL Publication 06-2, 2006

Sarwar, G., H. Simon, P. Bhave, and G. Yarwood (2012), Examining the impact of heterogeneous nitryl chloride production on air quality across the United States, *Atmospheric Chemistry and Physics*, *12*(14), 6455-6473, doi:10.5194/acp-12-6455-2012.

Sather, M. E., E. T. Slonecker, K. G. Kronmiller, D. D. Williams, H. Daughtrey, and J. Mathew (2006), Evaluation of short-term Ogawa passive, photolytic, and federal reference method sampling devices for nitrogen oxides in El Paso and Houston, Texas, *Journal of Environmental Monitoring*, *8*(5), 558-563, doi:10.1039/b601113f.

Schultz, M. G., D. J. Jacob, J. D. Bradshaw, S. T. Sandholm, J. E. Dibb, R. W. Talbot, and H. B. Singh (2000), Chemical NOx budget in the upper troposphere over the tropical South Pacific, *Journal of Geophysical Research-Atmospheres*, *105*(D5), 6669-6679, doi:10.1029/1999jd900994.

Shetter, R. E., et al. (2003), Photolysis frequency of NO2: Measurement and modeling during the International Photolysis Frequency Measurement and Modeling Intercomparison (IPMMI), *Journal of Geophysical Research-Atmospheres, 108*(D16), 15, doi:10.1029/2002jd002932.

Steiner, A. L., R. C. Cohen, R. A. Harley, S. Tonse, D. B. Millet, G. W. Schade, and A. H. Goldstein (2008), VOC reactivity in central California: comparing an air quality model to ground-based measurements, *Atmospheric Chemistry and Physics, 8*(2), 351-368.

Stutz, J., B. Alicke, R. Ackermann, A. Geyer, A. White, and E. Williams (2004), Vertical profiles of NO3, N2O5, O-3, and NOx in the nocturnal boundary layer: 1. Observations during the Texas Air Quality Study 2000, *Journal of Geophysical Research-Atmospheres*, *109*(D12), doi:10.1029/2003jd004209.

Talbot, R. W., et al. (1999), Reactive nitrogen budget during the NASA SONEX mission, *Geophysical Research Letters*, *26*(20), 3057-3060, doi:10.1029/1999gl900589.

Tang, W., D. S. Cohan, G. A. Morris, D. W. Byun, and W. T. Luke (2011), Influence of vertical mixing uncertainties on ozone simulation in CMAQ, *Atmospheric Environment*, *45*(17), 2898-2909, doi:10.1016/j.atmosenv.2011.01.057.

Volz-Thomas, A., I. Xueref, and R. Schmitt (2002), An automatic gas chromatograph and calibration system for ambient measurements of PAN and PPN, *Environmental Science and Pollution Research*, 72-76.

Warneke, C., J. A. de Gouw, J. S. Holloway, J. Peischl, T. B. Ryerson, E. Atlas, D. Blake, M. Trainer, and D. D. Parrish (2012), Multiyear trends in volatile organic compounds in Los Angeles, California: Five decades of decreasing emissions, *Journal of Geophysical Research-Atmospheres*, *117*, doi:10.1029/2012jd017899.

Washenfelder, R. A., A. O. Langford, H. Fuchs, and S. S. Brown (2008), Measurement of glyoxal using an incoherent broadband cavity enhanced absorption spectrometer, *Atmospheric Chemistry and Physics, 8*(24), 7779-7793.

Williams, E. J., J. M. Roberts, K. Baumann, S. B. Bertman, S. Buhr, R. B. Norton, and F. C. Fehsenfeld (1997), Variations in NOy composition at Idaho Hill, Colorado, *Journal of Geophysical Research-Atmospheres*, *102*(D5), 6297-6314, doi:10.1029/96jd03252.

Williams, E. J., F. C. Fehsenfeld, B. T. Jobson, W. C. Kuster, P. D. Goldan, J. Stutz, and W. A. McCleanny (2006), Comparison of ultraviolet absorbance, chemiluminescence, and DOAS instruments for ambient ozone monitoring, *Environmental Science & Technology, 40*(18), 5755-5762, doi:10.1021/es0523542.

Wong, K. W., H. J. Oh, B. L. Lefer, B. Rappenglueck, and J. Stutz (2011), Vertical profiles of nitrous acid in the nocturnal urban atmosphere of Houston, TX, *Atmospheric Chemistry and Physics*, *11*(8), 3595-3609.

Wong, K. W., C. Tsai, B. Lefer, C. Haman, N. Grossberg, W. H. Brune, X. Ren, W. Luke, and J. Stutz (2012), Daytime HONO vertical gradients during SHARP 2009 in Houston, TX, *Atmospheric Chemistry and Physics, 12*(2), 635-652, doi:10.5194/acp-12-635-2012.

Xue, L. K., et al. (2011), Source of surface ozone and reactive nitrogen speciation at Mount Waliguan in western China: New insights from the 2006 summer study, *Journal of Geophysical Research-Atmospheres*, *116*, doi:10.1029/2010jd014735.

Ziemba, L. D., J. E. Dibb, R. J. Griffin, C. H. Anderson, S. I. Whitlow, B. L. Lefer, B. Rappengluck, and J. Flynn (2010), Heterogeneous conversion of nitric acid to nitrous acid on the surface of primary organic aerosol in an urban atmosphere, *Atmospheric Environment*, *44*(33), 4081-4089, doi:10.1016/j.atmosenv.2008.12.024.